

**Experimental Investigation of the Performance of Intermeshed Steel
Beam Connections**

A THESIS

SUBMITTED TO THE GRADUATE SCHOOL OF
THE UNIVERSITY OF MINNESOTA

BY

Ramzi Labbane

IN PARTIAL FULFILLMENT OF THE REQUIREMENTS FOR THE DEGREE OF
Master of Science

ADVISER

Arturo E. Schultz

June 2019

© Ramzi Labbane 2019

ALL RIGHTS RESERVED

ACKNOWLEDGEMENTS

Firstly, I want to express my appreciation towards my advisor, Arturo E. Schultz, for the guidance he has provided me during my years in graduate school. I would like to thank him for granting me the opportunity to participate in this research project, and I am grateful for the knowledge he has shared to help me become a successful researcher. I would also like to thank fellow University of Minnesota researchers working on this project, Professor Jia-Liang Le and doctoral student Ebrahim Shemshadian, for their input and feedback on this research project. Additionally, I express my gratitude towards my fellow researchers working on this project at New York University (Debra Laefer and Brittney Oneill), Queens University Belfast (Patrick McGetrick, Tony Martin, and Pantelis Matis), and University College Dublin (Salam Al-Sabah and Linh Truong Hong) for their contributions and collaboration.

I would like to thank the Department of Civil, Environmental, and Geo-Engineering at the University of Minnesota for the educational and financial support I have received during my graduate studies. I would also like to express thanks to the faculty and staff members who were always willing to provide a helping hand. A special thank you goes to the Galambos Laboratory manager, Paul Bergson, for the mentoring and assistance he provided in my experimental work. I am also grateful for the other students with whom I experienced graduate school at the University of Minnesota. Many of them helped me with lab work, often on a whim and without hesitation, and I look forward to the years of friendship that we will share after graduate school.

Lastly, I would like to thank my parents and younger brother for their unending support of my academic endeavors.

ABSTRACT

Advanced manufacturing techniques, such as plasma cutting and water jet cutting, have not been fully capitalized on by the steel construction industry. These precise cutting techniques have the potential to transform how steel structures are designed and constructed. An innovative interlocking (herein referred to as “intermeshed”) steel connection system that relies on neither bolting nor welding has been proposed. The intermeshed connection was designed to resist loads typical in steel moment frames, and four full-scale beam specimens utilizing this connection as a splice were fabricated using precise, fully automated cutting techniques. An experimental testing program was conducted with these specimens to study the behavior of intermeshed connections under gravity loads. The experimental investigation demonstrated how different components of an intermeshed connection may interact to create a strong yet robust connection that exhibits stable and ductile response to vertical loading. The results of this study highlight how the steel construction industry can harness the advantages of advanced manufacturing techniques for intermeshed connections.

TABLE OF CONTENTS

ACKNOWLEDGEMENTS	i
LIST OF FIGURES	vii
LIST OF TABLES	xii
CHAPTER ONE	
Introduction	
1.1 Research Significance	1
1.2 Research Objective	2
1.3 Scope of Work	2
CHAPTER TWO	
Background	
2.1 Alternative Connections.....	4
2.1.1 Pin Fuse Connection	4
2.1.2 ATLSS Connections	5
2.1.3 ConX System	6
2.1.4 Comparison	8
2.2 Intermeshed Steel Connection Conceptualization	9
2.3 Advanced Manufacturing Techniques	11
2.3.1 Plasma Cutting	11
2.3.2 Water Jet Cutting	11
2.4 Front Intermeshed Connection.....	12
2.5 Side Intermeshed Connection	14
CHAPTER THREE	
Connection Design	
3.1 General.....	18
3.2 Angle Connection	19
3.2.1 Assumptions.....	19
3.2.2 Initial Inputs	20
3.2.3 Forces	25

3.2.4 Angle Design	26
3.3 Shear Plates	30
3.3.1 Initial Parameters	30
3.3.2 Forces	31
3.3.3 Shear Plate Design	33

CHAPTER FOUR

Laboratory Testing and Procedures

4.1 Experimental Program	37
4.2 Fabrication	38
4.3 Testing Setup and Loading	40
4.4 Testing Considerations.....	47
4.5 Instrumentation Plan	51
4.5.1 Instrument Locations	52
4.6 Assembly Procedures.....	57

CHAPTER FIVE

Test Results

5.1 Test 1 Results.....	62
5.1.1 Test 1 Displacement Data	63
5.1.2 Test 1 Strain Data.....	65
5.1.3 Test 1 Discussion	69
5.2 Modifications to Bracing and Instrumentation	73
5.3 Test 2 Results	79
5.3.1 Test 2 Displacement Data	79
5.3.2 Test 2 Strain Data.....	82
5.3.3 Test 2 Discussion	89
5.4 Test 3 Results	92
5.4.1 Test 3 Displacement Data	93
5.4.2 Test 3 Strain Data.....	95
5.4.3 Test 3 Discussion	101
5.5 Test 4 Results	104
5.5.1 Test 4 Displacement Data	104

5.5.2 Test 4 Strain Data.....	107
5.5.3 Test 4 Discussion	112

CHAPTER SIX

Evaluation of Experimental Observations and Measurements

6.1 Review of Test Observations	117
6.2 Demands on Angles	117
6.3 Beam Flange Development.....	119
6.4 Moment Capacity of Test Beams.....	121
6.5 Sources of Moment Overstrength	122
6.5.1 Moment Contribution of the Shear Plates.....	122
6.5.2 Moment Contribution from Bearing of Beam Webs	124
6.5.3 Decomposition of Moment Overstrength	125
6.6 Side Angle Contributions to Shear Resistance	127
6.7 Channel Restraint Forces	129
6.8 Local Nonlinearity	130
6.9 Potential Design Procedure Modifications	131
6.9.1 Asymmetrical Connections.....	131
6.9.2 Moment Overstrength	132

CHAPTER SEVEN

Summary, Observations, Conclusions and Recommendations

7.1 Summary	133
7.2 Observations	133
7.3 Conclusions.....	135
7.4 Recommendations.....	136

REFERENCES	138
------------------	-----

APPENDIX A

A.1 Design Spreadsheets	141
A.2 AutoCAD Design Details.....	143
A.3 Specimen Measurements.....	146

A.4 Mill Test Certificates	152
----------------------------------	-----

APPENDIX B

B.1 Stiffener Design.....	155
B.2 Original Bracing Design.....	156
B.3 Revised Bracing Design.....	157
B.4 Local Bearing at Angle Holes	158
B.5 Potential for Slippage of Angle.....	159

APPENDIX C

C.1 Expected Failure Load for Connection	161
C.1.1 W18x46 Maximum Moment Calculation	162
C.1.2 W21x57 Maximum Moment Calculation	162
C.2 Deflection Estimation.....	162
C.2.1 Deflection Calculations	163
C.3 Plastic Moment Calculations.....	164

APPENDIX D

D.1 Strain Calculations	165
D.2 Test 1 Supplementary Figures.....	166
D.3 Test 2 Supplementary Figures.....	167
D.4 Test 3 Supplementary Figures.....	169
D.5 Test 4 Supplementary Figures.....	171

LIST OF FIGURES

2.1: Pin-fuse connection (Gerfen, 2009).....	4
2.2: ATLSS Connection.....	6
2.3: ConXtech connection.....	7
2.4: Conceptualization of connection locations	10
2.5: 3D printed model of the front intermeshed connection	12
2.6: Finite element results	14
2.7: Initial side intermeshed connection concept.....	15
2.8: Modified side intermeshed connection	16
2.9: Circular hole corners.....	17
3.1: Angle leg to beam flange clearance	22
3.2: Plan view of teeth	23
3.3: Elevation of teeth and angle.....	24
3.4: Circular hole dimensions	24
3.5: Loading on a single tooth.....	28
3.6: Shear plate geometry	33
4.1: Plasma cutting.....	39
4.2: Water jet cutting.....	39
4.3: Test 1 loading.....	41
4.4: Test 2 loading.....	42
4.5: Test 3 loading.....	42
4.6: Test 4 loading.....	43
4.7: Loading locations for a) Test 1; b) Test 2 ; c) Test 3; and d) Test 4	44
4.8: Bracing setup	46
4.9: Channel restraints	49
4.10: Beam end view.....	50
4.11: Finite element beam flange stresses.....	52
4.12: Finite element angle stresses.....	53

4.13: Outer angle instrumentation.....	54
4.14: Inner angle instrumentation	54
4.15: Shear plate instrumentation	54
4.16: Beam instrumentation side view.....	55
4.17: Beam bottom flange instrumentation.....	56
4.18: LVDTs on tension angles	56
4.19: LVDTs on tension flange.....	57
4.20: Bracing with temporary wood braces	58
4.21: Bracing viewed from above.....	58
4.22: Test beam with temporary wood bracing	59
4.23: Test setup being moved with the crane.....	60
4.24: Bracing with steel angles in place.....	60
4.25: LVDT attachment to tension angle.....	61
5.1.1: Test 1 total load vs. vertical LVDT displacement	64
5.1.2: Test 1 total vertical load vs. horizontal LVDT displacement	64
5.1.3: Test 1 total vertical load vs. angle LVDT displacement.....	65
5.1.4: Test 1 load vs. compressive angle axial strain.....	67
5.1.5: Test 1 load vs. tensile angle axial strain	67
5.1.6 Test 1 load vs. flange strain	68
5.1.7: Test 1 load vs. beam bottom flange strain	68
5.1.8: Test 1 load vs. channel axial strain.....	69
5.1.9: Test 1 connection after 28 kips of load.....	70
5.1.10: Test 1 deformation in tension angles	71
5.1.11: Test 1 compression angle buckling.....	72
5.1.12: Compression angles post-testing	72
5.2.1: Bracing slotted holes.....	74
5.2.2: Test 1 spreader beam loading the bracing	74
5.2.3: Beam with permanent twist at support	75
5.2.4: String potentiometers in place of LVDTs 1 and 2.....	76

5.2.5: Angle Instrumentation Modifications	77
5.2.6: Beam instrumentation modifications	78
5.2.7: Shear plate instrumentation modifications	78
5.3.1: Test 2 load vs. vertical displacement	80
5.3.2: Test 2 uneven top flanges after testing	80
5.3.3: Lateral movement in the second beam test	81
5.3.4: Load vs. horizontal LVDT displacement.....	82
5.3.5: Load vs. angle LVDT displacement	82
5.3.6: Test 2 vs. compression angle load axial strain.....	84
5.3.7: Test 2 load vs. tension angle axial strain	85
5.3.8: Test 2 load vs. beam bottom flange strain	86
5.3.9: Test 2 load vs. beam flange axial strain.....	87
5.3.10: Test 2 load vs. shear plate axial strain	88
5.3.11: Web strains in whitewash	88
5.3.12: Test 2 load vs. channel flexural strain	89
5.3.13: Compression angles post-test viewed facing North and South.....	90
5.3.14: Lateral bending of the angles	91
5.3.15: Local deformation in a bracing angle	91
5.3.16: Modified bracing for Test 3 and Test 4	92
5.4.1: Test 3 load vs. vertical displacement	94
5.4.2: Test 3 load vs. horizontal LVDT displacement	94
5.4.3: Test 3 load vs. angle LVDT displacement.....	95
5.4.4: Test 3 load vs. compression angle axial strain.....	96
5.4.5: Test 3 load vs. tension angle axial strain	97
5.4.6: Test 3 load vs. beam flanges axial strain	98
5.4.7: Test 3 load vs. beam bottom flange strain	99
5.4.8: Test 3 load vs. shear plate axial strain	99
5.4.9: Test 3 load vs. compression channel flexural strain	100
5.4.10: Test 3 load vs. compression region channel axial strain.....	100

5.4.11: Test 3 movement of teeth and tension angle.....	101
5.4.12: Deformed beam flange loading the angle at peak load.....	102
5.4.13: Test 3 beam deformed shape	102
5.4.14: Test 3 connection post-test	103
5.4.15: Test 3 beam web yielding.....	103
5.5.1: Test 4 load vs. vertical displacement	105
5.5.2: Test 4 load vs. horizontal LVDT displacement	105
5.5.3: Test 3 load vs. angle LVDT Displacement.....	106
5.5.4: Test 4 connection prior to loading	106
5.5.5: Test 4 load vs. compression angle axial strain.....	108
5.5.6: Test 4 load vs. tension angle axial strain	109
5.5.7: Test 4 load vs. beam flange axial strain.....	110
5.5.8: Test 4 load vs. beam bottom flange strain	111
5.5.9: Test 4 load vs. shear plate axial strain	111
5.5.10: Test 4 load vs. channel flexural strain	112
5.5.11: Test 4 yielding of the beam web at center span.....	113
5.5.12: Deformed beam shape after bracing was loosened.....	114
5.5.13: Shear yielding observed outside the constant moment region.....	114
5.5.14: Test 4 top flange movement at angle centerline	115
5.5.15: Test 4 connection after unloading.....	115
5.5.16: Test 4 top view after unloading	116
6.2.1: Test 3 distribution of strain measurements in angles.....	118
6.2.2: Test 4 distribution of strain measurements in angles.....	118
6.2.3: Shear and moment diagram for Test 3 at peak load	119
6.3.1: Test 4 beam bottom flange strain distribution	120
6.5.1: Test 3 shear plate strain distribution at 90% of peak load	122
6.5.2: Test 4 shear plate strain distribution at 90% of peak load	123
6.6.1: Angle deformation with and without shear.....	128
6.7.1: Channel loading	129

6.8.1: Local plasticity in Test 3.....	130
A1: W18x46 Design Spreadsheet	141
A.2: W21x57 Design Spreadsheet	142
A.3: Test 1 Beam Dimensions	143
A.4: Test 2 Beam Dimensions	143
A.5: Test 1 and 2 Connection Details	144
A.6: Test 3 Beam Dimensions	145
A.7: Test 4 Beam Dimensions	145
A.8: Test 3 and 4 Connection Details	146
A.9: Grunau Metals mill test certificates for beams	152
A.10: Am-Tec Designs angle mill test certificates	153
A.11: Shear plate mill test certificate.....	154
B1: Loading on Revised Bracing.....	157
D1: Strain components.....	165
D2: Test 1 compression angle load vs. flexural strain	166
D3: Test 1 tension angle load vs. flexural strain.....	166
D4: Test 1 channel load vs. flexural strain	166
D5: Test 2 angle load vs. flexural strain	167
D6: Test 2 beam flange load vs. flexural strain	168
D7: Test 2 shear plate load vs. flexural strain.....	168
D8: Test 2 compression region channel load vs. axial strain.....	168
D9: Test 3 angle load vs. flexural strain	169
D10: Test 3 beam flange load vs. flexural strain	170
D11: Test 3 shear plate load vs. flexural strain.....	170
D13: Test 4 angle load vs. flexural strain	171
D14: Test 4 beam flange load vs. flexural strain	172
D15: Test 4 shear plate load vs. flexural strain.....	172
D16: Test 4 compression region channel load vs. axial strain.....	172

LIST OF TABLES

Table 1: Side Intermeshed Connection Test Specimens.....	38
Table 2: Mill Test Certificate Details	40
Table 3: Bracing Components	45
Table 4: Anticipated Forces at Failure.....	47
Table 5: Instrumentation Devices	51
Table 6: Beam Test 1 Loading Stages	62
Table 7: Beam Plastic Moments	121
Table 8: Test 3 Shear Plate Moments	124
Table 9: Test 4 Shear Plate Moments	124
Table A1: Beam 1 Specimen Measurements	147
Table A2: Beam 2 Specimen Measurements	148
Table A3: Beam 3 Specimen Measurements	149
Table A4: Beam 4 Specimen Measurements	150
Table A5: Angle Specimen Measurements.....	151

CHAPTER ONE

Introduction

1.1 Research Significance

In modern times, steel connections have almost exclusively been made with bolts and welds. There has not been significant research to develop alternative connection methods since bolting replaced riveting as the method of choice for connecting steel members. Both bolted and welded connections are labor intensive and represent a significant portion of the total cost of a steel structure. In fact, material cost is typically only a fraction of the total construction cost when accounting for labor and fabrication (AISC, 2019).

Bolted and welded steel members are not often reused due to the difficulty of deconstruction, even though steel is a highly recyclable material. Moreover, despite the introduction of new manufacturing equipment, few advances have been made in the development of alternative connections. Alternative connections executed using advanced manufacturing methods may reduce the amount of labor needed to fabricate and erect a steel structure, and they may also allow for deconstruction and reuse.

High definition plasma, laser, and water jet cutting, when combined with fully automated computer-controlled techniques, offer fast fabrication with high precision. This equipment is currently used to accelerate some conventional fabrication activities, such as the cutting of holes in lieu of drilling. However, the steel construction industry has not fully capitalized on the potential of advanced manufacturing equipment. The introduction of these cutting procedures may allow for an entirely new class of steel connections to be developed that improve both the efficiency of construction and the reuse of material. An intermeshed connection system that relies on neither bolting nor welding has been proposed to transform how structural steel is fabricated, assembled, deconstructed, and reused (Schultz et al., 2019).

1.2 Research Objective

The objective of this research is to develop an intermeshed steel connection that improves the efficiency of construction and reuse of material using advanced manufacturing techniques. The intermeshed connection consists of interlocking pieces that act together without relying entirely on bolts or welds to transfer forces. The primary objective of the connection is to resist gravity loads, although it may be able to transfer modest lateral loads, such as from wind. However, it is presumed that an external lateral load resisting system (i.e. separate braced frames or shear walls) will be designed to carry all lateral loads from cases such as wind events and seismic activity.

To gain acceptance from design professionals, an intermeshed connection design procedure that is accurate and can easily be replicated must be formulated. The procedure must allow designers to efficiently select the geometry of a connection that satisfies strength requirements. The validity of the proposed design procedure must be verified with experimental testing in order to be adopted by design and construction codes.

1.3 Scope of Work

The intermeshed steel connection project is a collaborative effort between University College Dublin (UCD), Queens University Belfast (QUB), New York University (NYU), and the University of Minnesota Twin Cities. UCD proposed the initial idea for the intermeshed connection, and in conjunction with QUB have assisted with computational analysis and small-scale testing of interlocking (herein referred to as “intermeshed”) steel connections. Finite element analysis was also performed at the University of Minnesota. This thesis focuses on the full-scale experimental testing conducted at the University of Minnesota.

A procedure to design the intermeshed connection was developed to create a realistic and practical connection. The procedure was based upon the 15th edition of the AISC Steel Construction Manual, the 2016 Seismic Provisions for Structural Steel Buildings, principles of statics, and properties of structural steel, as well as detailed

suggestions from the UCD research partners. The connection was designed to resist forces that may exist in a typical moment-resisting frame structure, and the ductility and strength of the connection were considered in the design procedure.

The experimental work involved four major-axis beam tests with the intermeshed connection located along the beam span and serving as splices. Two pure bending moment tests were conducted, as well as two tests with single point loads. In one of the pure bending tests, the connection was placed in the pure moment region, whereas in the other three tests, the connection was subjected to a combination of bending moment and shear forces. The specimens were instrumented extensively for comparison between experimental results and the expectations from the design procedure and computational models.

CHAPTER TWO

Background

2.1 Alternative Connections

In the past three decades, alternatives to traditional steel connections have been developed by several groups. These connections are sometimes proprietary, for which cases their use requires financial compensation to the developers. In this chapter, some of the alternative connections are described and reviewed. Comparisons to the proposed intermeshed steel connection are made.

2.1.1 Pin Fuse Connection

The pin-fuse connection, developed by Skidmore, Owings & Merrill, is an alternative connection that connects a beam to a column stub. The connection relies on slip critical bolts and a steel pin that resist axial and shear loads. The pin is the center of the rotational hinge formed, and the fuse in the system is created through frictional resistance of the bolts within the slotted holes (Cordova & Hamburger, 2011). The system is shown in Figure 2.1.

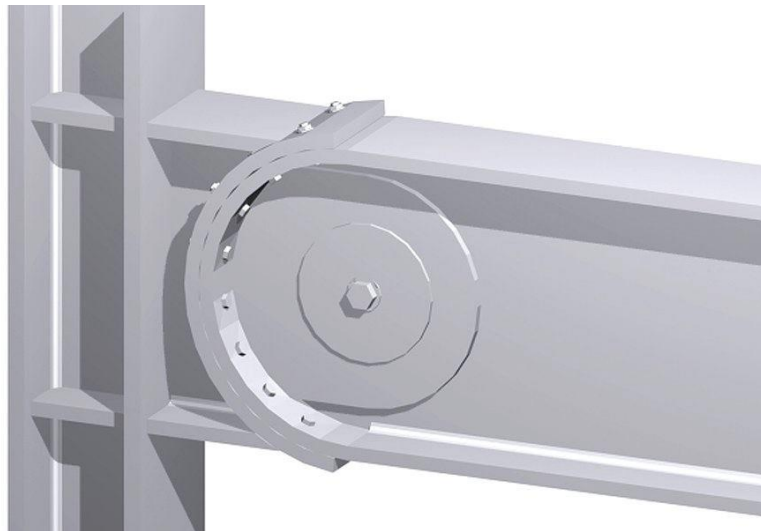


Figure 2.1: Pin-fuse connection (Gerfen, 2009)

The pin-fuse joint is designed so that the frictional resistance of the fuse may dissipate energy in large seismic events. In traditional moment frames, this could form plastic hinges that would affect the structural integrity of the frame. Since the pin-fuse connection is designed to act elastically in this scenario, it could be reused and repaired by loosening and retightening bolts back into their original positions. The ability to reuse material and avoid costly damages to the main load resisting system of beams and columns is congruent with the goals of the proposed intermeshed connection. However, the pin-fuse joint heavily relies on field bolting and is not universally accepted or listed as a prequalified connection in ANSI/AISC 358-16 (AISC, 2016).

2.1.2 ATLSS Connections

Research performed at Lehigh University was conducted to investigate alternative beam to column connections referred to as ATLSS connections (Advanced Technology for Large Structural Systems). A number of connections developed at Lehigh's ATLSS Center are classified as ATLSS connections. Pure shear, partial-moment, and full moment connections were proposed as part of the ATLSS connection research program. Most of the ATLSS connections involved dropping a beam with a male piece (tenon) into a column with a female piece (mortise), utilizing gravity loads to keep the connection in place (Perreira, Fleischman, Viscomi, & Lu, 1993). In Figure 2.2, the mortise, which is welded to the column, is shown next to the tenon, which is bolted to the beam. The ATLSS concepts were found to be most effective for shear transfer since moment connections required additional flanges that negatively affected the efficiency of assembly (Viana, Tommelein, & Formoso, 2017).

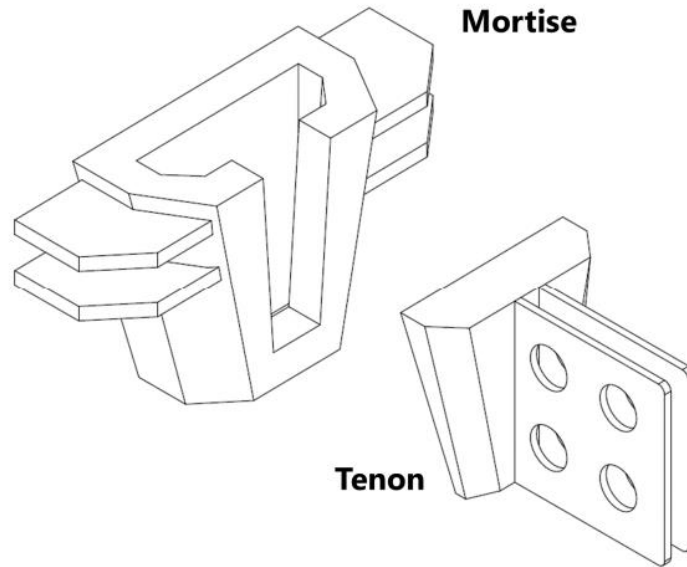


Figure 2.2: ATLSS Connection

The ATLSS connection is like the intermeshed connection since it aimed to improve how structures are assembled on site. However, the ATLSS connection has never been implemented commercially. The mortise and tenon pieces require casting by an entity other than the steel fabricator, and this feature complicates the path to market. The research into the ATLSS connection was conducted over twenty years ago, and the advanced manufacturing techniques available today were not all widely offered then. Unlike the ATLSS connection, the intermeshed connection research has been conducted with the intention of commercialization by utilizing advanced manufacturing equipment that is available to, and often used by, many steel fabricators. The newer manufacturing techniques may lead to a more marketable and universal connection system than what the ATLSS research produced.

2.1.3 ConX System

The ConX connection system was developed in the early 2000's by a private company, ConXtech, and it is commercially available. This connection consists of beams with

moment connections on as many as four sides of an HSS column. The technology is marketed as being ideal for buildings of up to twelve stories in height (“ConX Systems,” n.d.).

The connection itself requires no field welding, and bolting is not required until the assembly is already in place. A “collar corner” assembly is welded in shop to the HSS columns, and a “collar flange” is welded in shop to the beam flanges. Once the HSS columns in the structure are erected, they are filled in with concrete for stability. The beams are lowered into place to create a stable assembly. Then, high strength pretensioned bolts are used to interconnect the collar flanges and develop the full moment capacity of the system (Cordova & Hamburger, 2011). The ConX connection system is shown below in Figure 2.3 (AISC, 2016).

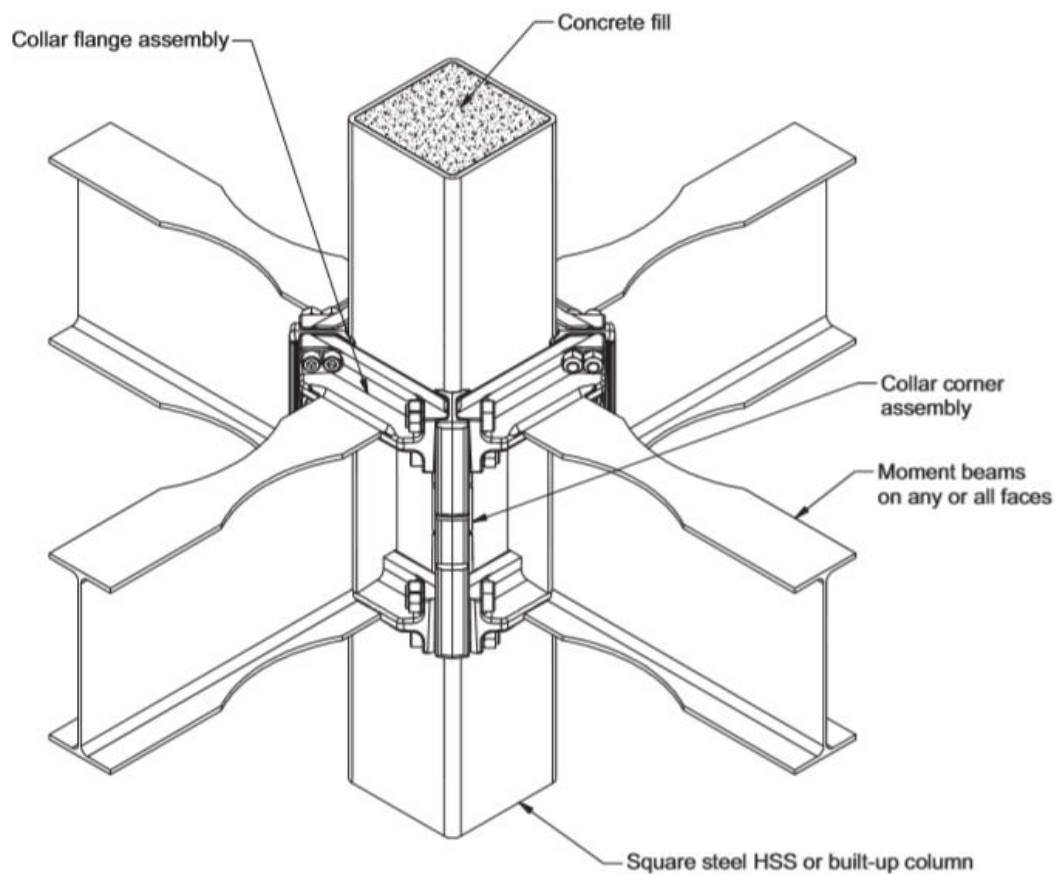


Figure 2.3: ConXtech connection

2.1.4 Comparison

A recent study researched the cost and construction productivity between alternative methods and conventional methods for steel connections. Both ATLSS and ConX connections were included in the study and referred to as steel quick connection systems (SQCS) (Shan, Kim, Goodrum, Caldas, & Haas, 2014). Alternative connections that have already been developed can be used to estimate how the proposed intermeshed steel connection may fare in the realm of cost and productivity.

Relative to traditional connection systems, the SQCS buildings were estimated to have a time savings of 51% during the construction process. The reduction in the number of hours of construction work required to complete a project would lead to a significant reduction in labor costs. However, the total cost of construction projects was found to be only negligibly lower for SQCS buildings in comparison to conventionally constructed buildings (Viana, Tommelein, & Formoso, 2017). The close comparison arises because the cost savings from the fewer labor hours were offset by the increased cost of steel fabrication. So, for the alternative connection methods already developed, there may not be significant cost savings at the end of the project. However, when schedule is a priority over cost, SQCS buildings could be a significantly better option than a building with traditional steel connections.

There are similarities between the intermeshed steel connection and the other alternatives researched, but there are also some stark differences. None of the alternative connections that have been developed have achieved universal acceptance by the steel construction industry, but the proposed intermeshed connection aspires to achieve this. The intermeshed connection also stands out because it relies on the advanced techniques such as water jet and plasma cutting during fabrication. Fabrication costs associated with the intermeshed steel connection will likely be different and potentially much lower than that of other SQCS systems.

An important similarity the proposed connection could share with other alternatives is that it may have time and labor cost savings similar to the SQCS buildings studied. Because of this, the studies on previous alternatives justify the development of

the intermeshed connection for increased construction efficiency. If codified and widely accepted by the steel construction industry, the intermeshed steel connection could reach commercial success unprecedented by the other alternative steel connections.

2.2 Intermeshed Steel Connection Conceptualization

Like other alternative connections investigated, the proposed intermeshed steel connection may be used to connect beams to the columns that support them in steel frame structures. Frames with uniform floor loads experience the highest negative moment at the face of each support and the highest positive moment at the center span. The moment in the beam is zero where negative moment changes to positive moment. This inflection point is located at roughly 20% of the span of the beam away from the support. Since the internal forces in the beam greatly vary along the span, the location of the connection will influence what loads it must be designed to withstand.

Due to interruption in load and stress path, it is unlikely that a connection consisting of intermeshed components will have the full capacity of the connected steel sections in axial, shear, and flexure (Schultz et al., 2019). Because of this, the intermeshed steel connection is anticipated to be most efficient when located near the inflection point away from the support. This can be achieved by executing the connections on-site to beam stubs that are shop welded to the columns prior to erection (Figure 2.4).

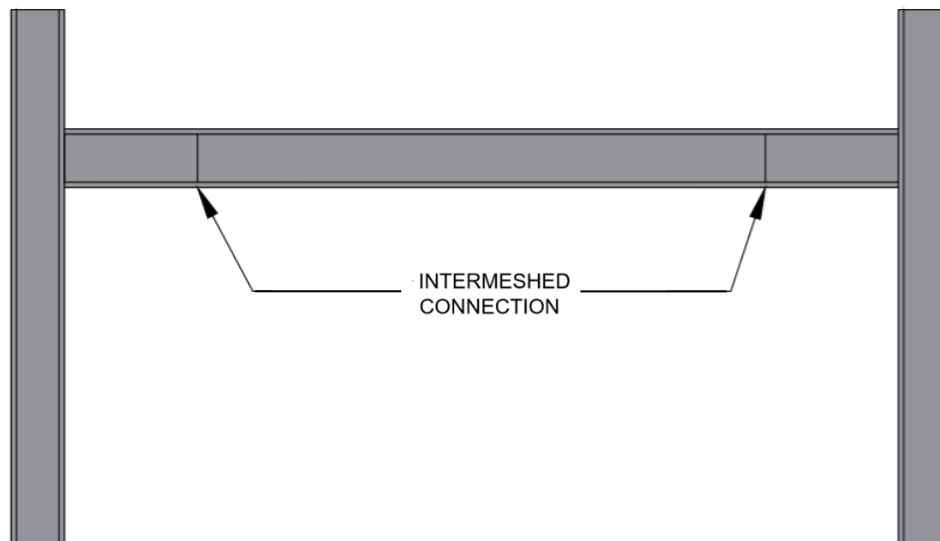


Figure 2.4: Conceptualization of connection locations

Locating the connection away from the supports leads to a reduction in both shear and moment demand from gravity loads, but these forces may still be significant. Shear forces are resisted in the beam web, so a connecting element in the web must be considered. Moment is transferred in the top and bottom flanges. Moment can be idealized as a force couple comprising of tension and compression resultants located at opposite (i.e. top and bottom) flanges. In an intermeshed connection, the compressive forces can be resisted through direct bearing contact, but the stress concentrations created by the tensile forces must be carefully considered when designing a functional connection system.

Since lateral loads are assumed to be resisted by structural core walls or braced frames, it is not necessary to use lateral loading as a controlling factor for connection design. However, small lateral loads could still be attracted by the intermeshed connections, and these would be resisted by connecting elements in the flanges of the beam. More importantly, gravity frames made using intermeshed connections must be able to resist the effects of lateral drifts imposed by the lateral load resisting system with no loss of vertical load capacity.

A “dovetail” type of flange connection with a stair stepped web was initially theorized. With this configuration, referred to as a front intermeshed connection, the beam could simply be lowered into place. This method assumed no reversal in direction of shear forces. Another type of connection, referred to as a side intermeshed connection, was envisioned with notches cut into the sides of the beam flanges that are then connected to each other via steel angles with rectangular holes. Both concepts are discussed in further detail in sections 2.4 and 2.5, and ultimately the side intermeshed connection was selected for the experimental testing program. Both configurations can be fabricated with advanced manufacturing techniques.

2.3 Advanced Manufacturing Techniques

The manufacturing techniques used in this research were plasma cutting and water jet cutting. Both techniques are appropriate for cuts that require high precision. The connections in this experiment relied on these for fabrication.

2.3.1 Plasma Cutting

Plasma cutting was first developed in the 1950’s and introduced to the steel construction industry in the decades following. It can be automated to cut all electrically conductive materials (“Facts About Plasma,” 2011). High definition plasma cutting is a thermal process achieved through a concentrated high-speed plasma stream. A concentrated electric plasma arc with a large kinetic energy is formed between a tungsten electrode and the material that is being cut (Krajcarz, 2014). The plasma stream is extremely hot at up to 30,000 K, and it cuts through the material by melting it (“Facts About Plasma,” 2011). The plasma cutter may be attached to a robotic arm with multiple degrees of freedom, giving it unlimited possibilities regarding the position and configuration of the cut surfaces.

2.3.2 Water Jet Cutting

First developed in 1968 and further advanced in the decades following, water jet cutting can be used to cut various materials, including structural steel. High pressure water jets

with abrasive additives are used to cut the material by eroding away at the surface (Krajcarz, 2014). This form of cutting may be a desirable alternative to plasma cutting due to its environmental friendliness and lack of thermal effects on the cut material (Dahil, Dahil, & Karabulut, 2014). Water jet cutting is also more precise than plasma cutting. As an emerging technology with certain advantages over other cutting methods, its use may become more widespread in the future.

2.4 Front Intermeshed Connection

The first connection that was investigated was the front intermeshed connection. The top and bottom flanges of connecting elements have teeth and notches cut into them that connect to each other like a dovetail joint. Bearing and friction in the teeth transfer compressive and tensile forces in the flanges. The stair stepped configuration of the beam web transfers the shear force through bearing. The connection geometry used for the investigation was developed based upon the expected load path. A basic mechanical model was used to aid with this (Shemshadian et al., 2019). An image of the front intermeshed connection is pictured below in Figure 2.5.

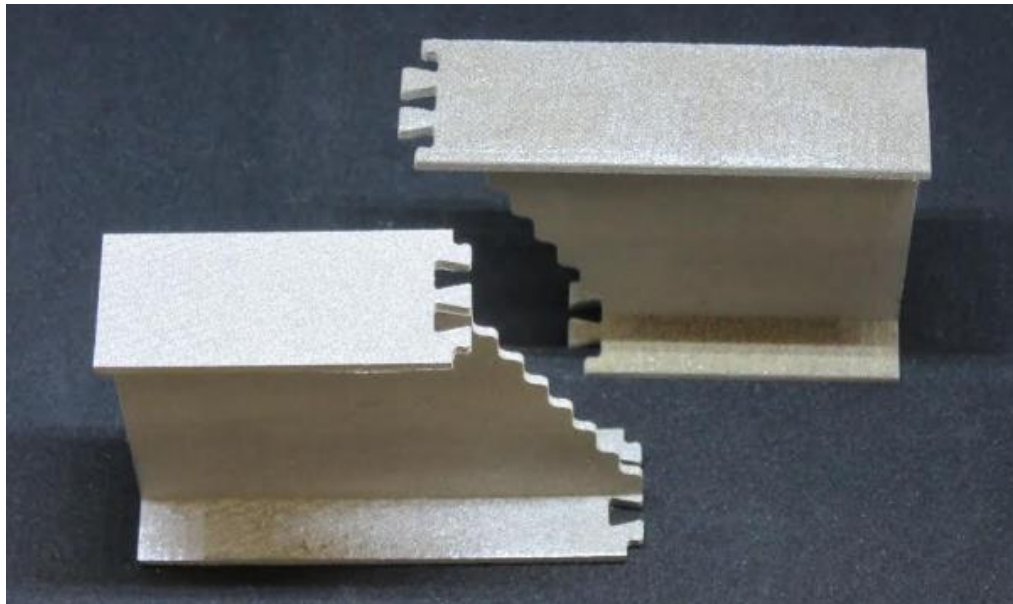
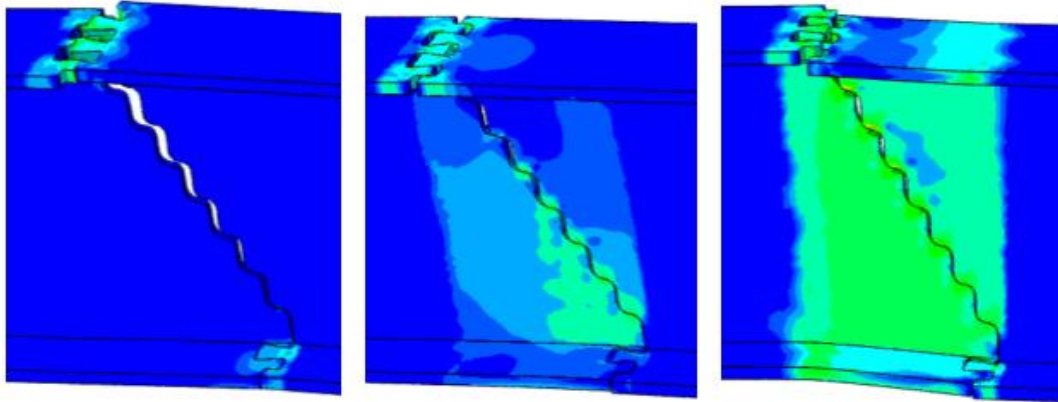


Figure 2.5: 3D printed model of the front intermeshed connection

To investigate the behavior of the front intermeshed connection, finite element analysis was performed in Abaqus under various loading conditions (Shemshadian et al., 2019). Initial analysis was performed to investigate failure modes and capacity of the connection, and further studies examined how different ratios of loads in compression, tension, shear, and flexure affected the capacity. One side of the connecting elements was modeled with a fixed boundary condition to simulate the column stub.

There was no reduction in beam capacity when shear and compressive forces were applied to the connection. However, there was a significant reduction in total strength due to tensile loads. In tension, the finite element model produced a failure that did not rupture the teeth. Instead, plastic deformations enabled the teeth to slip out from one another. This failure mode was consistent with small scale tests performed at QUB (Matis et al., 2019). The failure was similar for the pure tension case as well as for the flexural case. Once the teeth slipped out in tension there was no longer any flexural capacity.

When shear loads were combined with flexural loading, multiple failure modes were observed. Shear forces initially kept the flanges aligned and increased the strength of the connection. However, when shear forces were increased, a failure mode in which the flanges slipped apart transversely was observed. Therefore, the relative dominance of the shear forces over the flexural forces affected whether the combined loading scenario benefitted or impaired this type of connection (Shemshadian et al., 2019). Because of this behavior, it was deemed important to include combined shear and flexural loading for the experimental portion of the research.



a) Flexure b) Flexure and low shear c) Flexure and high shear

Figure 2.6: Finite element results

Although successful under certain loading combinations in the finite element analysis, the practicality of the front intermeshed connection was also questioned. Relative to traditional steel sections, the teeth have a complex geometry. The connection lacks adjustability, which could lead to issues with the field assembly of the connections with tight manufacturing tolerances. Ultimately, an alternative connection with similar features was selected for the experimental testing. However, the performance characteristics of the front intermeshed connection were carefully considered and used as guidance for designing the alternative.

2.5 Side Intermeshed Connection

The alternative connection chosen for experimental testing is referred to as the side intermeshed connection. Intermeshed external connectors located at the sides of the beam flanges transfer tensile and compressive flange forces. The initial concept for the side intermeshed connection required no bolting and had a stair stepped web joint like the front intermeshed connection, and it is shown in Figure 2.7. However, the stair stepped joint was ultimately replaced with a shear plate that requires minor bolting. This change was deemed necessary to achieve greater acceptance in the construction industry.

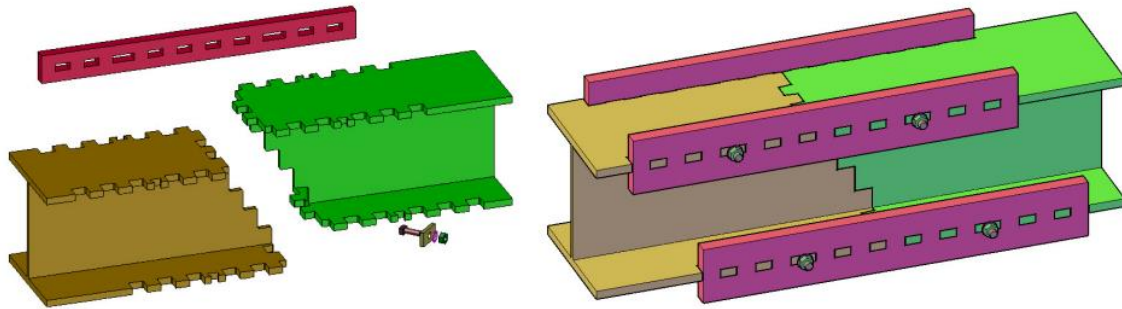
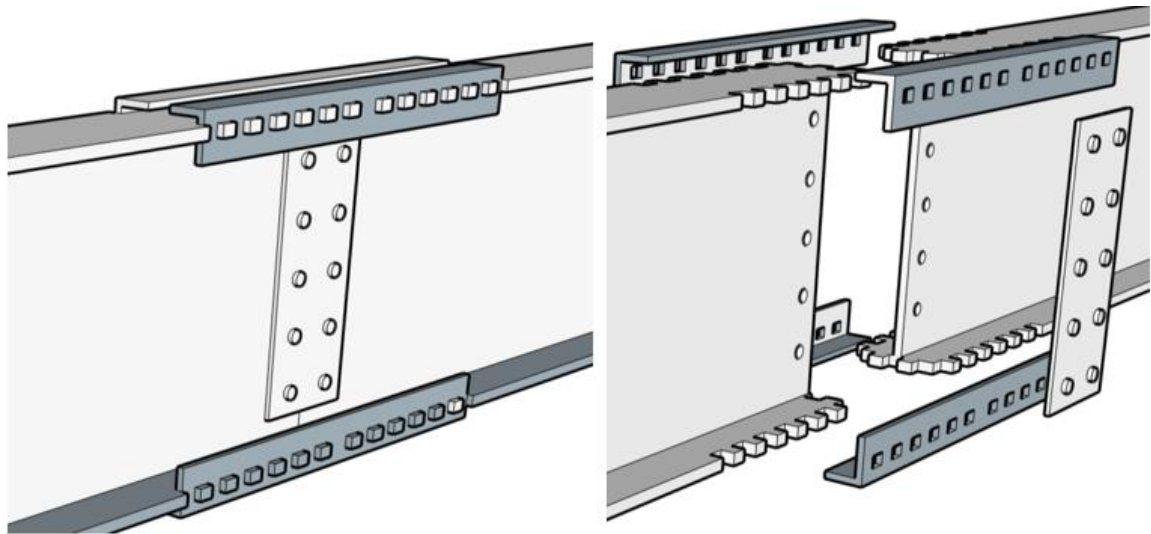


Figure 2.7: Initial side intermeshed connection concept

The side and front intermeshed connections are similar in that they rely on teeth cut into the flanges and rectangular holes to transfer tensile and compressive forces. However, the shape of the teeth and holes in the side intermeshed connection are rectangular instead of a dovetail shape. Also, the teeth that transfer tension and compression forces are located on the sides of the beam flanges rather than at the connection. The teeth are designed to resist minimal lateral loading only. The connecting elements are either plates or angles with rectangular holes located at each side of the top and bottom beam flanges, and the holes correspond to the location of the flange teeth. A pair of shear plates are bolted to the beam webs to transfer shear forces. The modified configuration that was selected for the side intermeshed connection is shown in Figure 2.8.



a) Assembled view

b) Exploded view

Figure 2.8: Modified side intermeshed connection

The side intermeshed connection was developed primarily to have a greater ease of fabrication and assembly than the front intermeshed connection. Larger tolerances are included in this configuration that correspond to allowable manufacturing tolerances specified by AISC. Tolerances at the holes increase the adjustability of the connection, allow connecting elements to be placed safely and easily, and accommodate imperfections in the connected members.

Another advantage of the side intermeshed connection could be the ease of the replacement of angles after an overloading event. If such an event were to occur, the angles acting as connecting elements should be the weakest component of the frame so that they experience failure first. This means the teeth should be designed more conservatively than the angles. This can be accomplished by designing the angles for the applied loads and by designing the teeth for forces that correspond to the capacity of the angles. This notion, referred to as capacity design, helps meet the goals of the intermeshed steel connection project for greater reuse of materials.

A concern with the side intermeshed connection is that the angles could potentially have high stress concentrations at the corners of the rectangular holes. Sharp

corners can experience a stress concentration factor of up to five (Sikora, 1973). Such large stress concentrations at the hole corners could result in a premature failure of the angle connector. To alleviate this issue, circular holes were added to the corners of the rectangular holes in the angles to create stress-reducing radii, and their effectiveness was verified with finite element analysis. The analysis found that the stress concentration was reduced to 1.7 at the corners, thus proving the usefulness of the corner holes (Shemshadian et al., 2019). Figure 2.9 shows the hole with the inclusion of circles at the corners, and the stress concentrations from the finite element analysis are also shown.

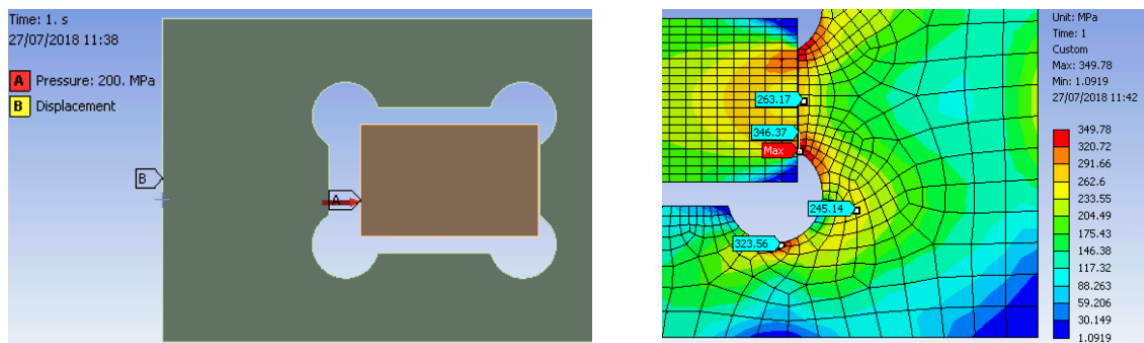


Figure 2.9: Circular hole corners

The qualitative configuration of the side intermeshed connection was decided upon for practicality purposes without consideration of the dimensions of the various connection elements. Although the depth of teeth and holes in the angles correspond to flange thickness, many other parameters must be determined based upon rational calculations, fundamental mechanics and engineering judgment and design criteria. The tooth length, number of teeth, and tolerances must be selected for the connecting angle elements to meet the expected connection performance. In addition to this, the plate at the web must also be designed to conservatively resist shear forces. A detailed design procedure for the side intermeshed connection was developed to select the connection geometries tested.

CHAPTER THREE

Connection Design

3.1 General

The procedure used to design the side intermeshed connection requires the design of the angles and web shear plates separately. In this procedure, it is assumed that the angles will take all the load due to moment, and the plates will take all the load due to shear. Several iterations may be necessary to develop an arrangement that is appropriate for a given combination of shear and moment. A spreadsheet or other computational tool may be used to iterate by updating the properties of the connection until an adequate design is reached.

As in a traditional steel structure, the connection would be designed after the beam section sizes have been selected to resist a given combination of gravity loads. Thus, some properties, such as the thickness of beam flanges and teeth, should not be adjusted when designing the connection. Other geometric parameters, such as the length of a single tooth, the number of teeth, and the size of the angles are dependent upon one another and must be chosen during the design of the connection. Once all geometries and material properties are stated, the capacity of the connection may be checked against the demand. The size of the connection components may then be increased or decreased to produce an adequate and optimally efficient configuration.

The method used to design the side intermeshed connection is extensively based upon the 15th edition of the AISC Steel Construction Manual. To ensure the practicality and sufficiency of the design procedure, the properties of structural steel, principles of statics, and the 2016 Seismic Provisions for Structural Steel Buildings were also referenced. Since this project is a collaborative effort with researchers in Europe, the Eurocode 3 (1992) requirements for steel connections were also carefully studied. However, ultimately no adaptations to the design procedure were adopted from the Eurocode.

3.2 Angle Connection

The angles and flange teeth are the defining characteristics of the side intermeshed connection. It requires a total of four angles: two for the top flange and two for the bottom flange. For simplicity and symmetry, all four angles and the corresponding flange teeth are identical. Since the side intermeshed connection can resist compressive forces through bearing contact of the beam sections, once such contact is established, tensile forces are assumed to be the controlling factor for the design of flange teeth and angles. The following section describes the process used to design the angles and flange teeth for tensile loads due to flexure.

3.2.1 Assumptions

The design of the angle connection follows the Load and Resistance Factor Design (LRFD) methods. The following assumptions are made.

- LRFD resistance factor, bending and yielding, $\phi = 0.9$
- LRFD resistance factor, rupture, $\phi = 0.75$
- Shear lag factor, $U = 0.80$.
- Yield strength factor, $R_y = 1.5$ or 1.1 (Grades 36 and 50, respectively)

The resistance factors selected are identical to those found in Chapter D of the AISC Specification. The shear lag factor, U , may be found in the same section. AISC Table D3.1 states that single angles “with four or more fasteners per line in the direction of loading” will have a shear lag factor of 0.80 (AISC, 2017). Side intermeshed connections have at least four teeth connecting to each angle in a typical loading scenario, and the flange teeth are essentially “fasteners”. It is assumed that the side intermeshed connection is similar enough to the criteria described in AISC that the shear lag factor of 0.80 is an appropriate approximation.

The ratio of the expected yield stress to the specified minimum yield stress is denoted as R_y (AISC, 2017). In steel manufacturing, the specified yield stress is the

minimum yield stress that the product must possess to meet the material specification from the American Society for Testing and Materials (ASTM). The true yield stress values of steel are commonly higher than the specified yield stress values as producers seek to satisfy, by a reliable margin, minimum specified values for product acceptance. Due to this situation, the true capacity of an angle may exceed its minimum capacity based upon the material specification. This issue is of importance in this project since failure should occur in the angles rather than the beams. The R_y value can provide a more realistic approximation for the capacity of the angles, and it may be estimated from the 2016 Seismic Provisions for Structural Steel Buildings Table A3.1. Although there may be less plastic deformation in these tests than there is in seismic design, it is assumed that R_y will provide a reasonable approximation for angle capacity.

No eccentric forces are presumed to act on the angle. Theoretically, force applied to the angle would have to be applied to the centroid of the angle for this to be true. Forces on the angle are small area loads from the bearing contact with the flange teeth. To keep actual eccentricities minimal, the location where flange teeth bear on the angle should coincide with the centroid of the angle. To accomplish this, an angle with equal leg lengths may not be appropriate. To move the centroid of the angle closer to the center of bearing contact with the teeth, the leg of the angle parallel to the beam web can be longer than the leg parallel to the flange. If the bearing forces coincide with the centroid of the angle, eccentric forces are assumed to be insignificant.

3.2.2 Initial Inputs

The following geometric properties must be specified to begin the design of the connection.

- Beam
 - Depth (d)
 - Width (w)
 - Flange thickness (t_f)
 - Web thickness (t_w)
 - Shape factor (Z_p)
 - Beam web area (A_w)
- Angle
 - Angle leg dimensions (l_v and l_h)
 - Thickness (t_a)
 - Angle area (A_a)
 - Angle to flange clearance (C)

Each of these values may be found in the AISC Steel Construction Manual or product tables from steel producers. Although the beam size will be known from the framing plan in a structure, the angle sizes must be selected as part of the design of the connection. The clearance (C) refers to the distance from the outer face of the beam flange to the closest face of the angle leg parallel to the flange. The clearance is shown in Figure 3.1. The angle must be placed so that its clearance is greater than or equal to the radius at the corner of the angle. In turn, the thickest steel element that a plasma or water jet cutting machine must penetrate is the legs of the angles.

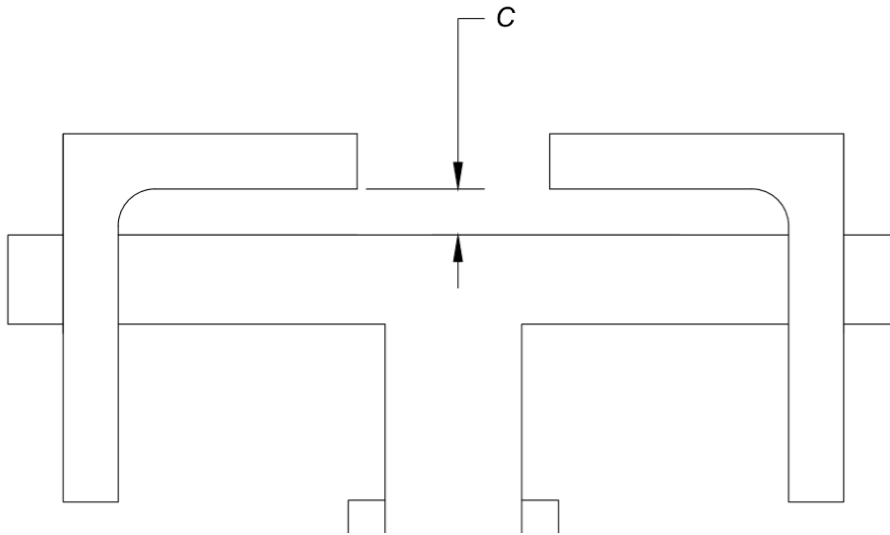


Figure 3.1: Angle leg to beam flange clearance

The following material properties should be used because they represent appropriate ratios of beam-to-angle strengths.

- F_y beam = 50 ksi
- F_y angle = 36 ksi
- F_u angle = 58 ksi

Additionally, the yield and rupture strengths listed are what are most commonly used in the steel construction industry today. The main load resisting elements, such as beams, are regularly Grade 50 steel. The connecting elements, such as plates and angles, are most often Grade 36 steel. These properties are recommended for side intermeshed connection design.

Finally, the designer must select the configuration of teeth in the beam flanges. The following geometric parameters may be easily changed, but values must be chosen considering, in part, engineering judgment.

- Number of teeth (n)
- Tooth width (b)
- Tooth depth (l_t)
- Tolerances (g_0, g_1, g_2)

The variable, n , refers to the number of teeth on one side of a single beam flange. Therefore, the number of holes cut into any given angle will be $2n$ since the angles connect to two beam flanges. A tooth width at or near one inch was selected here. The tooth depth must be adequate in length to fully support the angle, but it must not be so intrusive into the flange width that it greatly affects the capacity of the beam section. A tooth depth of less than one inch was used in this study.

Finally, values for the tolerances in the rectangular holes in the angles must be specified. If the tolerances are not already identified, $1/16''$ is recommended as being appropriate for each one. Tolerances in beam section camber, determined from AISC 1-22 through 1-26, were examined to obtain this value. Figure 3.2 and Figure 3.3 show where the tolerances (g_0, g_1, g_2) are located around the flange teeth.

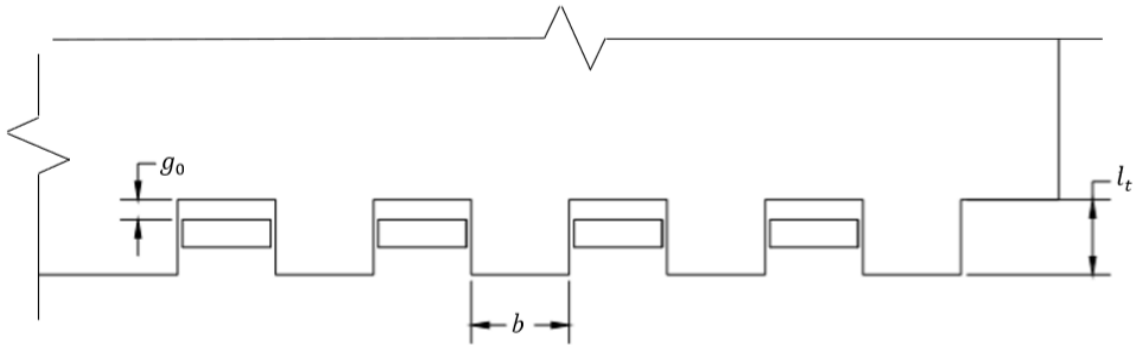


Figure 3.2: Plan view of teeth

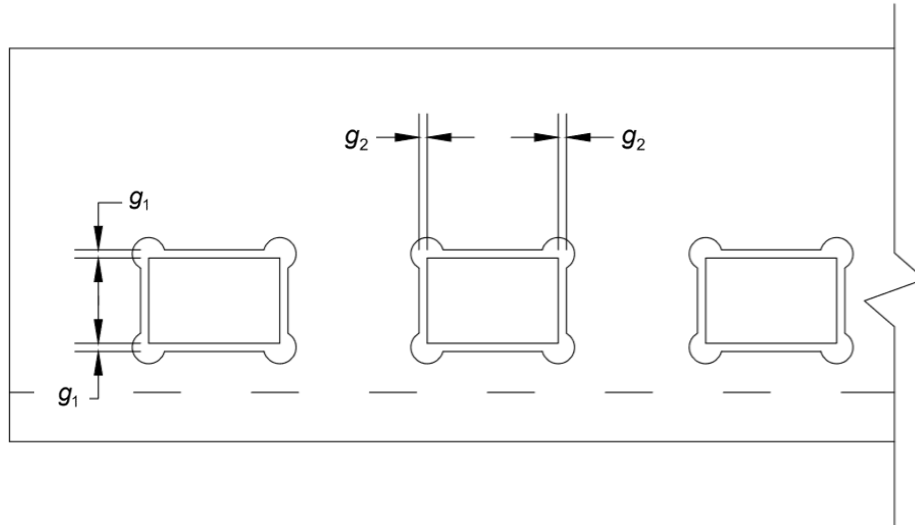


Figure 3.3: Elevation of teeth and angle

Dimensions for the circular cuts at hole corners were chosen so that an adequate amount of stress could be relieved without significantly reducing the angle cross section. The geometry of the circular cuts is shown in Figure 3.4, and each cut will be identical for any angle.

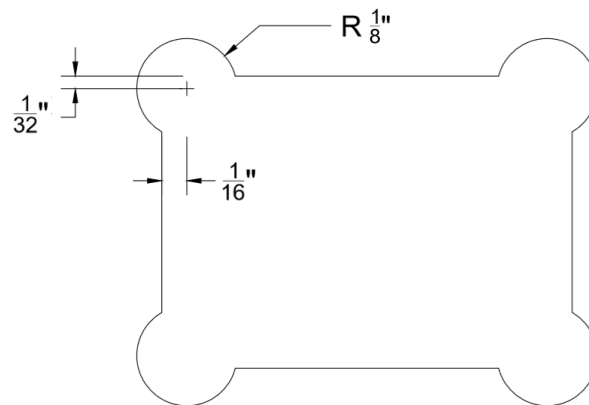


Figure 3.4: Circular hole dimensions

3.2.3 Forces

For practical reasons, these connections are not recommended for placement near the location where maximum moment will be experienced. Therefore, the full moment capacity of the beam is not required for the connection. The fraction of this capacity that is sought becomes a design choice. One third the total moment capacity of the beam was selected as the design moment, but this value can easily be changed based upon engineering judgment. Moreover, given the conservative approach that is outlined here for the connection design, it is likely that the connection will be stronger than assumed.

The fraction value of one third was selected based upon the size of the connection and the probable moment demand. It was important to limit the length of the connection for practicality purposes. Excessively long connections (beyond approximately 1.5 times the beam depth) would affect the economy and constructability of this system. The value of one third was found to produce connections of reasonable length for each case examined, and it resulted in ample moment capacity, thus allowing for some flexibility in exactly where the connection is placed.

In practice, moment at the location of the connection should always be checked so that it does not exceed one third (or the value selected) of the beam capacity. The calculation for design moment is given by Equation 1.

$$M_d = \frac{1}{3} F_y Z_p \quad [1]$$

M_d = design moment

Z_p = shape factor, AISC Table 1-1

The flange force in the selected angle section is determined from static equilibrium of moments and by neglecting the contribution of the web to moment resistance. It is given by Equation 2.

$$F_f = \frac{M_d}{d_b + C + t_a} \quad [2]$$

F_f = flange force

The force per angle (F_a) will be one half of the flange force.

3.2.4 Angle Design

The capacity of the angles must be investigated for the cases of both yielding and rupture.

$$P_y = \phi F_y A_a \quad [3]$$

P_y = yield capacity

$$P_r = \phi F_u A_{ea} \quad [4]$$

P_r = rupture capacity

A_{ea} = angle cross section effective area

$$A_{ea} = U[A_a - t_a(t_f + 2g_1)] \quad [5]$$

U = shear lag factor, 0.80

$$\text{Angle utilization (\%)} = \max\left(\frac{F_a}{P_y}, \frac{F_a}{P_r}\right) \times 100 \quad [6]$$

Angle utilization should be below 100% to prevent yielding ($F_a \geq P_y$) or fracture ($F_a \geq P_r$) at the design moment. The size of the angle must be increased if this requirement is not met, but a utilization approaching 90 to 100% is ideal for efficiency

purposes. Given the large reductions in cross-sectional area at the hole locations in the angles, rupture failure is most likely to control design.

After yield and rupture strength has been checked, the shear force in a single tooth should also be checked. The shear force in each tooth is determined from the maximum force an angle will likely experience when it fails due to gross section yielding. This is an ideal scenario because when failure occurs it will do so in the angles rather than the beams.

$$F_{amax} = 1.1A_aF_yR_y \quad [7]$$

F_{amax} = maximum force from an angle

$R_y = 1.5$ (from grade 36 angle)

1.1 = accounting for uncertainties, adapted from seismic provisions (see seismic design provisions Chapter E, section 6b).

$$V_{ed} = \frac{F_{amax}}{n} \quad [8]$$

V_{ed} = force in a single tooth

$$V_{rd} = \phi \frac{R_y A_t F_y}{\sqrt{3}} \quad [9]$$

V_{rd} = tooth resistance

A_t = area of single tooth = $b * t_f$

$\sqrt{3}$ = Reduction in tensile capacity of $\sqrt{3}$ from Von Mises yield criterion

$R_y = 1.1$ for a Grade 50 beam

$$\text{Shear utilization (\%)} = \frac{V_{ed}}{V_{rd}} \times 100 \quad [10]$$

Shear utilization should be below 100% to ensure that a failure does not occur in the teeth on the flange. If a value of greater than 100% is obtained, the number of teeth should be increased.

To ensure the teeth are not damaged, an upper limit should be chosen for shear utilization below 95%. The R_y values incorporated into the angle and tooth equations are based upon assumptions rather than factual data from testing.

Finally, the moment experienced in each tooth must be checked. No bending stress reduction factor is included. In the European Standard EN 1993-1-1 section 6.2.8, a factor is included to account for the effect of shear force on moment resistance (Eurocode 3, 1992). This standard utilizes the values of shear force and shear resistance to calculate a factor by which the yield strength of the steel may be reduced. The AISC code does not contain any equivalent reduction factor. Since the rest of the design process is conservative in nature and based upon the AISC code, a bending stress reduction factor was not used for this design. The moment in a single tooth is based upon the loading shown in Figure 3.5.

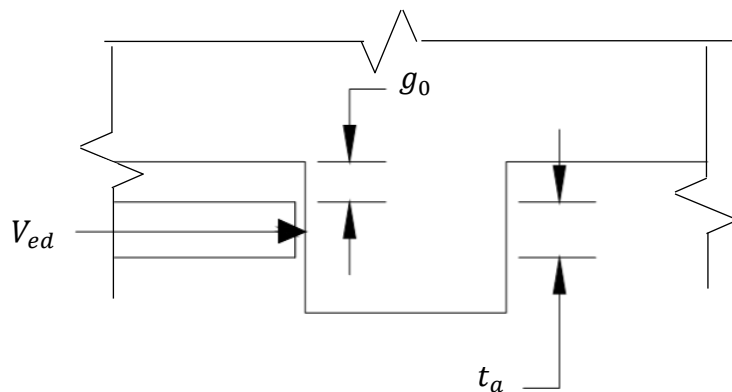


Figure 3.5: Loading on a single tooth

$$M_{ed} = V_{ed} \left(\frac{t_a}{2} + g_0 \right) \quad [11]$$

M_{ed} = moment applied to tooth

$$M_{rd} = \phi R_y F_y M_{pt} \quad [12]$$

M_{rd} = tooth moment resistance

$R_y = 1.1$ (grade 50 beam)

M_{pt} = plastic section modulus for tooth

$$M_{pt} = \frac{t_f b^2}{4} \quad [13]$$

$$\text{Moment utilization (\%)} = \frac{M_{ed}}{M_{rd}} \times 100 \quad [14]$$

Moment utilization should always be below 100% to ensure that a failure does not occur in the teeth on the flange. If a value of greater than 100% is obtained, the number of teeth should be increased.

To avoid damaging the flange teeth, an upper limit for moment utilization may be chosen below 100%. Like the shear utilization ratio, an upper limit of 95% is recommended if a reduction is desired, and engineering judgment should be used when selecting an acceptable upper limit for the moment utilization ratio.

A spreadsheet or other computational tool can easily be used to iterate these design calculations and select a geometry that meets the requirements for yielding, rupture, tooth shear, and tooth moment. The parameters that can be easily changed to design an appropriate section are the angle size and the number of teeth. The final step in designing the side intermeshed connection is to design the shear plates that transfer shear in the beam web.

3.3 Shear Plates

In a traditional wide flange beam, the web is responsible for carrying shear forces. Since the angle connectors in the side intermeshed connection only contact the beam flanges, they are assumed to carry no shear force. Because of this, a path must be provided to transfer shear forces from one side of the connection to the other within the beam webs. Therefore, bolted shear plates are included on both sides of the beam webs to transfer shear. Although one of the original concepts included a stair stepped web, as shown in Figure 2.5, the bolted shear plate was deemed more effective. This was due to the slipping seen in the finite element model and the added difficulty in fabrication and assembly.

The shear plates are placed symmetrically at the connection, and they should be centered along the depth of the beam webs. The shear splice connection is designed to nearly match the shear capacity of the beam section. This is a conservative approach for the tests being performed since the forces are relatively low, and in reality the angles will carry at least some portion of the shear force. Nonetheless, it is desirable to provide ample margin against shear failure in the web when testing the intermeshed connection.

3.3.1 Initial Parameters

The same geometric properties of the beam that were defined for the angle design were used to design the shear plates as well. Additional properties that must be specified are the material properties and dimensions of the plates. The material properties specified in this document are commonly used for connecting elements, but they can easily be modified. The values of L_{ev} and L_{eh} (Figure 3.6) are also commonly used for plates, but they may be modified if desired. Eccentricity (Figure 3.6) is defined as the spacing between the lines of bolts on each side of the connection, and it may be taken as two times L_{eh} . AISC Figure 10-12 may be used to aid with the dimensioning of the shear plate, and it was used to produce Figure 3.6.

Bolt type and bolt size must also be chosen as part of the design. A325 bolts with a diameter of $\frac{3}{4}$ " are commonly used and are recommended for this purpose. The bolt

shear strength is based upon these properties, and it can be found in AISC Table 7-1. Three inches is the standard center to center spacing for bolts in the vertical direction, s , and it is the recommended spacing for this connection (Figure 3.6). The relevant geometric and material properties for shear plates and bolts are defined below.

- Plates
 - $F_y = 36$ ksi
 - $F_u = 58$ ksi
 - $L_{ev} = 1.25''$
 - $L_{eh} = 1.50''$
 - $l =$ Length
 - $t =$ Thickness

- Bolts
 - Bolt type
 - Bolt size
 - $\phi r_{nv} =$ Bolt shear strength
 - $e =$ Eccentricity
 - $s =$ Vertical bolt spacing

3.3.2 Forces

To find the shear capacity of a beam, the equation from AISC Specifications Section G2-1 was adapted. Shear strength is calculated by multiplying the web area by the yield strength of the material. In Section G2-1, this value is multiplied by 0.6. In the side intermeshed connection design, due to the conservative nature of the added shear plates, a factor of 0.6 was deemed appropriate. The shear demand on the shear plates has been assumed to approximately equal the shear capacity of the beam, and the force in each plate, r_u , is half of the total shear demand.

$$V_n = 0.6F_y A_w \quad [15]$$

V_n = total shear demand

The bolt shear strength may be found in AISC Table 7-1, but the bolt bearing strength must be obtained using Equation 16. Whichever one is more critical is used to find the total capacity of a vertical line of bolts.

$$\phi r_{nb} = 2.4\phi d_b t_w F_u \quad [16]$$

ϕr_{nb} = Bolt bearing strength

$\phi = 0.75$

d_b = bolt diameter

The bolts are designed for a single side of the connection, and both sides should be symmetrical. An initial value for the number of bolts on one side of the connection must be selected. One-half of the eccentricity, rounded up to the nearest inch, should be used to find the coefficient for eccentrically loaded bolt groups, C , in AISC Table 7-6. The value of C must be greater than C_{min} in Eq. [17]. ϕr_n for a single bolt is the minimum of the bolt bearing strength (ϕr_{nb}) and the bolt shear strength (ϕr_{nv}), and V_n is the force per plate. ϕr_{nv} is found in AISC Table 7-1.

$$C_{min} = \frac{V_n}{\min(\phi r_{nb}, \phi r_{nv})} \quad [17]$$

$$\phi r_{nt} = C * \min(\phi r_{nb}, \phi r_{nv}) \quad [18]$$

ϕr_{nt} = total capacity for a single vertical line of bolts

The value of ϕr_{nt} must be greater than the shear force per plate. The number of bolts must be increased if this is not true.

3.3.3 Shear Plate Design

The vertical bolt spacing, L_{ev} , L_{eh} , and eccentricity have been used to determine the width and length of each shear plate. Figure 3.6 demonstrates how plates are dimensioned using these parameters. The thickness of the plate must be selected during design, and if the plate cannot resist the loads, plate thickness should be increased. The plates must be checked for bolt bearing, flexural yielding, flexural rupture, shear yielding, shear rupture, and block shear. For each of these checks, the capacity calculated (ϕr_n or ϕM_u) must exceed the demand (r_u or M_u).

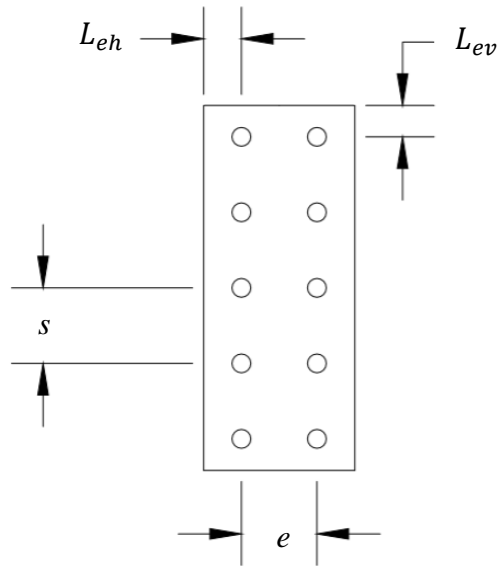


Figure 3.6: Shear plate geometry

a. Bolt Bearing

The bearing strength of a single plate is given by AISC J3-6a, and it is multiplied by the coefficient for eccentrically loaded bolt groups to give the total bolt bearing strength.

$$\phi r_n = C * 2.4d_b t_p F_u \quad [19]$$

ϕr_n = bolt bearing strength

t_p = plate thickness

b. Flexural Yielding

The applied moment due to shear force and eccentricity is given by Equation 20. The moment capacity of the plate is given by Equation 21.

$$M_u = R_u * \frac{e}{2} \quad [20]$$

R_u = Shear force on a single plate

$$\phi M_u = \phi F_y S_x \quad [21]$$

S_x = section modulus of the plate

c. Flexural Rupture

Equation 22 may be used to solve for the rupture capacity of the plate due to flexure.

$$\phi M_u = \phi F_u S_{net} \quad [22]$$

S_{net} = net section modulus of plate, taken from AISC Table 12-1 (1994 manual)

d. Shear Yielding

The yield strength of a steel plate may be calculated using Equation 23, which is from D2-1 in the AISC manual.

$$\phi r_n = \phi F_y A_g \quad [23]$$

A_g = gross area of shear plate

e. Shear Rupture

The rupture strength of a steel plate may be calculated using Equation 24, which is from D2-2 in the AISC manual.

$$\phi r_n = \phi F_u A_n \quad [24]$$

A_n = net area of plate

$$A_n = [l - n(d_b + 2g)]t \quad [25]$$

n = number of bolts

g = bolt hole tolerance 1/16"

f. Block Shear

Block shear should be checked, and it may be done so using AISC Tables 9-3a, 9-3b, and 9-3c. The final value is multiplied by two for the strength check since each side of the plate will have a column of bolts.

$$\phi r_n = \min[2(V_v + V_t)t, 2(V_v + V_r)t] \quad [26]$$

V_t = tension value from 9-3a

V_v = shear value from 9-3b

V_r = rupture value from 9-3c

CHAPTER FOUR

Laboratory Testing and Procedures

4.1 Experimental Program

The experimental program at the University of Minnesota aimed to investigate the performance of the side intermeshed connection and verify the design procedure described in Chapter 3. The program consisted of four tests (Table 1). One of the tests had the connection located in a pure bending moment region along the span of the beam, and the other three tests had the connection in locations that had combinations of bending moment and shear (Figure 4.7). A pure moment test was important since the angle connectors and flange teeth were designed for the sole purpose of resisting a pre-selected value of bending moment. Tests that included bending moment with shear were also imperative since in practice these connections would be placed in moment frames with shear forces. These loading scenarios were created by placing one or two point loads along the span of the beam.

Each connection was loaded about the major axis of bending of the beam sections to simulate the effect of gravity loads. Originally, minor axis tests were also considered to demonstrate the effects of lateral loading on the connection. However, ultimately minor axis tests were found to be of lesser importance for the testing program since the intermeshed connection was not envisioned for use in cases for which the beams resist lateral loads that produce minor axis bending.

Wide flange Grade 50 steel beams were used for the testing since these are most commonly used for the framing in a structure. The beam sizes, W18x46 and W21x57, were selected from sizes often used for beams and based upon engineering judgment. These beam sizes can be found in structural framing of buildings. Twelve-foot span lengths were chosen for the testing program for economical constraints. Beams that are significantly longer would be expensive and difficult to assemble in the laboratory, and, more importantly, realistic tests of the connection region do not require full-length beams. Table 1 contains the description of each test.

Table 1: Side Intermeshed Connection Test Specimens					
Series	Loading Description	Point Loads	Span (ft)	Design Moment (k-ft)	Rolled Shape
1	Pure bending	2	12	126	W18×46
2	Bending plus shear	1	12	126	W18×46
3	Bending plus shear	1	12	179	W21×57
4	Bending plus shear	2	12	179	W21×57

The W18x46 and W21x57 side intermeshed connections were both designed according to the procedure described in Chapter 3. Both W18x46 specimens were nominally identical, as were the two W21x57 specimens. The W18x46 beam included 2½ x 2 x 3/8 angles, and the W21x57 included 3 x 2 x 3/8 angles. Once the specimens were designed, design (AutoCAD) drawings were created and sent to the selected fabricators. Additional information about the connection design, including calculations and dimensioned AutoCAD drawings, are included in Appendix A.

4.2 Fabrication

Local and regional fabricators were contacted to investigate the feasibility of fabricating the beams, angles, and plates for the side intermeshed connection. Due to the nature of this experiment, it was imperative to ensure that the fabricators chosen had the capabilities to cut the specimens with either high-definition plasma or water jet, while guaranteeing adequate precision. Grunau Metals of Oak Creek, WI, was selected to fabricate the beams and plates. Grunau Metals used a Python X Robotic CNC Plasma Cutting System for their fabrication. The plasma cutting of one of the beam specimens is shown in Figure 4.1. Grunau was originally selected to fabricate the side angles as well, but they could not guarantee that the circular cuts at hole corners could be cut with the necessary precision using the plasma cutter. Am-Tec Designs of Scandia, MN, was selected to fabricate the angles. Am-Tec used an OMAX A-Jet water jet cutting machine to cut the angles. The water jet cutting of one of the angles is shown in Figure 4.2.



Figure 4.1: Plasma cutting



Figure 4.2: Water jet cutting

Once the specimens arrived in the lab, they were measured with calipers to check the accuracy of the fabrication. On the beams, every tooth was measured and found to be well within the specified tolerance value of a one-sixteenth of an inch. Every hole on every angle was also measured. Both the width and the height of each hole was found to be well within the tolerance value. The measurements verified that both plasma cutting and water jet cutting are acceptable for this type of connection. The measurements of the specimens are included in Appendix A.

Mill test certificates were received from both fabricators, and the pertinent details of each mill test certificate are included in Table 2. The values in the table are averaged values from multiple pieces. The mill certificate documents are included in Appendix A. It is interesting to note that the angles and shear plates, cut from A36 steel, had actual yield stresses comparable to that for which the wide flange sections were cut from Grade 50 steel. It is also of interest to note that both steel grades had similar elongations, with values that exceeded 25%.

Item	Yield Strength (ksi)	Tensile Strength (ksi)	Gage Length (in)	% Elongation
W18x46	52.7	68.6	8	27.85
W21x57	55.02	72.13	8	25.4
L2½ x 2 x 3/8	58.6	75.3	8	26.65
L3 x 2 x 3/8	51.95	72.65	8	27.5
Shear Plate	53.2	74.7	8	27.5

4.3 Testing Setup and Loading

The experimental program was conducted at the University of Minnesota’s Theodore V. Galambos Structural Engineering Laboratory. An MTS 600-kip load frame located in the Galambos Lab floor was selected as the loading mechanism. The beams were simply supported with various loading schemes. To create a pure bending moment scenario, a load distribution beam was attached to the load frame to apply two point loads to the

beam being tested (Figure 4.3). When only one point load was applied, moment and shear forces both existed at any given location along the span. The location of the connection was changed, thus creating slightly different ratios of moment to shear (Figures 4.4-4.6). In the first two tests, the connection was placed at center-span, producing a moment to shear ratio of approximately 6 in Test 2. In the final two tests, the connection was placed near one of the end supports, producing a moment to shear ratio of 2.

Stiffeners were welded to the beams by the fabricator at the point load locations, and they were also added at the end reaction locations. Calculations performed to size the stiffeners are shown in Appendix B. A 3D visualization of Test 1, the pure moment test, is shown in Figure 4.3. Figures 4.4 – 4.6 show a 3D visualization of the tests that created both moment and shear at the connection. Figure 4.7 is a dimensioned 2D drawing showing the locations of the connections and loads.

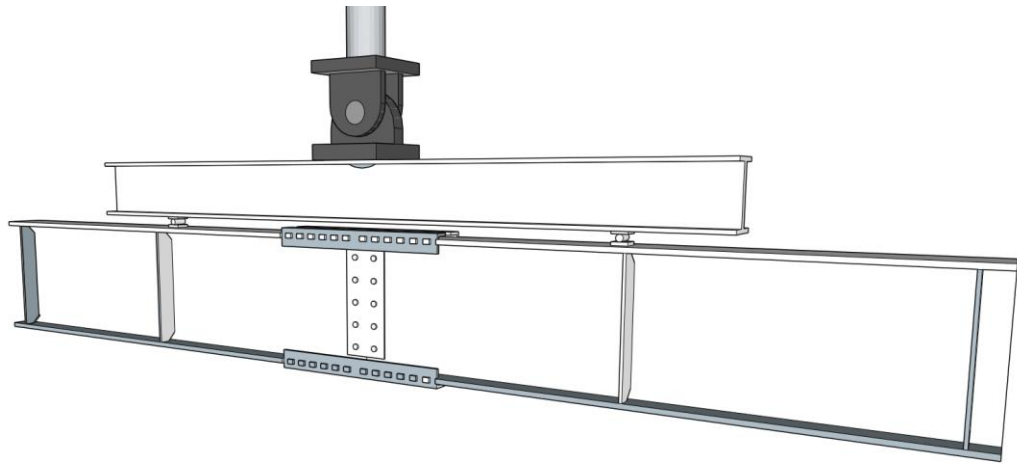


Figure 4.3: Test 1 loading

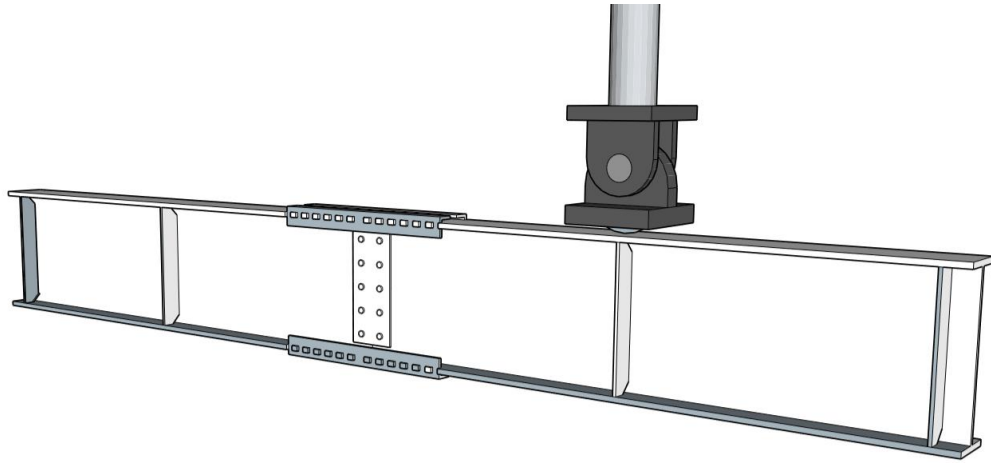


Figure 4.4: Test 2 loading

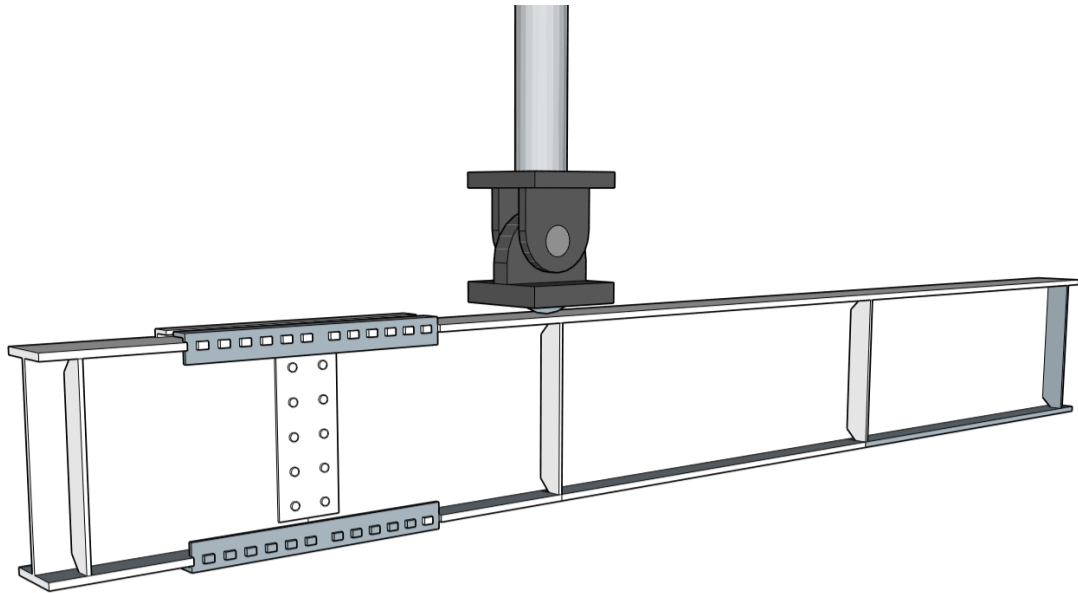


Figure 4.5: Test 3 loading

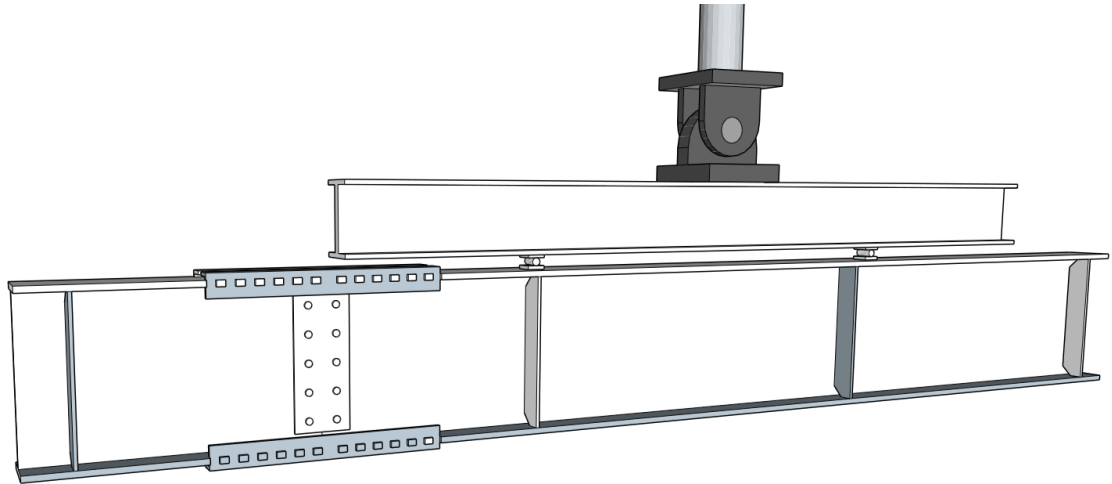


Figure 4.6: Test 4 loading

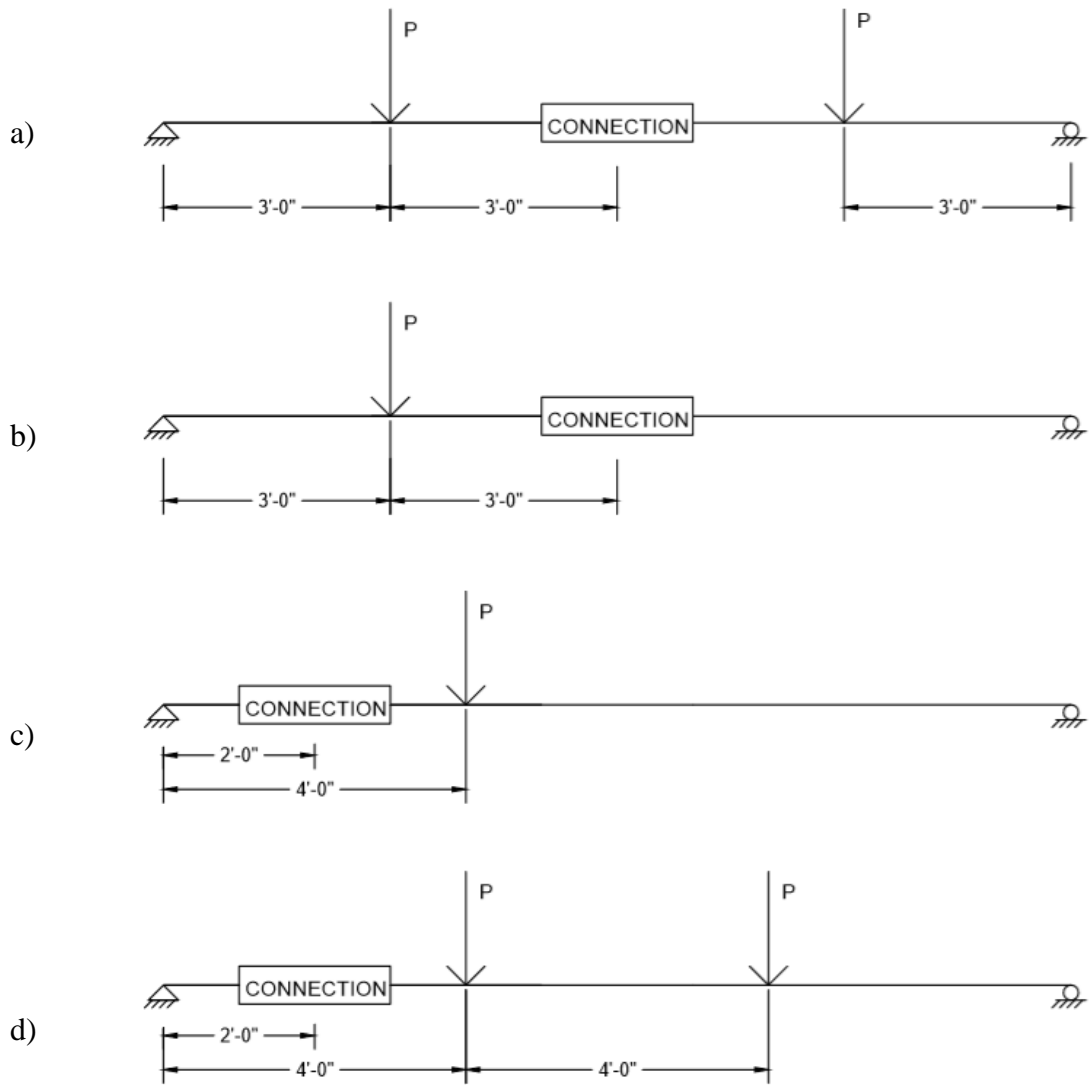


Figure 4.7: Loading locations for a) Test 1; b) Test 2 ; c) Test 3; and d) Test 4

To avoid unwanted lateral deflections in the beams, bracing was added to the sides of the test specimen. Bracing is commonly designed using the “two percent rule” (Winter, 1960), which means bracing should be able to resist at least two percent of the compressive load in the member it is restraining. In this case, the member being restrained is the compression flange. Calculations, included in Appendix B, show that

the bracing needed to resist lateral deflection, thus justifying the construction of the bracing system.

The bracing design was modified as the program progressed from one test to the next due to the need for additional lateral restraint. The bracing plan used in the first test (Figure 4.8) consisted of a light gage built-up steel section (EFCO) attached to two floor beams placed parallel to the test specimen. Two wide flange support beams were also clamped to the floor beams to provide support for the test specimen. Four three-foot-long EFCO steel members were attached vertically on top of the steel floor beams. Two ¾” diameter rods were then attached to each of the EFCO members, and 3 x 3 x ¼” steel angles were attached to the ends of the rods. The angles contacted the flanges of the beams. All components used for this bracing were readily available in the Galambos Lab, and they are listed in Table 3. The bracing setup is depicted in a 3D visual representation (Figure 4.8). The revised bracing details for the subsequent tests are included in Chapter 5 following the presentation of the results of Test 1.

Table 3: Bracing Components			
Item	Description	Quantity	Size
Floor beams	Support beams clamped to these	2	W14
Support beams	Support the test specimen	2	W14
Vertical bracing supports	EFCO members	4	Three foot members
Bracing rods	Attach to EFCO and support angles	8	¾” rods, ~30” in length
Bracing angles	3 x 3 x ¼” size angles	4	Extend along the depth of the beam

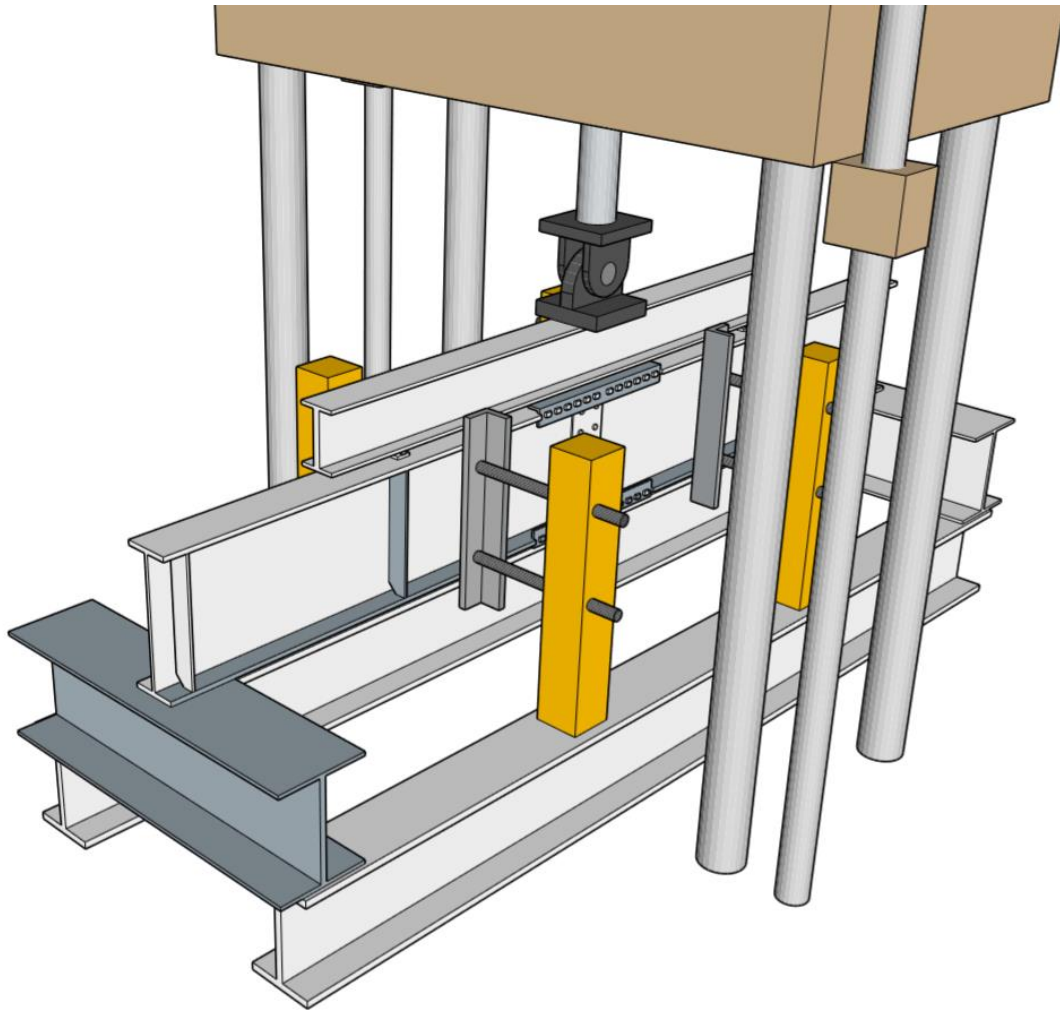


Figure 4.8: Bracing setup

Although the connections were designed to resist a specific load under major axis bending, they were tested beyond this load to a peak load. Since angle rupture controlled failure in the design procedure, the force capacity of the angle, F , was calculated by multiplying rupture strength by effective area. This value was then multiplied by two since there are two angles resisting rupture, as shown in Equation 27.

$$F = 2F_u A_e R_t \quad [27]$$

The value of moment at failure could be calculated by using Equation 28. The couple forces between the top and bottom angle legs were used to calculate the moment. The value for distance, d_r , was taken as the distance between the center of the horizontal legs of the top and bottom angles. Equation 29 was used to calculate d_r , in which the dimensions C and t_f are defined in Figure 3.1.

$$M = Fd_r \quad [28]$$

$$d_r = d + 2C + t_f \quad [29]$$

Once the failure moment was estimated, principles of statics were used to obtain the load, P , that was expected to occur at failure. The calculations are included in Appendix C, and the maximum expected loads are tabulated in Table 4.

Table 4: Anticipated Forces at Failure					
Series	Shape	Load P (k)	# of Point Loads	Shear (k)	Moment (k-ft)
1	W18x46	75	2	0	226
2	W18x46	151	1	38	226
3	W21x57	225	1	150	300
4	W21x57	150	2	150	300

4.4 Testing Considerations

A locking mechanism to prevent the angles from slipping out, thus causing a premature failure, was considered for the testing. The slip out force of the angles relative to the beams was estimated as two percent of the buckling force because of the two-percent rule for lateral restraint, and it was then compared to the frictional resistance from bearing contact. This bearing contact surface is where the flange teeth meet the inside surface of the angle holes. No excess deformation was predicted to occur at the hole due to bearing contact, and this check is included in Appendix B. The frictional resistance of the teeth at

the angle holes exceeded the slip out force, so no extra restraint was deemed necessary. Calculations are included in Appendix B.

Despite the high frictional resistance, a mechanism to prevent movement of the angles was deemed best practice for the testing program. Assumptions made about the behavior of the angles may not be entirely accurate, so a simple restraint system was created. Additionally, this restraint was also conceived as a means to determine the magnitude of the restraint forces needed to keep the angles from slipping out of the flange teeth and bending away from the beams. Four $\frac{3}{4}$ " strips of a C7x9.8 steel channel were placed above and below the angles to hold them in place, and the setup was kept in place with vertical steel members. This scheme is shown in Figure 4.9. Although steel washers were packed between the interior surfaces of the legs of the restraint channels and the exterior faces of the vertical legs of the side angles, small movements were still allowed by this restraint system. However, it prevented the angles from moving excessively and slipping off the flanges. One strain gage was placed on the top and bottom of the web of the channels. The configuration of this restraint system was intended purely for the testing program, and the development of an alternative long-term solution is proposed Chapter 7.

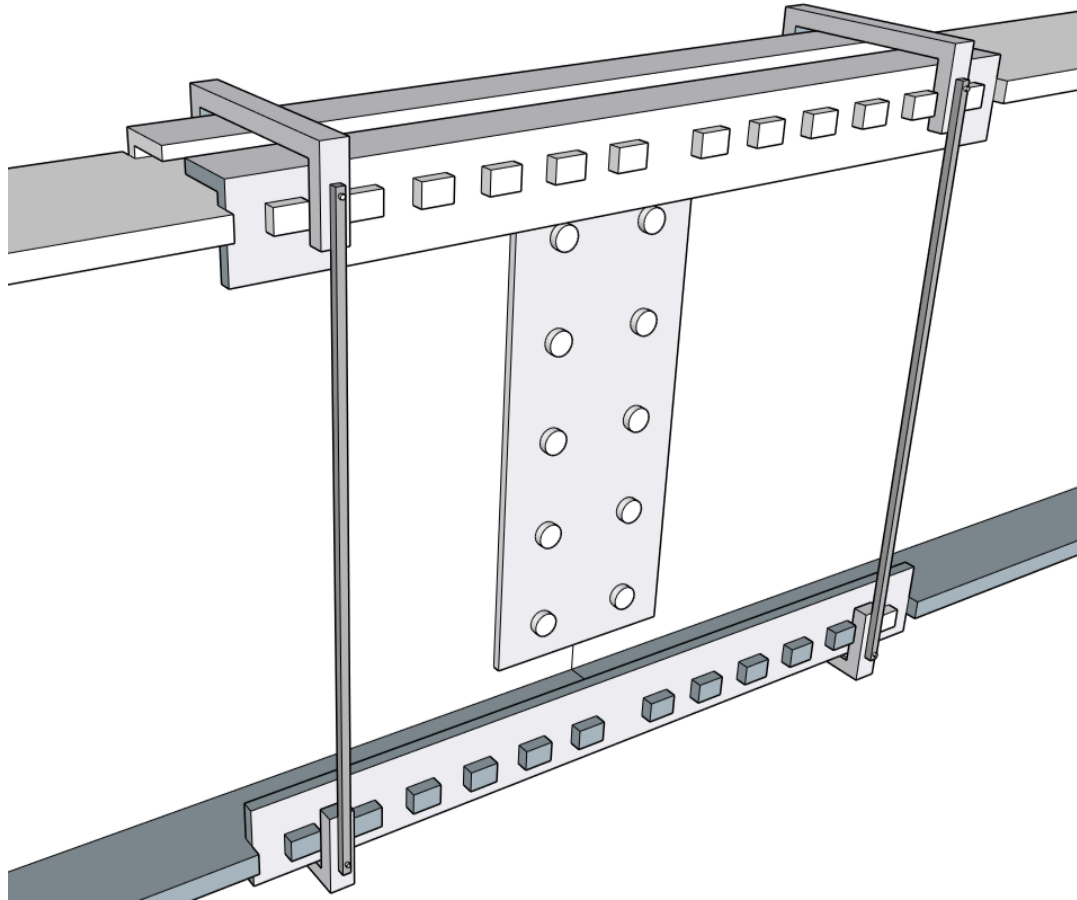


Figure 4.9: Channel restraints

The maximum expected deflections at failure were also estimated. First, the theoretical maximum deflection for each beam was calculated as if there was no splice along the span. Then, the maximum amount of vertical deflection due to vertical tolerances at the holes was added. Finally, since the beams could also slip apart horizontally due to tolerances at the holes, there could be additional vertical deflection associated with horizontal movement. Each beam was estimated to deflect up to roughly 1.5 inches for the maximum expected vertical loads given in Table 4, and calculations are included in Appendix C. Larger deflections were possible due to plasticity of the specimen and the potential for higher failure loads than estimated.

Reuse of beams after the initial testing program was considered viable. Although angles were not to be reused since they would be tested to failure, the beams were not expected to experience large permanent deformations. Therefore, additional angles could theoretically be attached to the beam sections to run additional tests in the future. To avoid retesting the same flange teeth that may have already experienced high stresses, each section of the test specimen could be reversed 180 degrees so that new flange teeth could be tested. Figure 4.10 shows the test specimen with identical flange teeth cut into both ends.

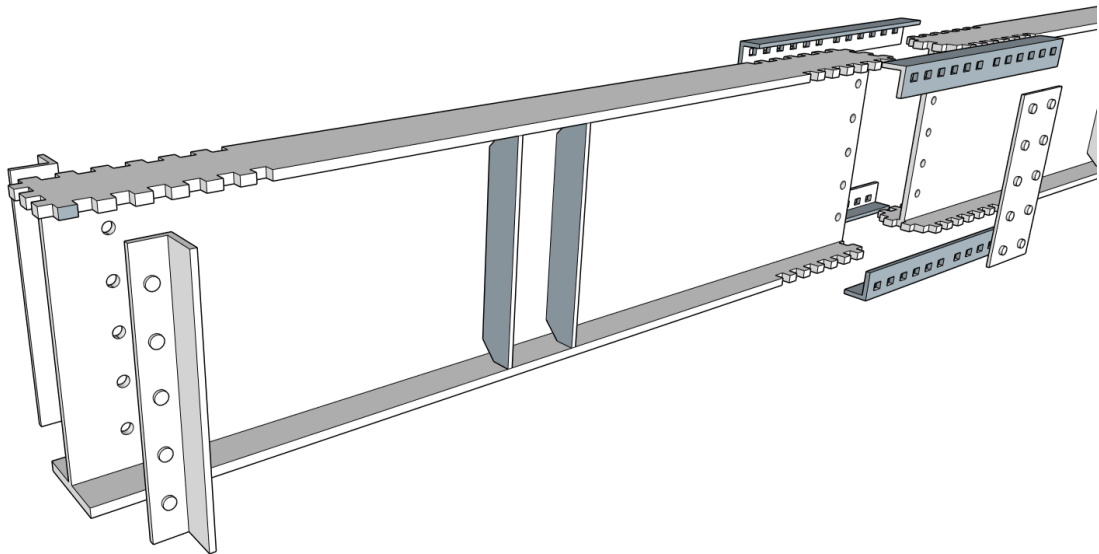


Figure 4.10: Beam end view

Angles were attached with A325 steel bolts to the ends of the beams to act as stiffeners when reusing beams. Angles were selected because they could easily be attached and removed. The holes used to bolt the angles to the beam end were identical to the holes used at the connection for the shear plates. In this way, the connection could be assembled the exact same way no matter which direction the section was facing.

Additional transverse stiffeners were also added to ensure there would always be a stiffener directly under point loads (Figure 4.10).

4.5 Instrumentation Plan

Each test required instrumentation to measure strains and displacements. The instruments consisted of strain gages, strain gage rosettes, string potentiometers, and Linear Variable Differential Transformers (LVDTs). The strain gages measured strain in one direction, and the rosettes measured strain at angles of zero, forty-five, and ninety degrees with respect to a pre-selected direction (usually the direction of the longitudinal axis of the beams). String potentiometers and LVDTs were used to measure displacements. Strain gages and rosettes were ordered from Texas Measurements (College Station, Texas), and string potentiometers and LVDTs from the University of Minnesota’s MAST Laboratory were calibrated for reuse. LVDTs with a range of +/- 1.0 inch were used on the beams, and smaller LVDTs with a range of +/- 0.1 inches were used on the angles. Table 5 lists the measurement devices used as instrumentation. In addition to these devices, the internal LVDT and load cell within the load frame also generated signals that were recorded along with those for the instruments described above.

Table 5: Instrumentation Devices		
Item	Supplier	Type
Strain Gage	Texas Measurements	FLA-3-11-3LJCT
Strain Gage Rosette	Texas Measurements	FRAB-3-11-3LJBT
LVDT (Large)	Macro Sensors	S01250-1000
LVDT (Small)	Macro Sensors	PRH 812 100
LVDT Conditioner	Schaevitz Sensors	ATA 2001
String Potentiometer	TE Connectivity	Classic String Pot Series

Additional materials were required for instrumentation installment. When applied to steel surfaces, strain gages were applied to surfaces that had been smoothed, sanded, and cleaned. A grinder, sandpaper, and acetone were used to accomplish this. Cyanoacrylate adhesive, obtained from Texas Measurements, was used to attach the

strain gages to the steel surfaces. The gages were then protected by a layer of strong bond (SB) tape and covered with an aluminum adhesive located in the Galambos Laboratory. Mounting bases and plastic twist ties were used to relieve wire stress and organize the wiring. LVDTs were attached with discharge capacitor stud welds or clamps.

4.5.1 Instrument Locations

Identical instrumentation was initially intended for each test, but the instrumentation was slightly modified as testing progressed and data was collected and reviewed. The instrumentation locations for Test 1 are presented in this section, and the revisions are given following the results of Test 1 in Chapter 5.

The beams had strain gages installed on the flanges as well as the web. Strain gages were attached on the bottom flange of the beam along the length of the connection. Finite element analysis performed by UCD produced the stress distribution shown in Figure 4.11.

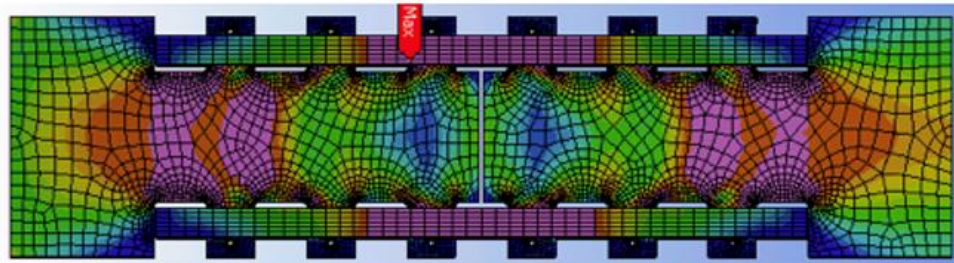


Figure 4.11: Finite element beam flange stresses

The UCD model showed the stresses radiating out from the teeth towards the center of the flange at roughly a forty-five-degree angle. Because of these results, the strain gages on the flange were placed in the center at approximately forty-five-degrees from each tooth. To understand the stress state in the beam, strain gages were also

located outside of the connection region on the top and bottom flanges, and a rosette was located at the center of the web as well.

The same finite element model from UCD demonstrated the distribution of angle stresses. Starting from the outside ends of an angle, the stresses built up from each additional tooth until the center of the angle was reached. Therefore, stresses were always highest around the center two holes in the angle, and rupture would occur in this location. The high stress concentration at the center of the angle is shown in Figure 4.12, which was taken from UCD's finite element analysis.

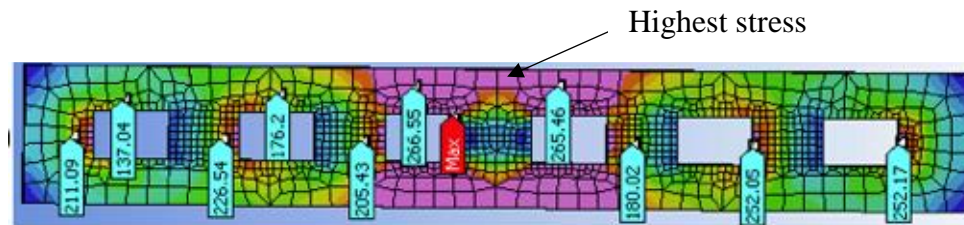


Figure 4.12: Finite element angle stresses

Since the maximum stresses and strains that occurred in the angle were towards the center in the finite element model, all instrumentation was placed at the center of the angle. Strain gages were placed on the inside and outside of each leg of the angles.

LVDTs were located on the tension flange of the beam and the tension angles. Two LVDTs on the beam measured the separation between the tension flanges. The other two beam LVDTs measured vertical displacement by recording the change in distance between the bottom flange and the floor below. On each tension angle, one LVDT was located under each of the two centermost holes.

Images of the instrumentation for angles, shear plates, and beams are shown in Figures 4.13 – 4.19. Squares denote strain gages, circles denote rosettes, and rectangles denote LVDTs.

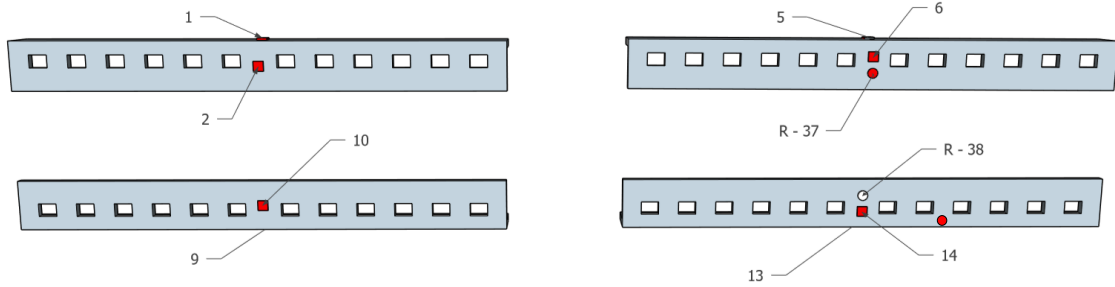


Figure 4.13: Outer angle instrumentation

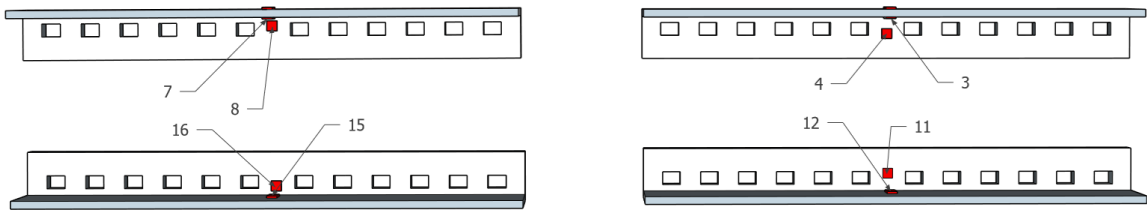


Figure 4.14: Inner angle instrumentation

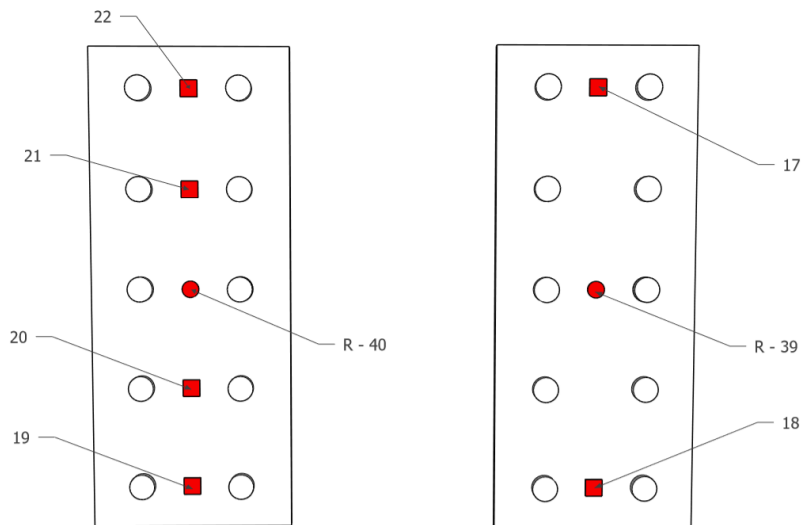


Figure 4.15: Shear plate instrumentation

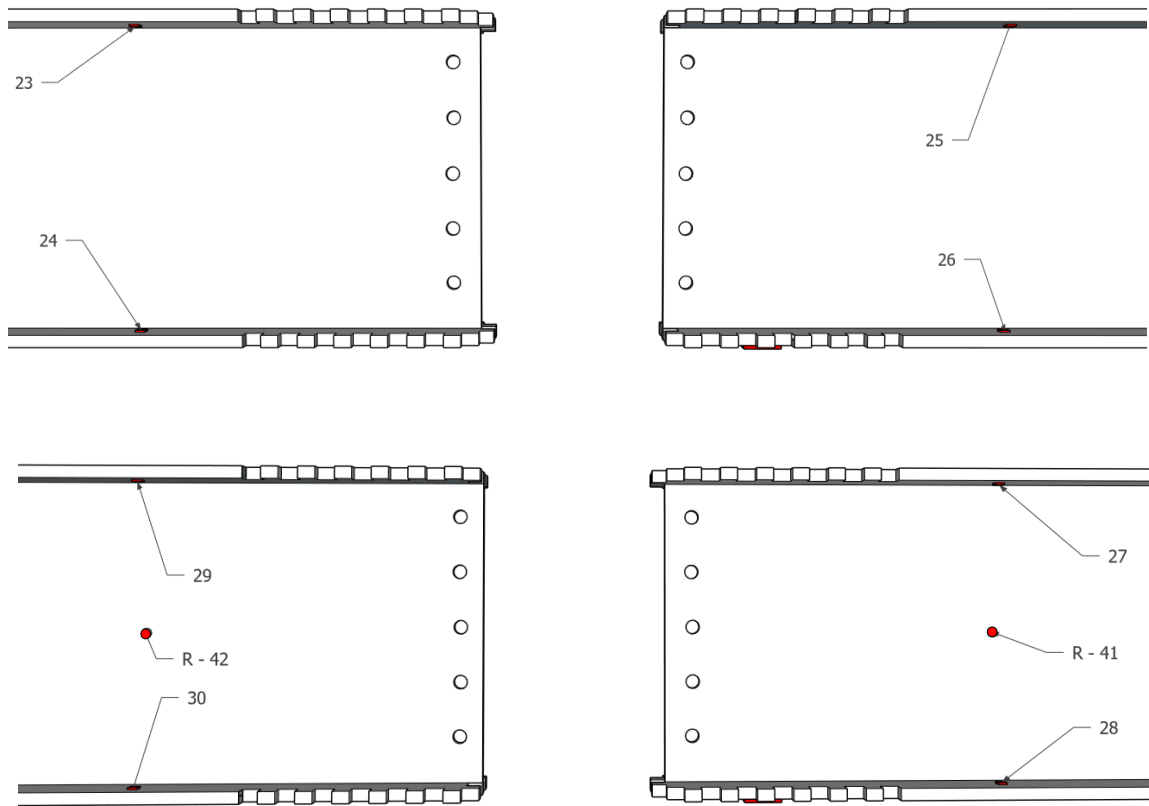


Figure 4.16: Beam instrumentation side view

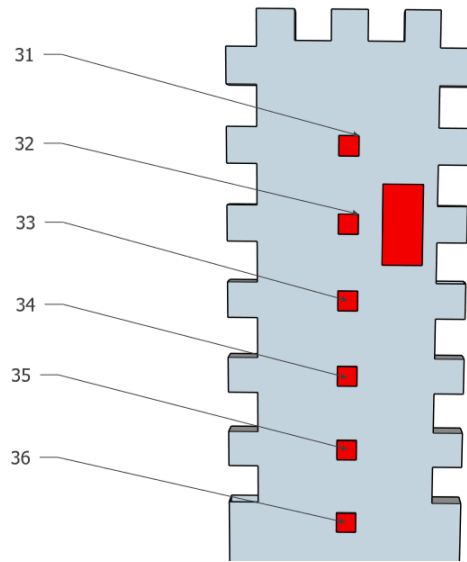


Figure 4.17: Beam bottom flange instrumentation

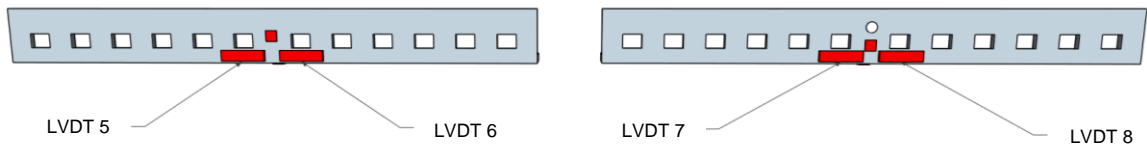


Figure 4.18: LVDTs on tension angles

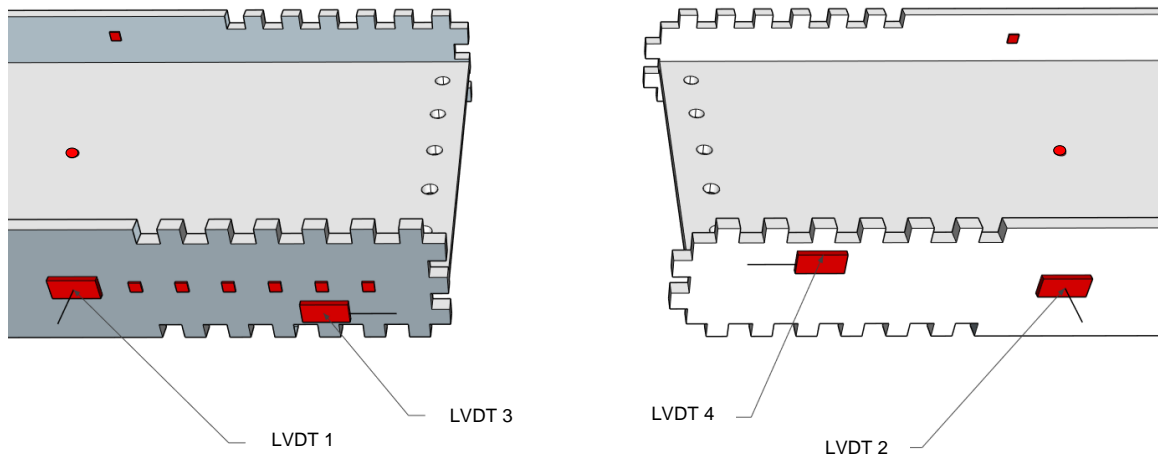


Figure 4.19: LVDTs on tension flange

4.6 Assembly Procedures

The testing setup was constructed in the Galambos Lab. Clamps were used to attach the vertical EFCO members to the beams below, and clamps were also used to secure the support beam. The bracing rods were placed in the EFCO, and the bracing angles were cut and drilled. Figures 4.20 and 4.21 show the bracing setup, and the wood members shown were temporarily in place of the angles before the angles were drilled.



Figure 4.20: Bracing with temporary wood braces



Figure 4.21: Bracing viewed from above

The specimens were delivered with one shear plate attached and one unattached. The second shear plate was bolted before moving the beam. The test specimen was lowered using the gantry crane in the Galambos Lab and placed on rollers, and then the temporary wood bracing members were moved into contact with the beam flanges. With nearly the entire test setup in place, the crane was used to move the entire arrangement on to small dollies which were used, in turn, to roll the entire assembly underneath the load frame. The instrumented beam in the testing setup is pictured in Figure 4.22, and Figure 4.23 shows the entire arrangement being moved with crane.



Figure 4.22: Test beam with temporary wood bracing



Figure 4.23: Test setup being moved with the crane



Figure 4.24: Bracing with steel angles in place

Before LVDTs were attached, whitewash consisting of a mixture of lime and water was added to beam webs and angles. The whitewash was used to demonstrate yielding of the specimen. The angle LVDTs are pictured in Figure 4.25.



Figure 4.25: LVDT attachment to tension angle

The spreader beam was lowered onto the test specimen, and the entire setup was rolled underneath the load frame. The spreader beam was clamped onto the load frame, and the dollies were removed. All wiring was attached, and working channels were verified in the data acquisition system.

CHAPTER FIVE

Test Results

5.1 Test 1 Results

The first beam test was a pure bending moment test of a W18x46 steel wide-flange beam, and it was conducted in four separate stages using a displacement-controlled protocol. Loading was paused in each stage for photographs and visual inspection of the connection. The first three stages were conducted to examine beam behavior under load checkpoints that were deemed significant, as noted in Table 6. Deflections during the third stage caused the load distribution beam to interfere with and transfer some load to the bracing. The bracing was adjusted to avoid this interference, and then the fourth stage of testing was conducted. Table 6 describes each stage of testing.

Stage	Maximum Load	Load Pauses	Comments
1	28 k	None	1/3 design load
2	56 k	28 k	2/3 design load
3	200 k	84 k 126 k	Pauses at design load (84 k) and the estimated failure load (126 k). Beam unloaded at approximately 200 k to adjust bracing.
4	225 k	None	Peak load reached at lateral torsional buckling

The figures presented in this section show LVDT and strain gage data for each of the four tests combined in single plots. Some strain gages and strain gage rosettes did not measure data or did not record strains accurately, and these were omitted from the results. Where gages were located on both sides of a cross section, such as on the angles, strains were decomposed into axial and flexural components based upon superposition of linear, elastic stresses (Appendix D).

5.1.1 Test 1 Displacement Data

The following plots, Figures 5.1.1 – 5.1.3, present the data recorded from LVDTs. The sequence of loading and unloading for each of the four stages is clearly demonstrated in the peaks and valleys of the load vs. displacement plots. Increasing displacements were measured at relatively low loads at the beginning of stage one due to the shear plate bolts slipping into place and engaging with the plate, and this is labeled as initial seating in Figure 5.1.1. In each plot, elastic behavior is observed when the slope of the line is linear. The initiation of global yielding in the load-deflection diagram is observed when the linear region of the curve changes slope and flattens. This indicates that plasticity was experienced in at least one element of the connection. After yielding has occurred in an element, the unloading of the specimen is represented as a line that decreases to zero load but includes a residual displacement. When the beam is then reloaded, it follows approximately the same curve as unloading until it reaches a load that had not previously been reached. The curves are labeled in Figure 5.1.1.

The vertical LVDT displacement is closely correlated with the horizontal LVDT displacement (Figures 5.1.1 and 5.1.2). Each plot displays curves that follow the same pattern. Based upon these plots, it may be concluded that horizontal displacement was directly correlated to vertical displacement. Some of the displacements in the LVDT data were due to the closing of tolerances at bolt holes and angle holes. The bolts were audibly slipping into contact with the plate and beam web, and the flange teeth were observed gradually moving into bearing contact with the angle holes when this was happening. The beam flanges at the top moved closer together, and the flanges at the bottom moved farther apart.

The angle LVDT data recorded one brief period in which the angles were carrying load asymmetrically (Figure 5.1.3). LVDT 5 measured a reduction in displacement near its yield point, and at this point the adjacent LVDT 6 recorded an increase in displacement. The displacement reduction measured in LVDT 5 appears to be from a brief period when the opposite side of the angle carried more load. This irregularity was short-lived, and the LVDTs once again recorded symmetrical displacements soon after.

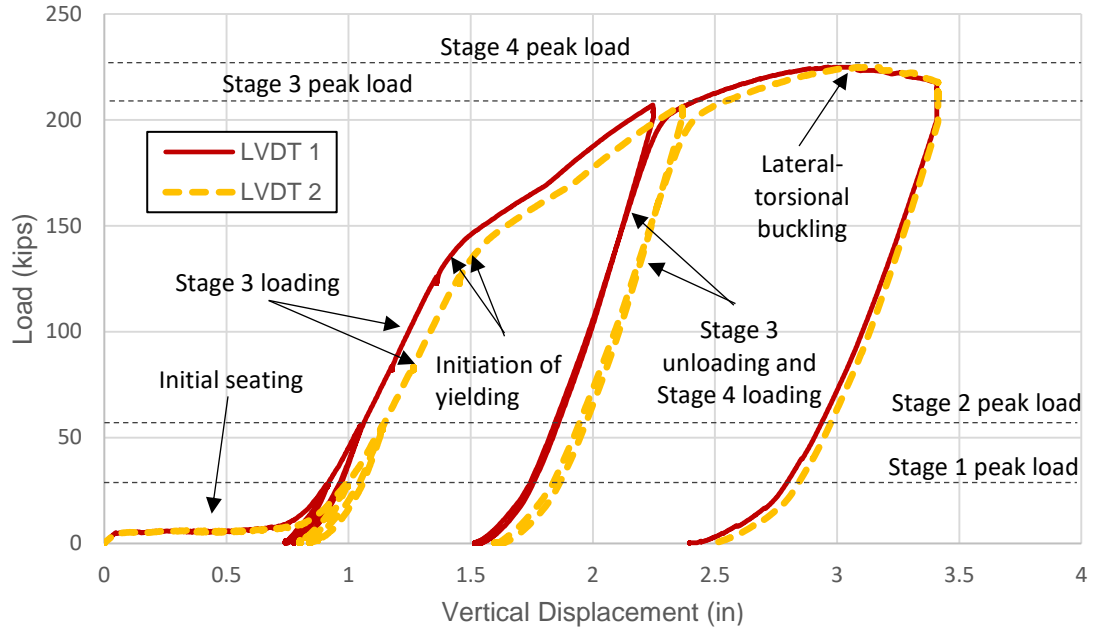


Figure 5.1.1: Test 1 total load vs. vertical LVDT displacement

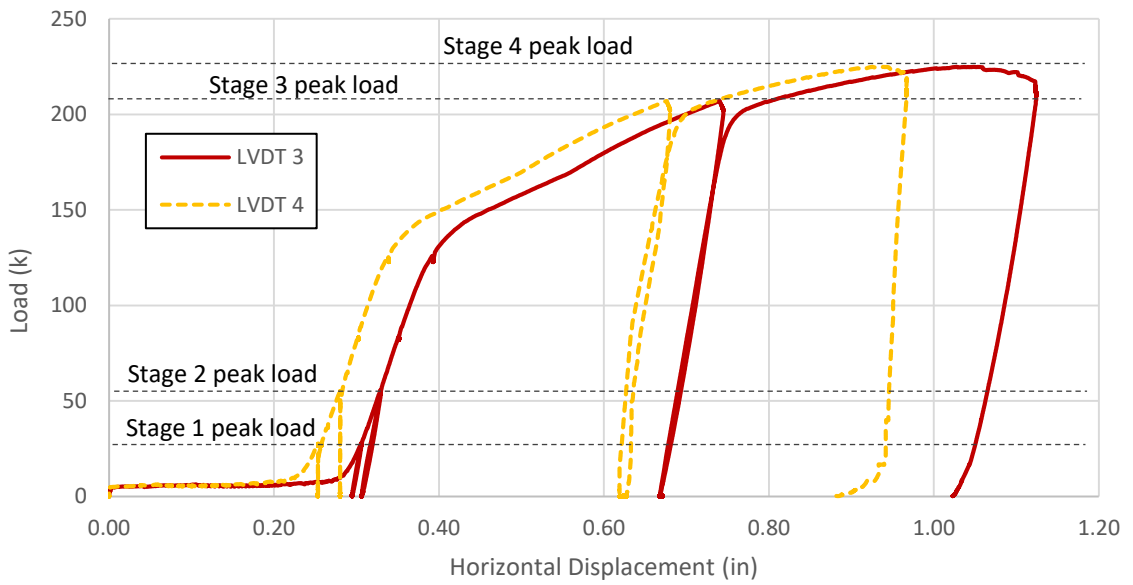


Figure 5.1.2: Test 1 total vertical load vs. horizontal LVDT displacement

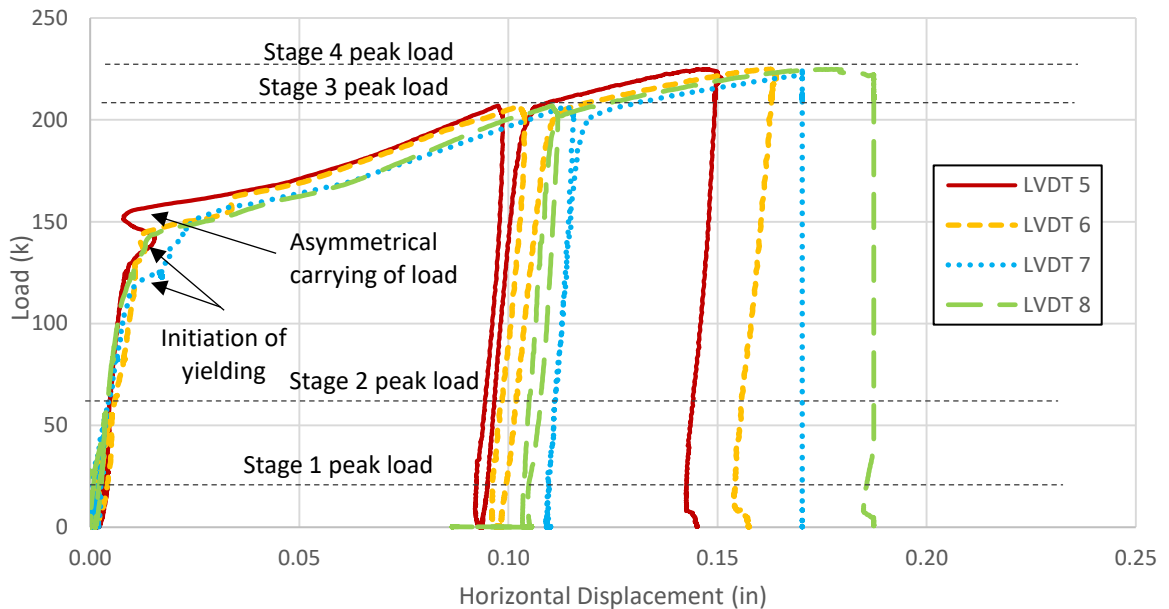


Figure 5.1.3: Test 1 total vertical load vs. angle LVDT displacement

5.1.2 Test 1 Strain Data

Load vs. axial strain data is presented in Figures 5.1.4 – 5.1.8. During the first two stages of loading, all elements in the connection behaved elastically. All strain measurements returned to approximately zero after unloading. Higher strain measurements were recorded once contact was established.

Inelastic behavior was first observed in the third stage of loading, and it started in the angles at about 125 kips of load. Yielding was recorded in the compression angles (Figure 5.1.4), but smaller strains were recorded in the tension angles due to strain gage placement in the center of the angle instead of the section over the first hole (Figure 5.1.5). The tension angle LVDTs recorded elongation of the centermost holes corresponding to approximately 20% strain (Figure 5.1.3), but the tension angle strain gages failed to record this elongation.

After the beam was unloaded during the third stage, residual strains existed in the angles and bottom beam flange (Figures 5.1.5 - 5.1.7). The shear plate instruments

measured no plasticity, and the plots have been excluded due to unreliable data from those strain gages. During the fourth stage, a maximum load of 225 kips was recorded, and the specimen underwent lateral torsional buckling. The angles in compression were forced to bend out-of-plane due to lateral torsional buckling, and this behavior was recorded near the peak load in Figure 5.1.4. The various connection elements continued to deform inelastically after the peak load was reached, and the test was stopped.

Two strain gages on the beam compression flange recorded inelastic behavior, as did three gages at the center of the bottom flange (Figure 5.1.6 and 5.1.7). The gages on the bottom flange were located beneath the beam web in the connection region, as indicated in Figure 4.17. The gages located farthest from the connection centerline recorded the highest strains (Figure 5.1.7). This behavior was consistent with the predictions made in finite element analysis for the distribution of forces in the flange.

The strain data recorded on the channels is in Figure 5.1.8, and one channel recorded unreliable data that was omitted. The channels recorded strains that were either positive or negative depending on their placement at the top or bottom channels. The axial strains were used to approximate the stress and lateral force acting on the channel. The maximum stress calculated was 11.6 ksi, and the maximum force calculated was 1.8 kips.

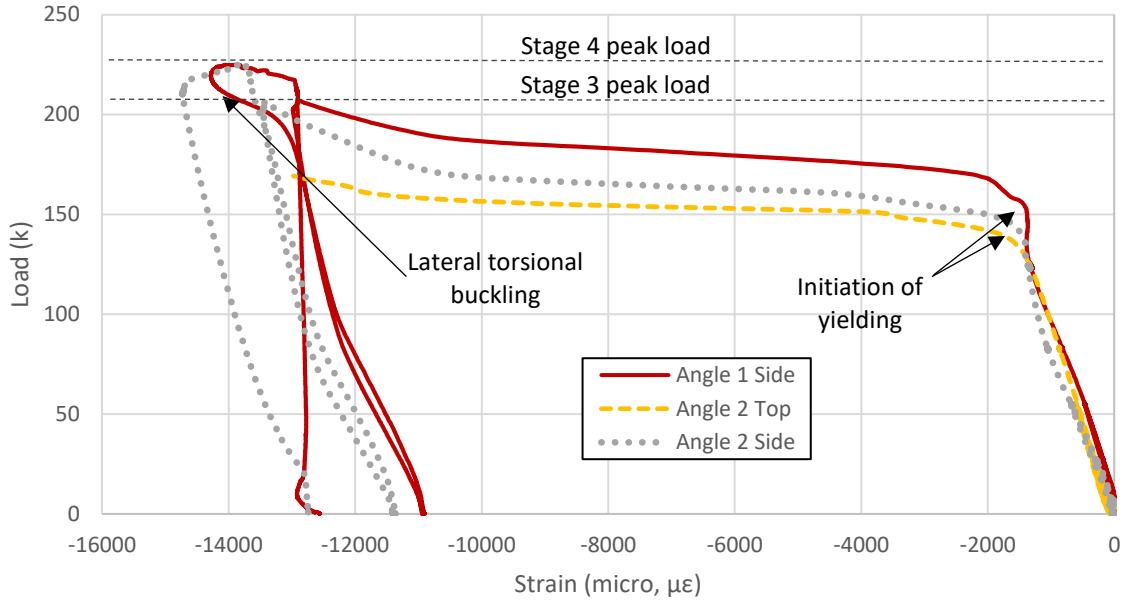


Figure 5.1.4: Test 1 load vs. compressive angle axial strain

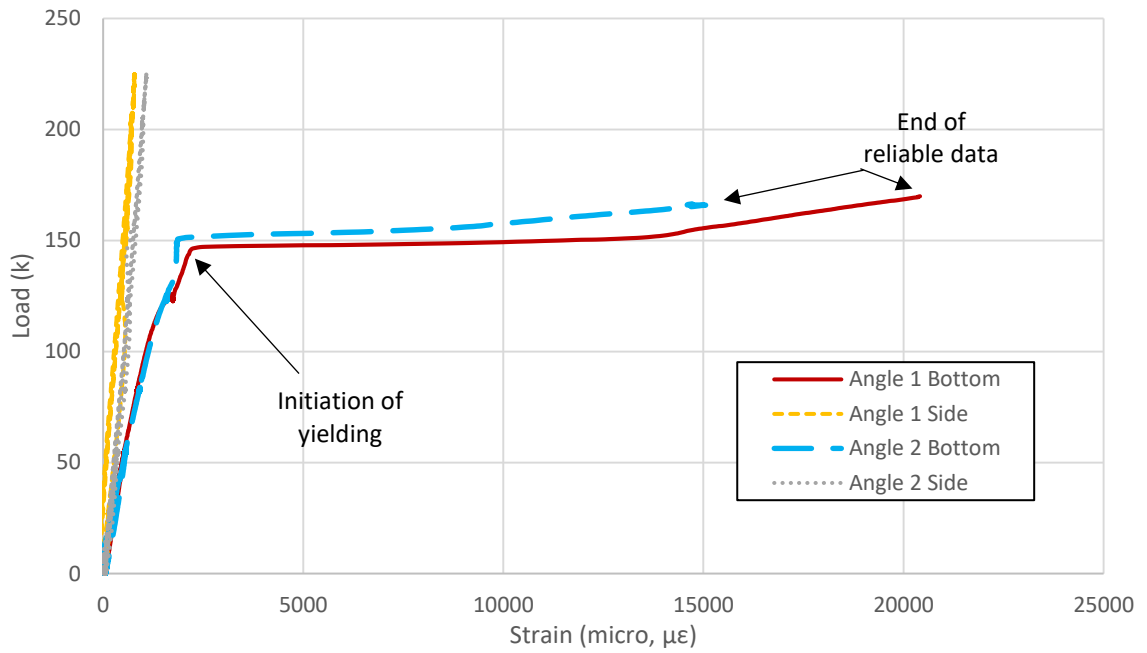


Figure 5.1.5: Test 1 load vs. tensile angle axial strain

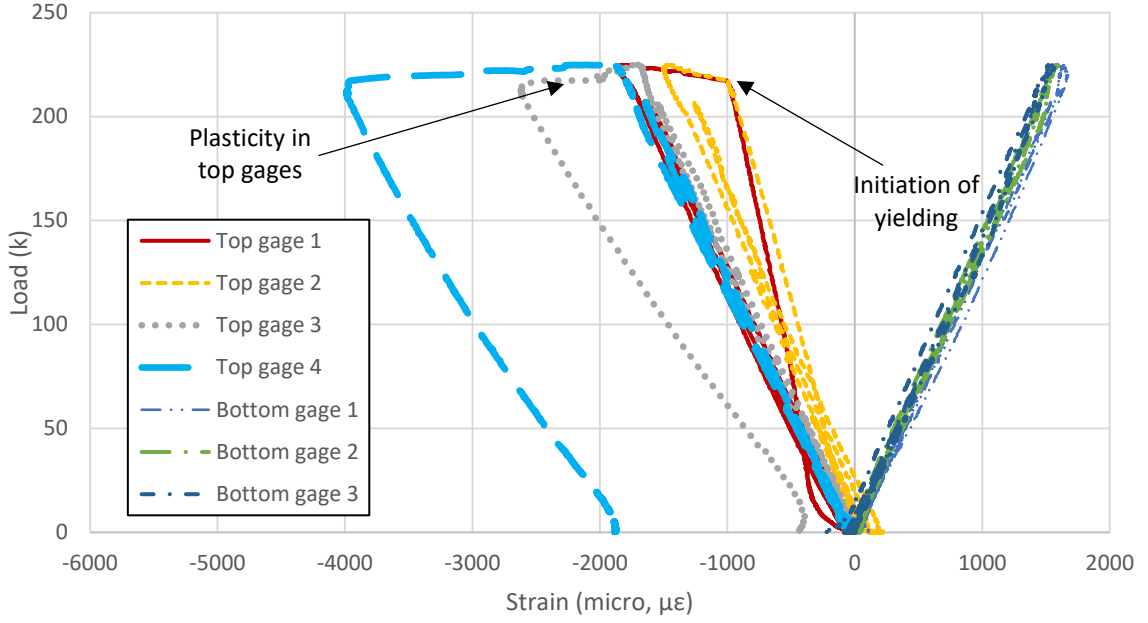


Figure 5.1.6 Test 1 load vs. flange strain

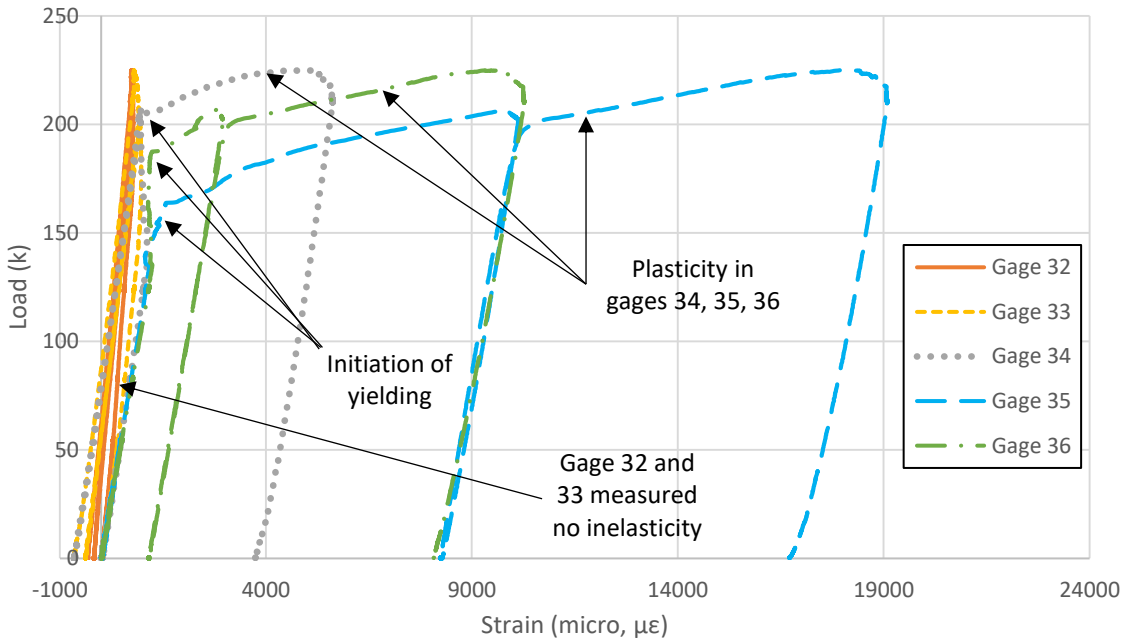


Figure 5.1.7: Test 1 load vs. beam bottom flange strain

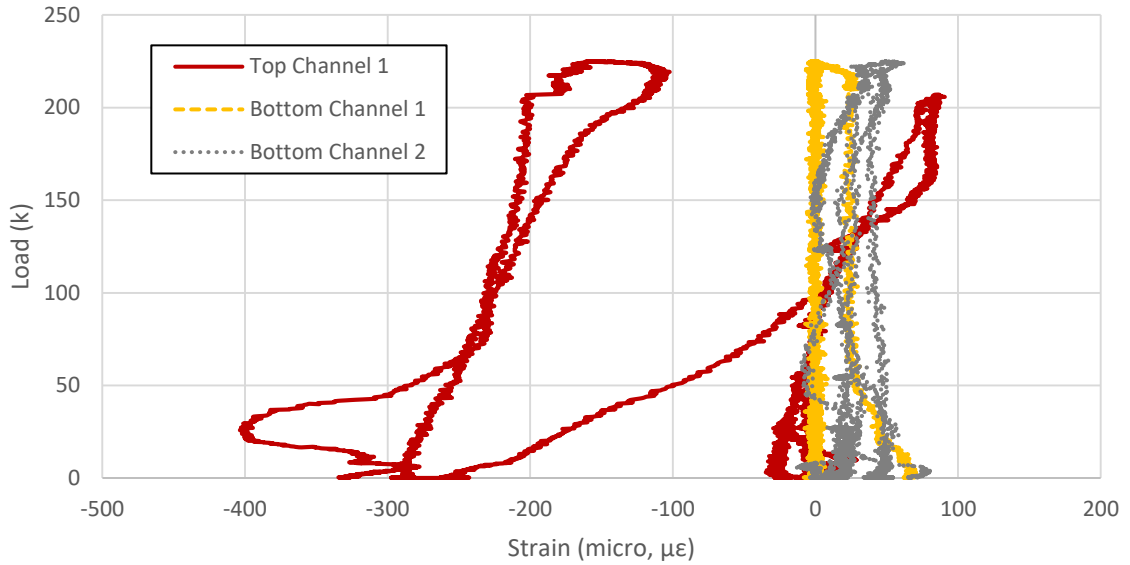


Figure 5.1.8: Test 1 load vs. channel axial strain

5.1.3 Test 1 Discussion

The beam and connection responded to vertical loading that produced constant moment in the manner that was expected, at least initially. However, the magnitude of deflection needed to fully engage the connection, about 0.75 inches, was much larger than expected. Once the flange teeth and the shear plate bolts had made contact with the corresponding surface in the angles and the beam webs, the connection generated internal resistance to offset the applied loads. Figure 5.1.9 shows images of the connection before and after loading. In the post-loading image, the teeth in compression have moved closer together, and the teeth in tension have moved farther apart. Figure 5.1.10 contains images that show how the centermost holes in tensile angles deformed in comparison to the other holes.

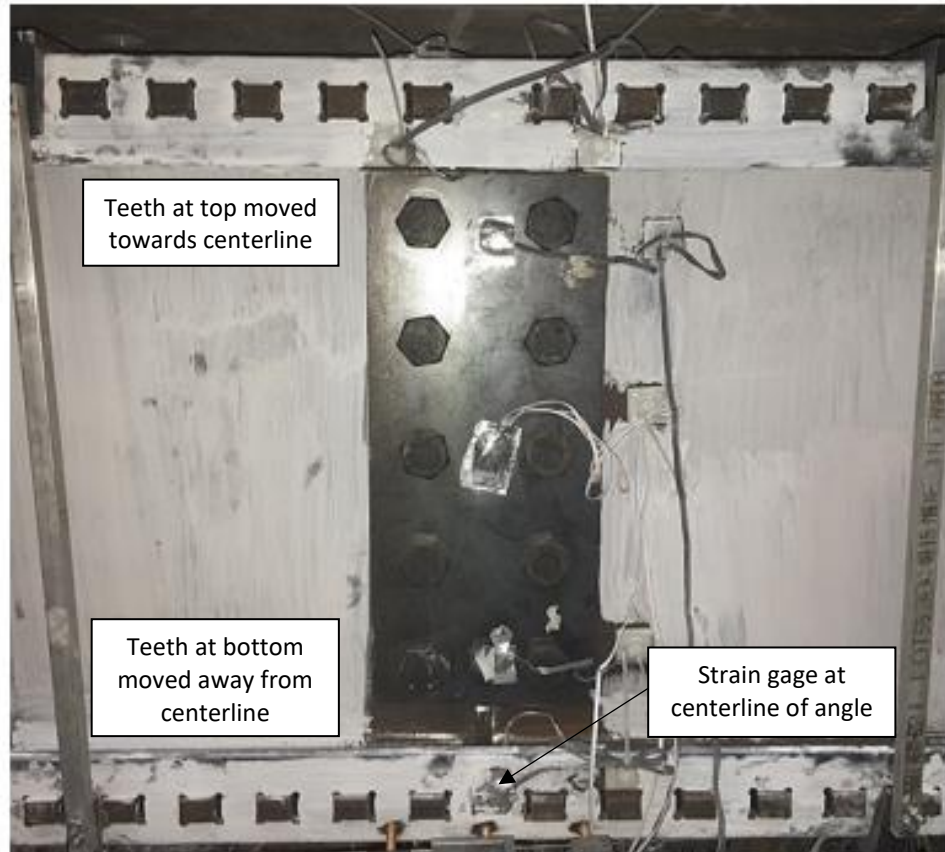
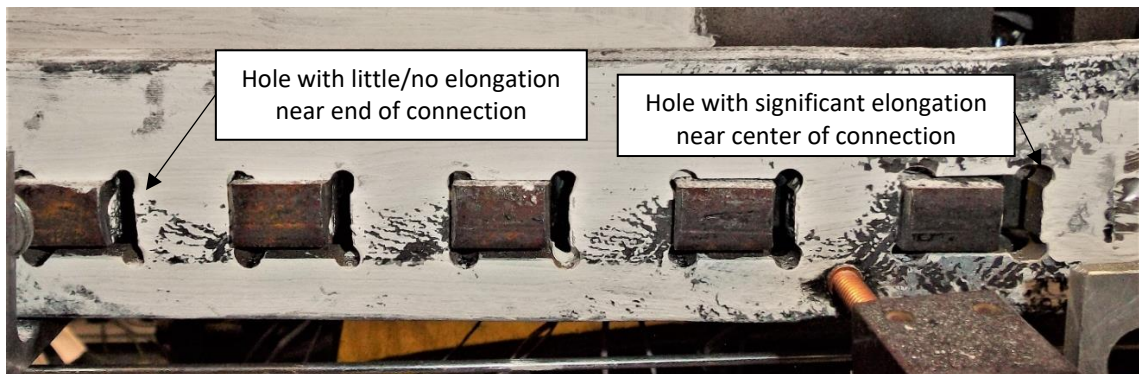
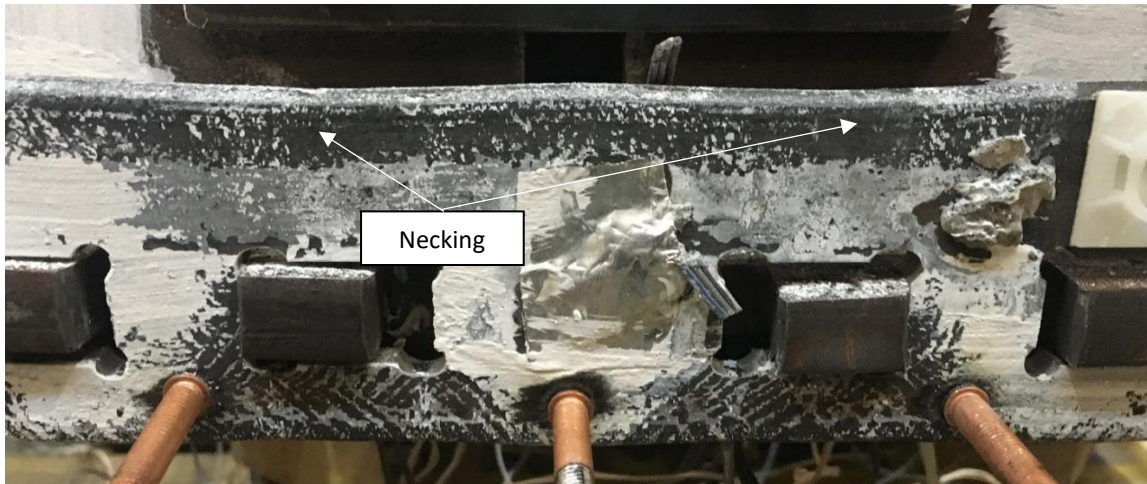


Figure 5.1.9: Test 1 connection after 28 kips of load



a) The elongation of the centermost hole



b) Necking above center holes

Figure 5.1.10: Test 1 deformation in tension angles

The angles in compression experienced relatively high strains that were measured at up to nearly 0.015 (Figure 5.1.4). However, once the angles became plastic due to the large axial strains, connection resistance to lateral-torsional buckling was reduced. This effect, combined with insufficient stiffness from the lateral bracing system, allowed the beam to undergo lateral-torsional buckling before the beam section reached its plastic moment capacity. Figure 5.1.11 contains images of the compression angle after the lateral torsional buckling failure of the beam. The approximate lateral-torsional buckling load is labeled in Figure 5.1.1. The curvature of the angle was due to the lateral pressure being applied by the beam as it deflected laterally and twisted. The beam flanges were forced in opposite torsional directions, causing the angle to experience the bending observed after the test.



Figure 5.1.11: Test 1 compression angle buckling

Because of angle deformation, the channel restraints were necessary to keep the compression angles in place. Unfortunately, the channels were not snug tight, so there was some room for movement of the angles before loading of the channel restraints occurred. Figure 5.1.12 is a photo taken after one of the channels was removed post-testing.



Figure 5.1.12: Compression angles post-testing

The results of the first beam test were generally consistent with the assumptions for the conceptual model used to define the design procedure, as well as the finite element analysis. Additionally, unexpected issues, such as interference between the bracing and the loading beam, as well as the slightly premature failure due to lateral torsional buckling, were not anticipated. Adjustments to the bracing system and instrumentation scheme were made to maximize the amount of behavioral data that could be obtained from subsequent tests.

5.2 Modifications to Bracing and Instrumentation

The first test was stopped when the vertical load capacity of the beam dropped to about 93% of the peak value observed during the test. The loss of capacity was due to lateral torsional buckling of the beam. An end view of the final state of deformation of the beam after unloading is shown in Figure 5.2.3. To avoid a lateral torsional buckling failure and permanent twisting deformation in subsequent tests, bracing restraints were added to the test setup at the support locations. Additionally, the steel angle braces were made adjustable by slotting the connection holes to avoid interference with the loading beam when the deflections of the test beam became large (Figure 5.2.2). Once the load distribution beam deflected downward several inches, the steel angles would need to be moved to avoid interference with the loading beam and subsequent sharing of the load. Slotted holes were drilled in the angles so they could be repositioned vertically without unloading the test beam (Figure 5.2.1).



Figure 5.2.1: Bracing slotted holes

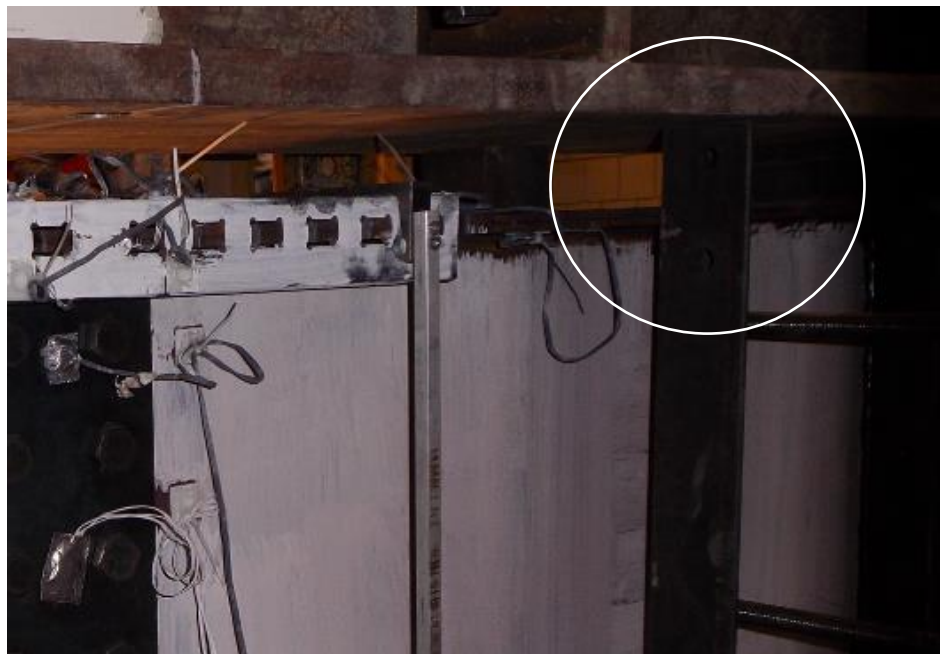


Figure 5.2.2: Test 1 load distribution beam loading the bracing

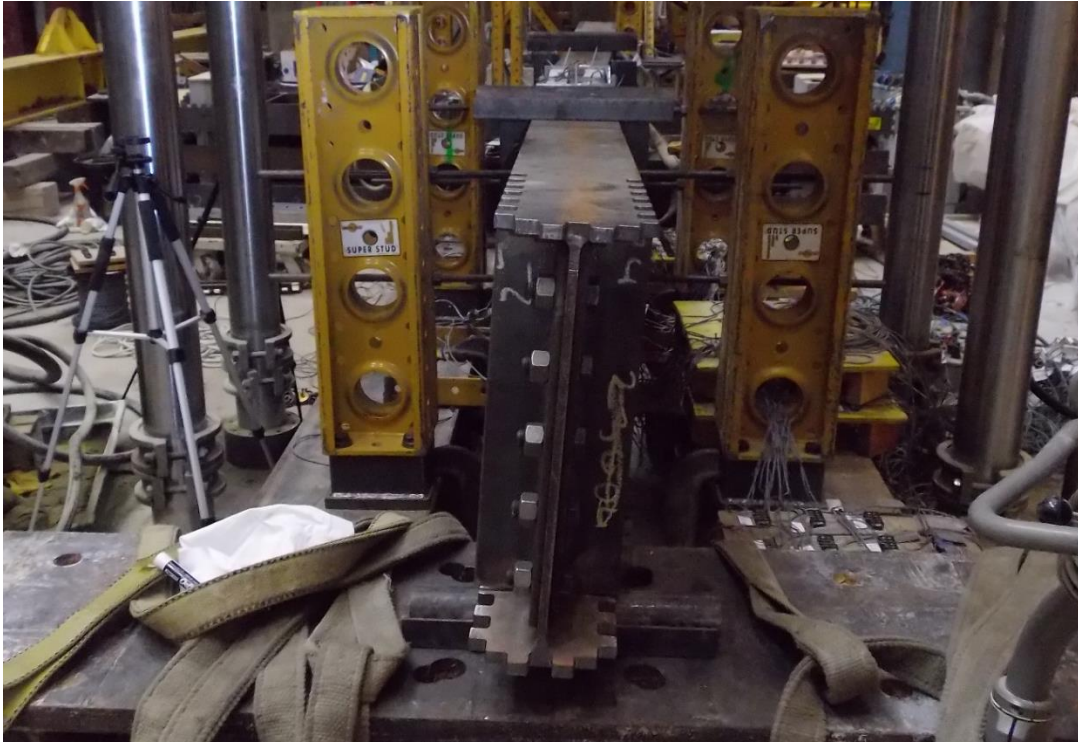


Figure 5.2.3: Beam with permanent twist at support

The instrumentation was modified as well. In Test 1, the two LVDTs (LVDT 1 and LVDT 2) that measured vertical displacement were reset at the beginning of each new stage of testing. They could measure a range of displacements up to but not exceeding two inches, and actual displacements exceeded three inches. To simplify the displacement measurements, these LVDTs were replaced with string potentiometers in the following tests. The string potentiometers had a range of 10 inches, and they were attached to each beam flange approximately one inch from the connection centerline (Figure 5.2.4).

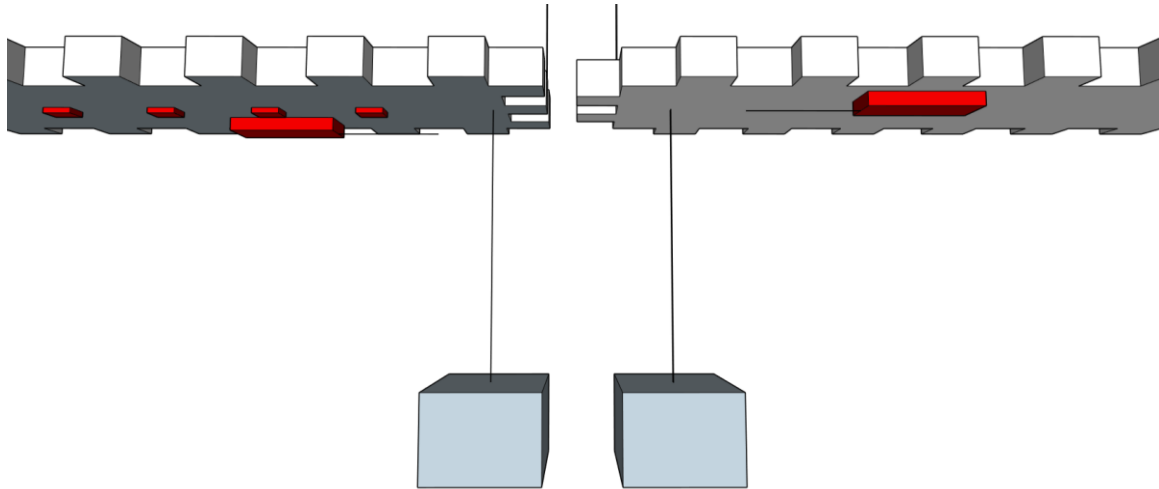


Figure 5.2.4: String potentiometers in place of LVDTs 1 and 2

Strain gage locations were adjusted as well. The gages on the tension angles did not measure strains in the first test that were as large as expected due to their placement at the center of the angle (Figure 5.1.9). Unlike the UCD finite element stress distributions suggested (Figure 4.12), the region directly above the two centermost holes showed the most elongation. In retrospect, these locations represented the smallest cross section for axial loading of the angles, and the largest strains should be expected at these locations. The strain gages were moved to these locations (Figure 5.2.5).

Since strain gages on the beam flanges were located on only one side of each flange (Figure 4.16), strains could not be separated into flexural and axial components. That is, any local flexural deformation of the flanges would produce strains that are localized to the strain gage location. Thus, strain gages were placed on both sides of the beam flanges in subsequent tests (Figure 5.2.6).

Some strain gage locations in Test 1 were removed for subsequent tests. Only one plate was instrumented in the following tests (Figure 5.2.7). On the bottom flanges of the beam, only three of the six gages recorded strains resulting from plasticity. Out of the three that measured low strains, two of them were removed because a clear indication of the strain distribution could be obtained with fewer gages (Figure 5.1.7). Finally, only beam flanges on one side of the connection were instrumented following Test 1 (Figure

5.2.6). There were few differences in the measured strain distributions for the gages in the beam flanges on both sides of the connection.

The modified angle strain gages are identified in plots of the resulting measurements based upon their location on the angle. For example, Gage 1 and Gage 2 are labeled as being at the “top” of a compression angle on the horizontal leg, and gages 3 and 4 are labeled as being on the “side” of the angle on the vertical leg. Gages 5 and 6 correspond to locations at the hole on the angle. These labels are included in the top right of Figure 5.2.4.

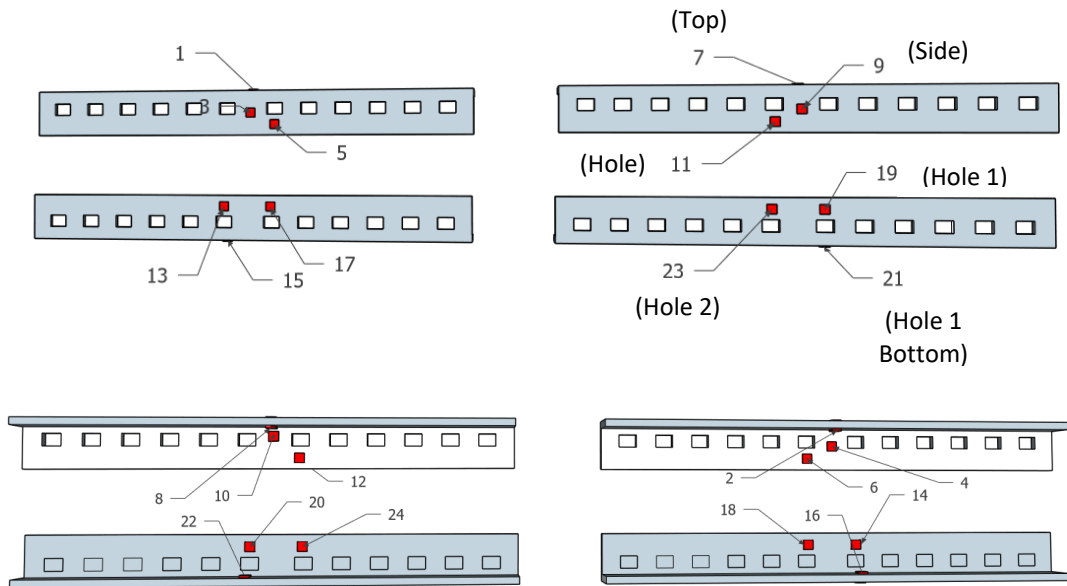


Figure 5.2.5: Angle Instrumentation Modifications

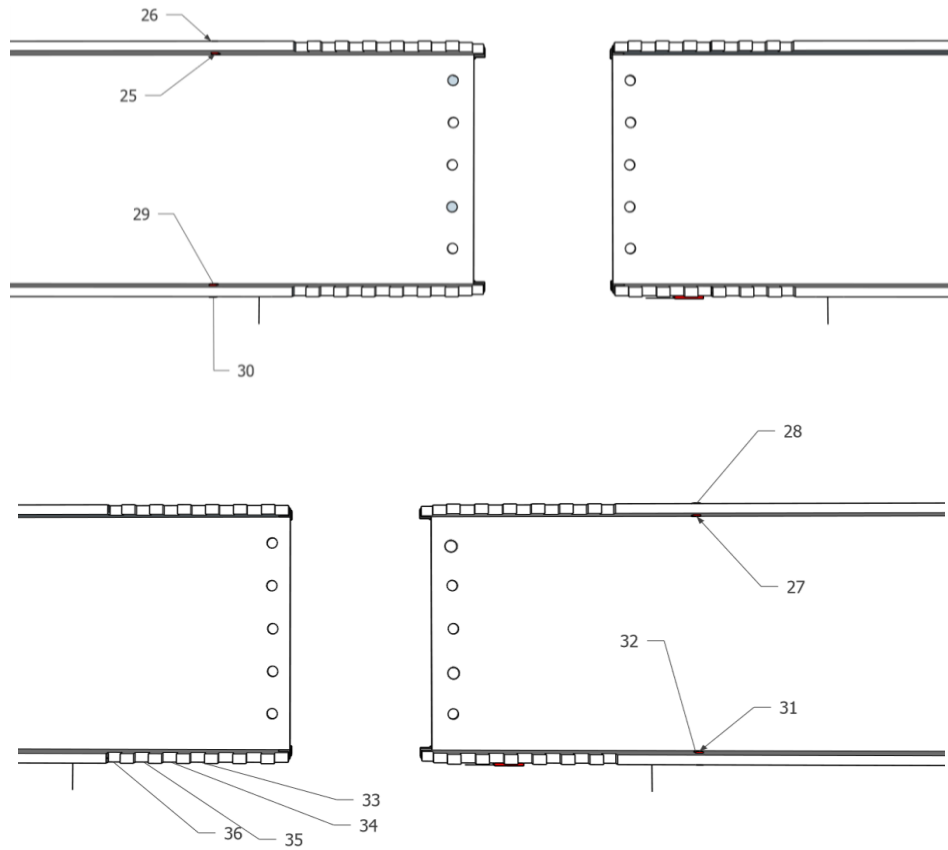


Figure 5.2.6: Beam instrumentation modifications

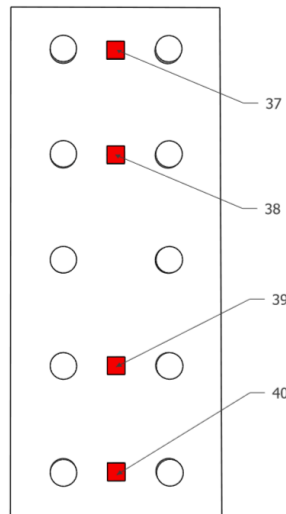


Figure 5.2.7: Shear plate instrumentation modifications

5.3 Test 2 Results

The second beam, another W18x46, was tested with a single point load over a stiffener, and with the connection under both shear force and bending moment, as noted in Table 1 and Figure 4.4. The test was conducted in one stage with two pauses. The beam and connection responded to vertical loading that produced constant shear and moment in the manner that was expected. Like the beam in Test 1, the magnitude of deflection needed to fully engage the connection was much larger than expected. Once the flange teeth and the shear plate bolts had made contact with the corresponding surface in the angles and the beam webs, the connection generated internal resistance to offset the applied loads. The first pause in loading was after the beam had deflected roughly two inches, and this pause was done so that the bracing could be moved to avoid interference between the loading head and the bracing system by utilizing the new slotted holes. The pauses can be observed as small load drops in the displacement (Figures 5.3.1, 5.3.4 and 5.3.5) and strain curves (Figures 5.3.6 through 5.3.12). A peak load of 182 kips was reached, and the beam section failed at a moment equal to its calculated plastic moment capacity. Additional comments on plastic moment are included in Chapter 6.

5.3.1 Test 2 Displacement Data

The maximum deflection measured was 3.5 inches. String Pot 2 measured slightly more displacement than String Pot 1 since it was located on the side of the connection adjacent to the point load. The beam flanges on either side of the connection were not level with one another at the end of the test. The vertical slip of the beam flanges was consistent with independently conducted finite element model predictions for connections loaded with both moment and shear. An image of the uneven beam flanges after testing is pictured in Figure 5.3.2. Out of plane movement of the beam was also observed at the peak load, and this is pictured in Figure 5.3.3.

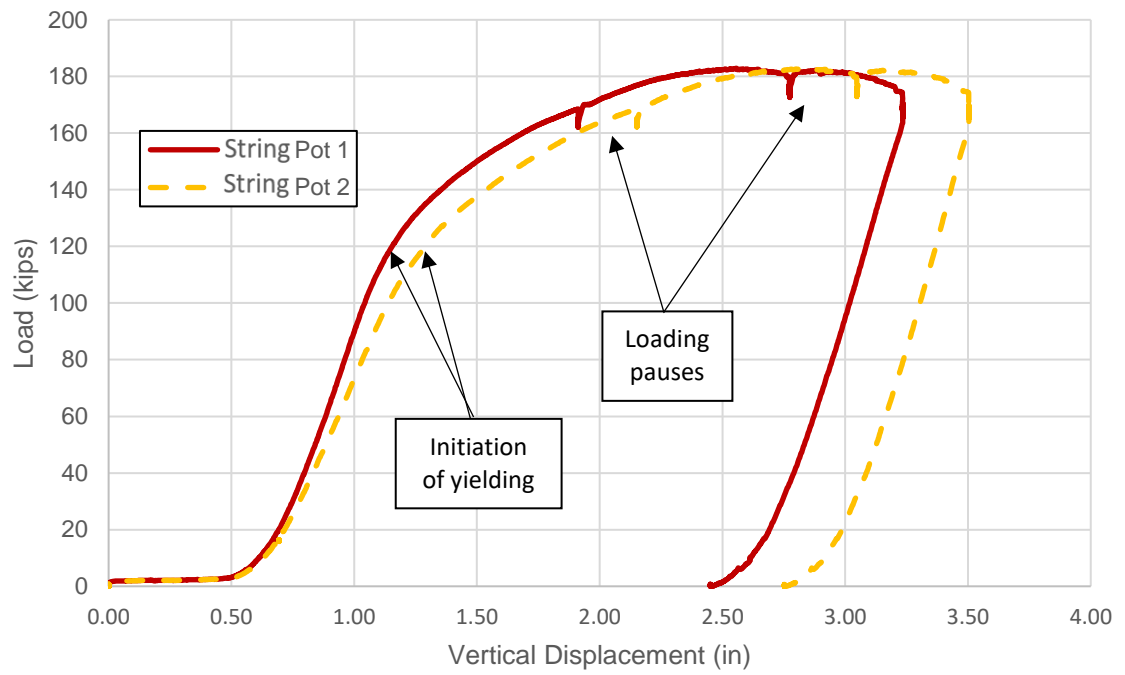


Figure 5.3.1: Test 2 load vs. vertical displacement



Figure 5.3.2: Test 2 uneven top flanges after testing

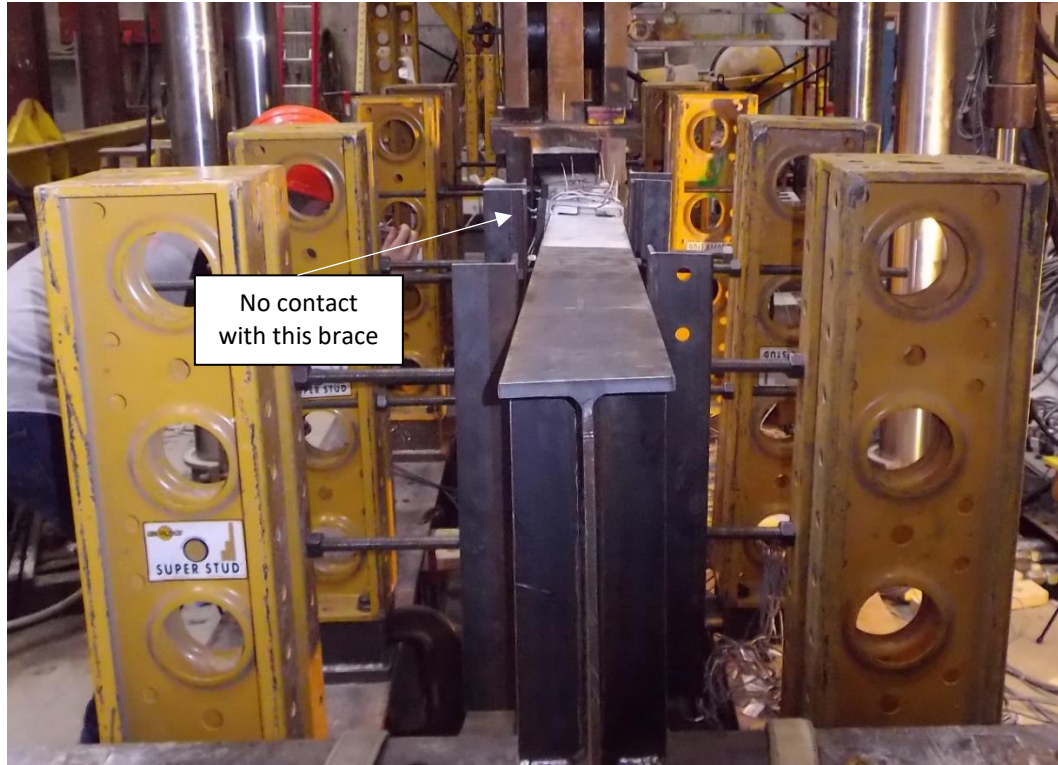


Figure 5.3.3: Lateral movement in the second beam test

The LVDTs were placed identically to the first test, but the displacements measured were smaller due to the lower moment at the connection. The shear forces and vertical slip of the beam flanges also influenced the measured displacements. In Figure 5.3.5, LVDT 5 and LVDT 8 show similar load displacement curves with higher displacements than the other two LVDTs. This occurred because LVDT 5 and LVDT 8 were both located on the sides of the angles nearest the point load. The data from Test 2 demonstrated that angles may not be loaded equally on each side of the connection when variable shear forces and bending moments are present. This was also demonstrated in the data presented for Tests 3 and 4 in sections 5.4 and 5.5.

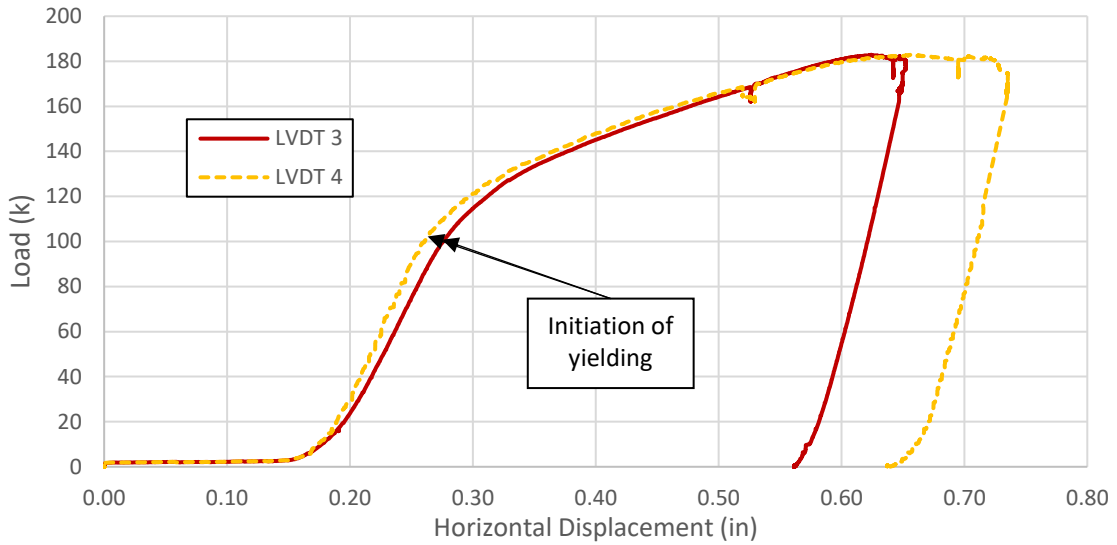


Figure 5.3.4: Load vs. horizontal LVDT displacement

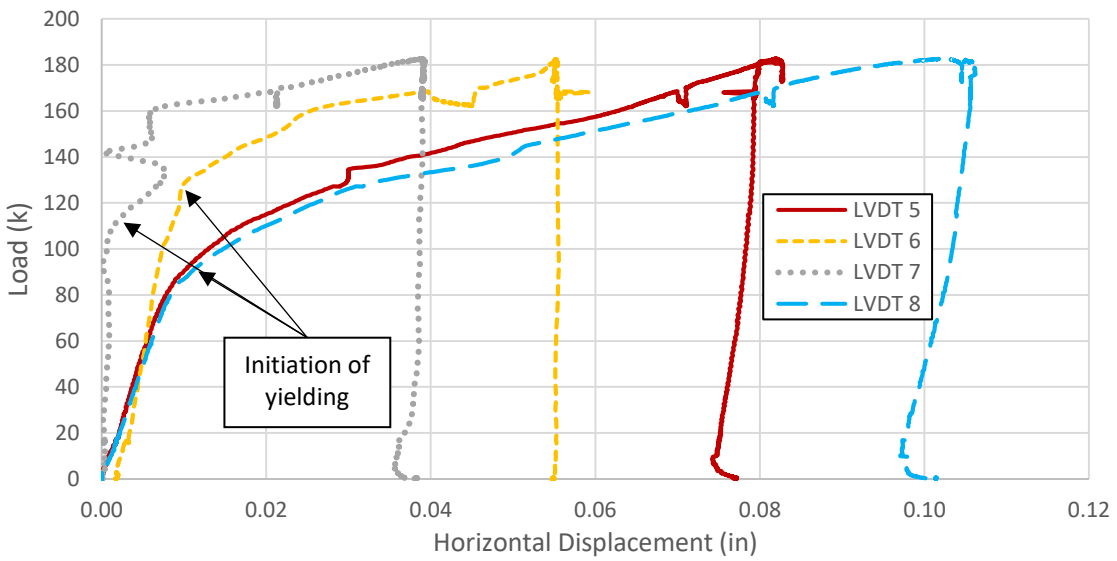


Figure 5.3.5: Load vs. angle LVDT displacement

5.3.2 Test 2 Strain Data

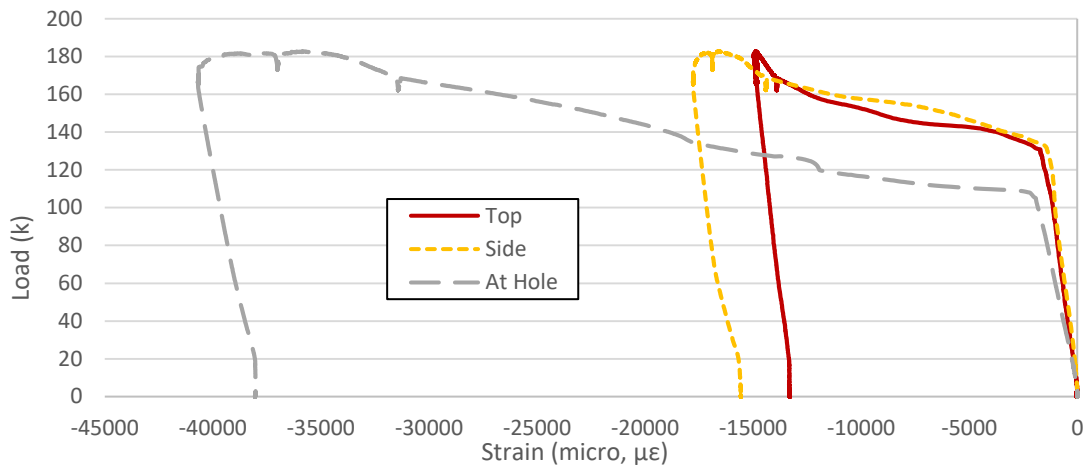
Strain gage data was recorded for the compression angles, tension angles, beam flanges, shear plates, and channels corresponding to the original instrumentation plan with the modifications described in Section 5.2. Strain gage data was separated into axial and

flexural components in this test, as described in Appendix D, and data is presented in Figures 5.3.6 through 5.3.10. Additional strain data is included in Appendix D.

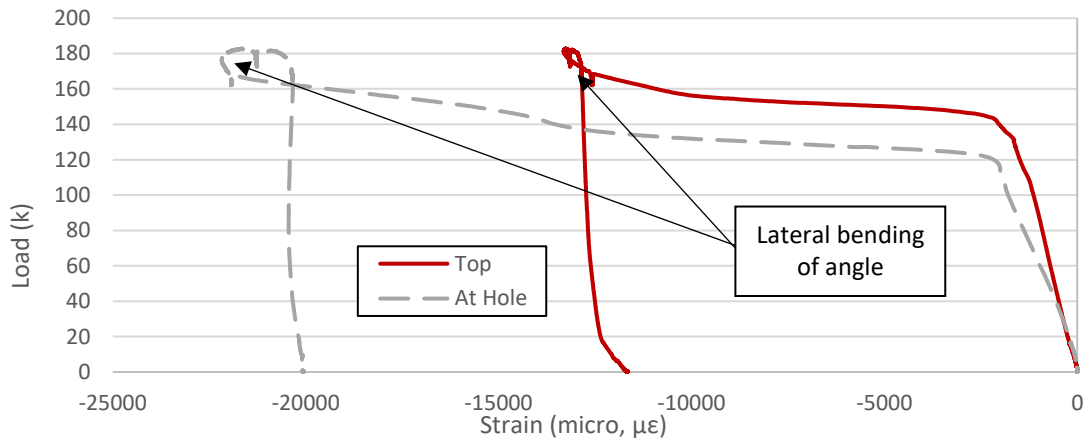
Several gages on the tension angles recorded a sudden loss in strain corresponding to loading in the strain hardening region of the load vs. strain curves (Figure 5.3.7). Despite the temporary decrease in strain, load continued to increase. These temporary reductions in strain measurements are likely due to the redistribution of stress within the angles, potentially due to slip of connection components and/or lateral movement.

Similar to Test 1, the bottom beam flange strain gages within the connection recorded plasticity only at Gages 34, 35, and 36 (Figure 5.3.8). In the beam section, inelastic behavior was recorded in axial strain measurements in both the top and bottom flanges, but not until the approximate peak load had been reached (Figure 5.3.9). The flexural strains, located in Appendix D, were insignificant in comparison.

The shear plate instruments recorded low strains in tension, but compression strains were not properly recorded at the top of the plate due to an unreliable strain gage reading (Figure 5.3.10). At the top, the plate was being compressed and bent from the out of plane movement of the specimen, and this may have crushed this strain gage. The web of the beam adjacent to the shear plate demonstrated yielding, shown in Figure 5.3.11.

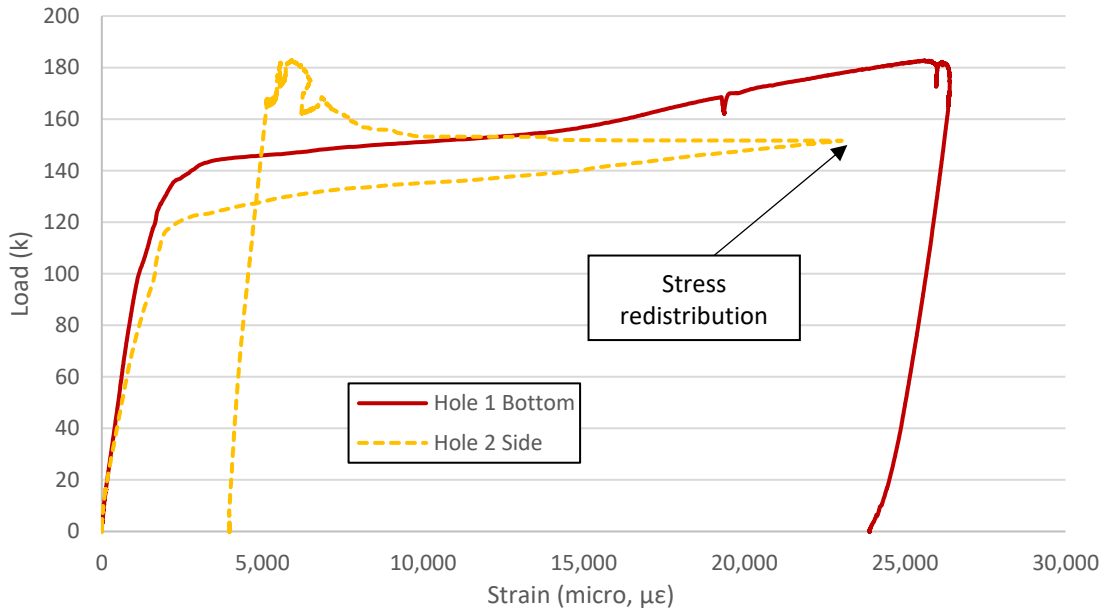


a) Angle 1

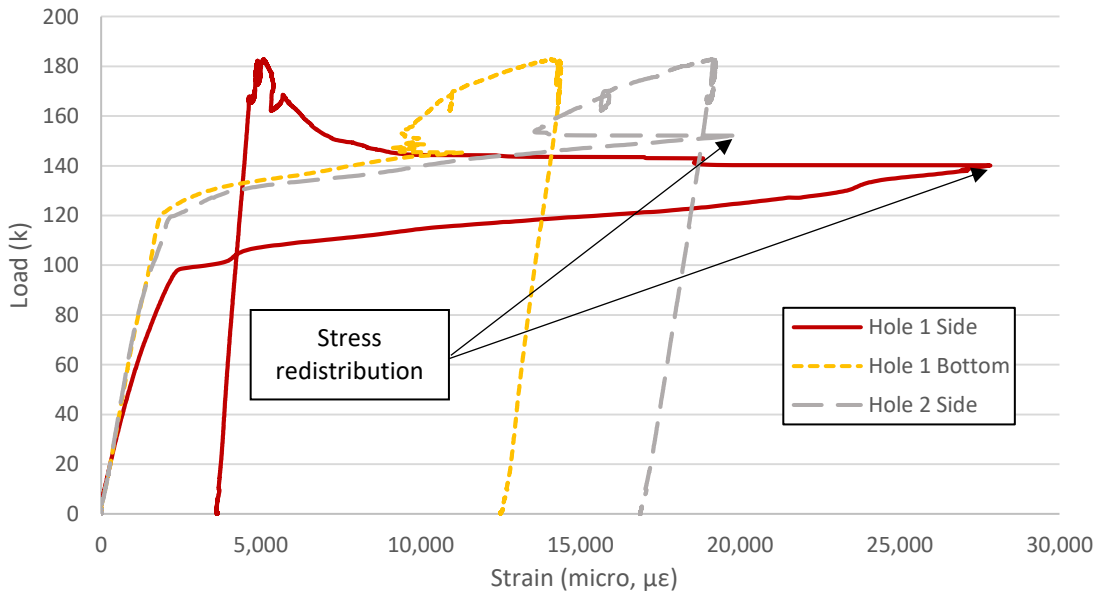


b) Angle 2

Figure 5.3.6: Test 2 vs. compression angle load axial strain



a) Angle 1



b) Angle 2

Figure 5.3.7: Test 2 load vs. tension angle axial strain

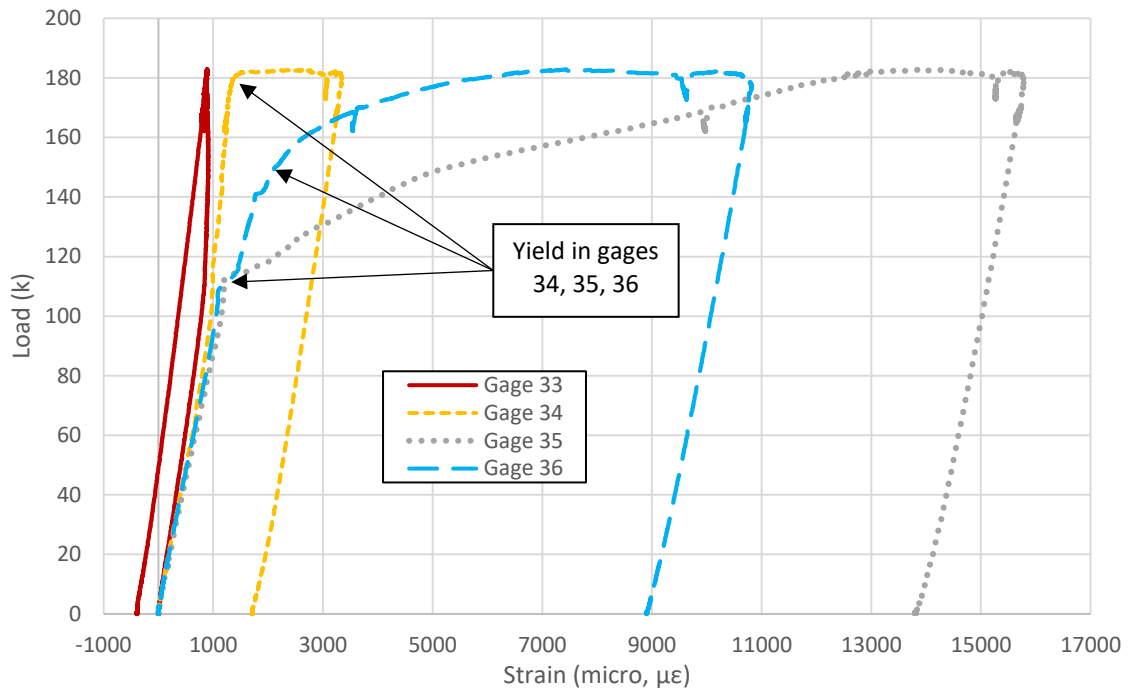
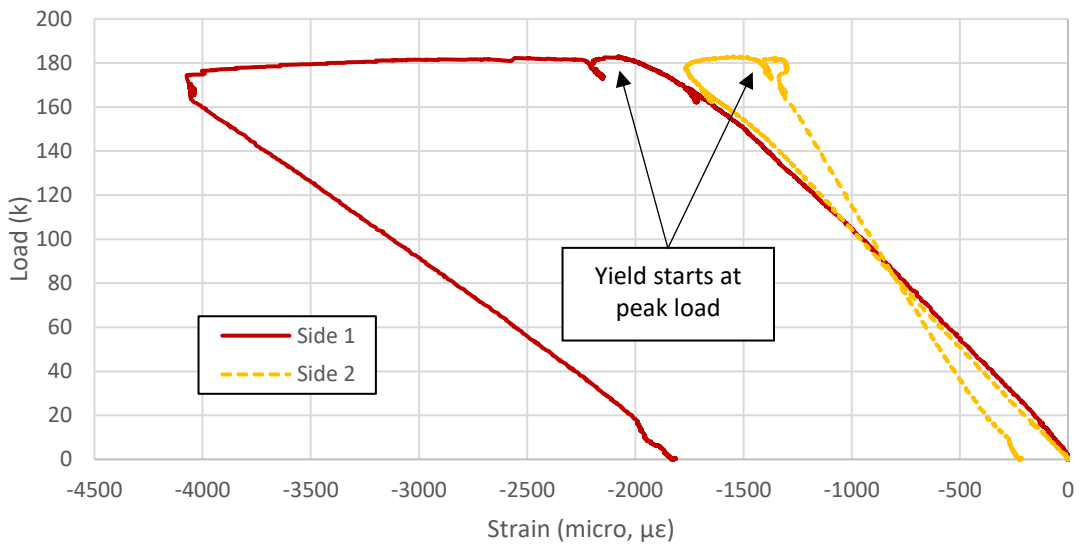
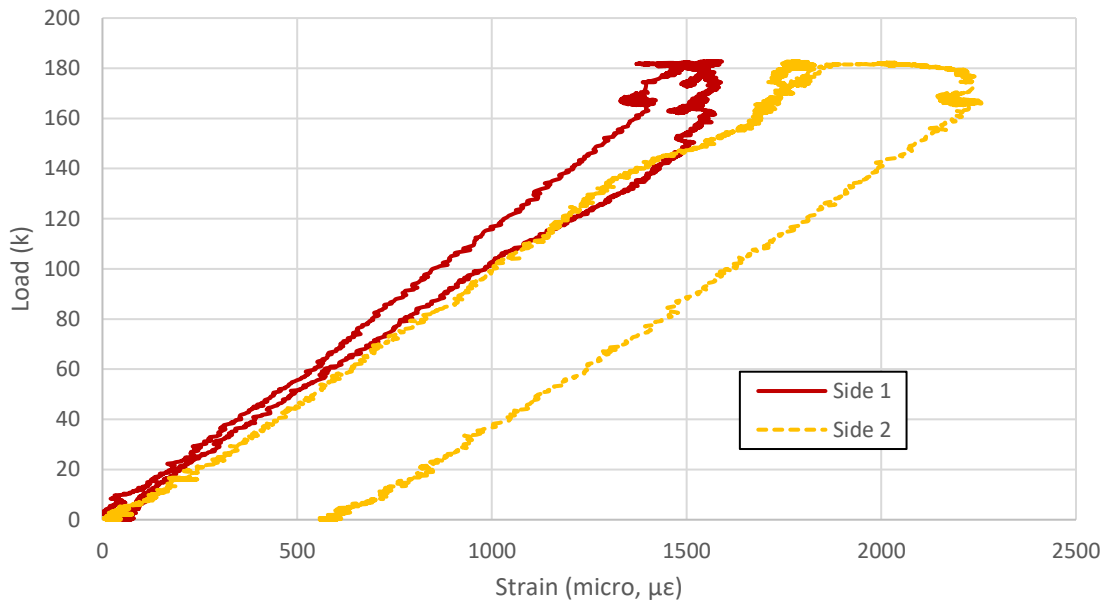


Figure 5.3.8: Test 2 load vs. beam bottom flange strain



a) Top Flange



b) Bottom Flange

Figure 5.3.9: Test 2 load vs. beam flange axial strain

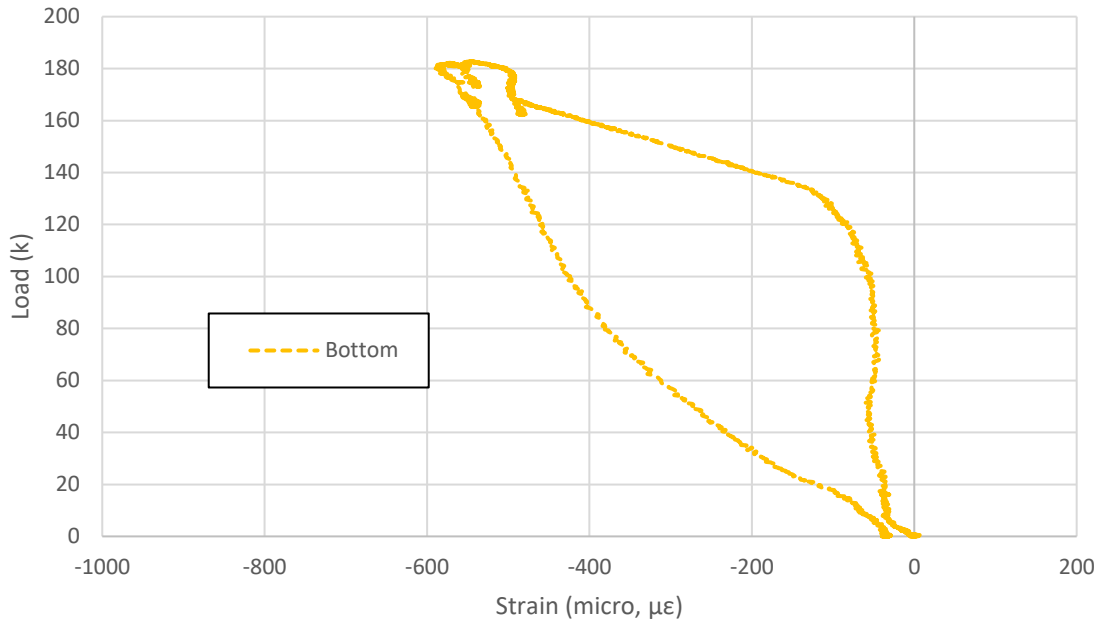


Figure 5.3.10: Test 2 load vs. shear plate axial strain



Figure 5.3.11: Web strains in whitewash

The channels restraining the compression angles experienced little axial strain (Appendix D). Flexural strain occurred because the components experiencing load were the legs of the channel. This eccentric load caused bending in the web of the channel,

which is where the strain measurement was recorded. The flexural strain data for the channels restraining compression angles is presented in Figure 5.3.12. The strain measurements did not decrease after unloading due to plastic behavior in the beam and compression angles.

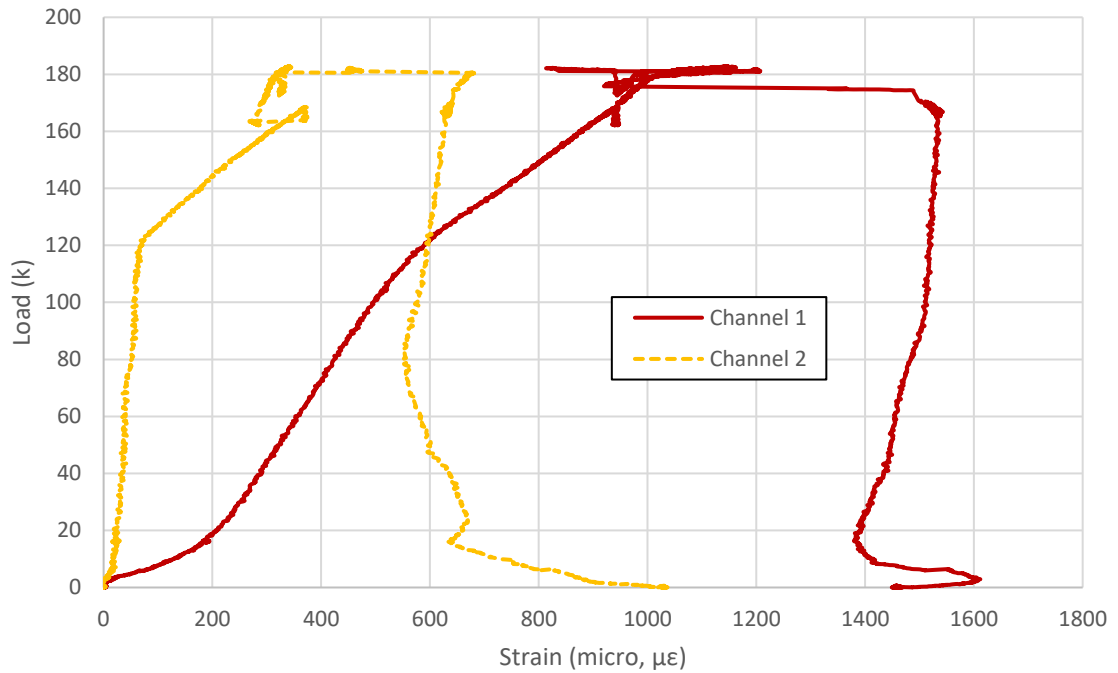
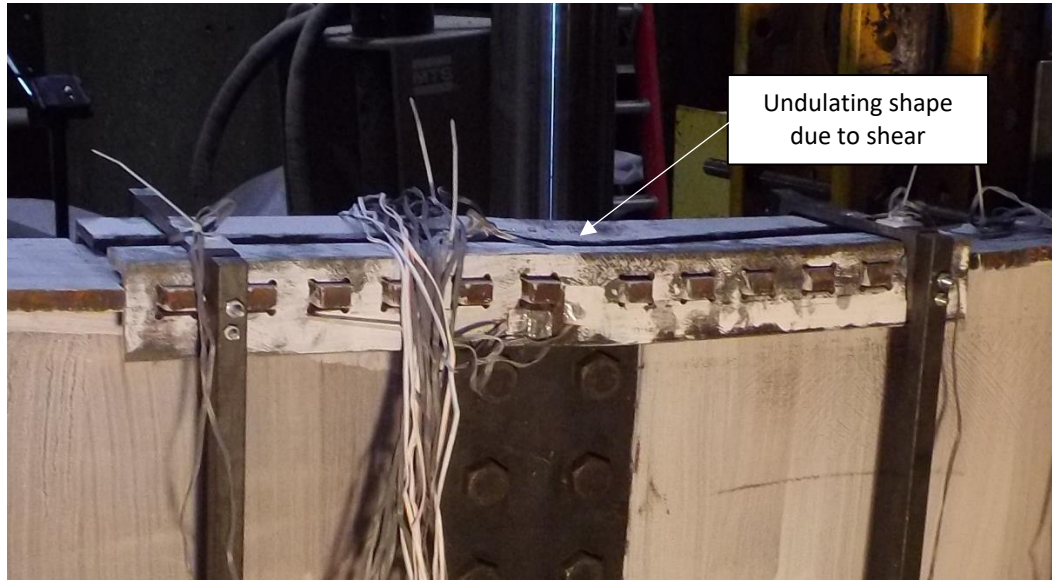


Figure 5.3.12: Test 2 load vs. channel flexural strain

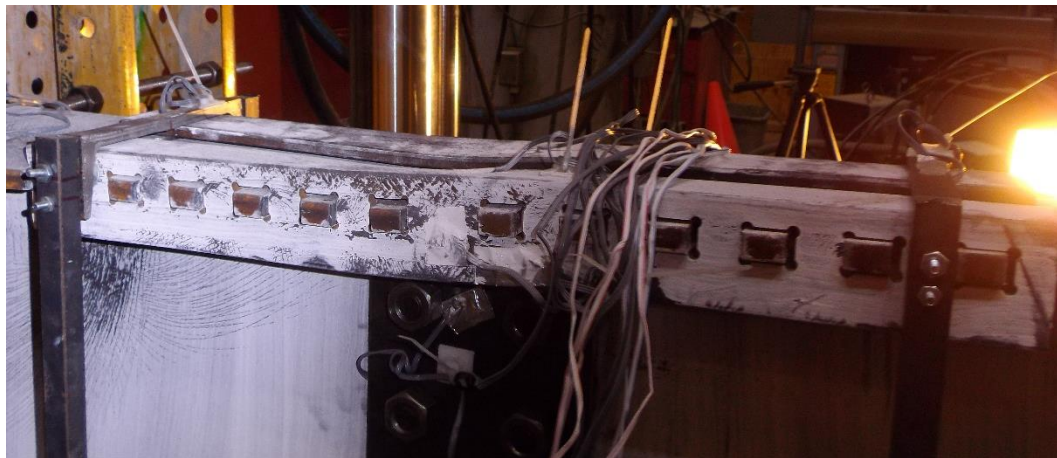
5.3.3 Test 2 Discussion

Shear force produced permanent vertical slip between the two beam flanges, and the angles have an undulating appearance post-test because of this, as shown in Figure 5.3.13. These permanent deformations indicated that the angles resisted some of the shear force and yielded because of it. There was also lateral bending of the angles, but it was limited by the channel restraints (Figure 5.3.14). The stiffened bracing system enabled the beam to resist loading that developed the theoretical plastic moment capacity.

However, the small lateral displacements that were observed indicated that the beam may have been experiencing the initiation of lateral-torsional buckling at the end of the test.



a) View facing North



b) View facing South

Figure 5.3.13: Compression angles post-test viewed facing North and South

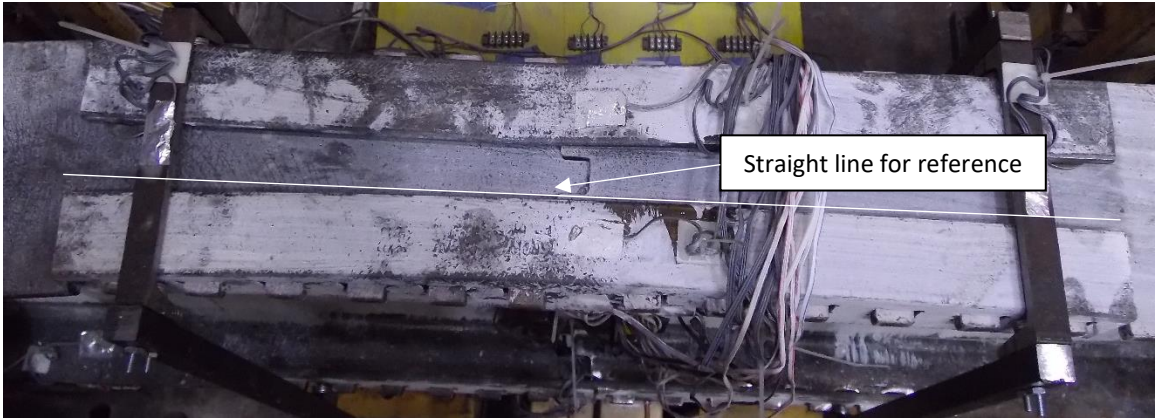


Figure 5.3.14: Lateral bending of the angles

Measurable out of plane movement at peak load occurred because the forces on the bracing were underestimated. The bracing was not stiff enough to carry the lateral loads without experiencing significant deflections. The bracing angles experienced local lateral deformations that allowed the beam to deflect (Figure 5.3.15). The EFCO members were not stiff enough, and the most heavily loaded EFCO members deflected in a cantilever mode.



Figure 5.3.15: Local deformation in a bracing angle

Because of the flexibility of the bracing in the second test, the EFCO braces were replaced with four W12x35 steel pedestals. Rather than clamping these members to the beams below, each W12x35 bracing member was bolted to the support beams with four 7/8-inch A490 bolts. C8x11.5 channel sections were attached to the wide flange sections with 7/8-inch diameter rods (Figure 5.3.16). The replacement of the braces was designed to increase the stiffness of the system enough to prevent measurable out of plane movements. Calculations of the stiffness of the replacement bracing are included in Appendix C.

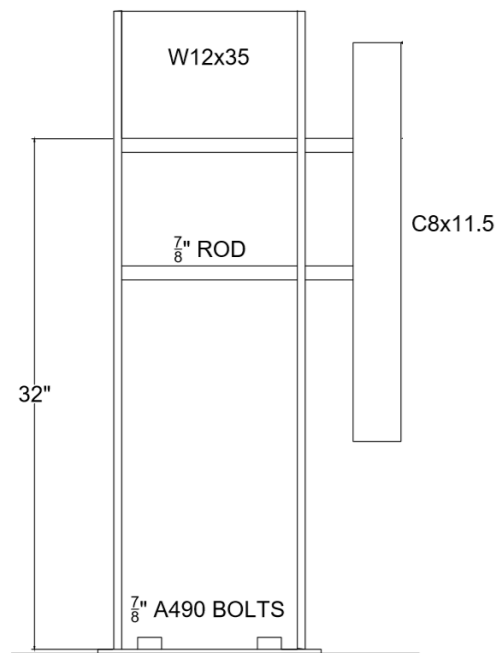


Figure 5.3.16: Modified bracing for Test 3 and Test 4

5.4 Test 3 Results

The third beam, a W21x57, was tested with one point load and was subjected to a combination of bending moment and shear (Table 1 and Figure 4.7). The test was paused once under load to prevent interference between the loading head and braces. Additional

adjustments to bracing were not possible due to friction between the surface of the top beam flange and bracing. Therefore, the beam was unloaded, the bracing was adjusted, and then the beam was reloaded. A maximum load of 232 kips was reached, and the beam section reached its calculated plastic moment capacity. Additional comments on the plastic moment capacity are included in Chapter 6 (Table 7). The initiation of lateral-torsional buckling was also observed at the failure.

5.4.1 Test 3 Displacement Data

A maximum displacement of nearly 2.5 inches was measured in Test 3. Similar to Test 2 (Figure 5.3.2), vertical misalignment of the flanges gradually occurred once load was applied. The behavior can be seen in the load vs. deflection data shown in Figure 5.4.1. The data obtained using the LVDTs is included in Figures 5.4.2 and 5.4.3. The pause, unloading, reloading, and initiation of lateral-torsional buckling is clearly displayed in the load vs. vertical displacement plot in Figure 5.4.1.

LVDT 3 failed to record data properly when following the pause, and this data was omitted in Figure 5.4.2. It is likely the result of a loose clamp that was restraining the LVDT rod. Regarding asymmetrical displacement of the angle LVDTs, the data shown in Figure 5.4.3 is like the angle LVDT data from Test 2 (Figure 5.3.2). The two LVDTs located nearest the point load, LVDT 6 and LVDT 7, experienced more deflection than LVDT 8. LVDT 5 did not properly record data and was omitted the results. This, again, was most likely due to a loosened attachment of the LVDT rod.

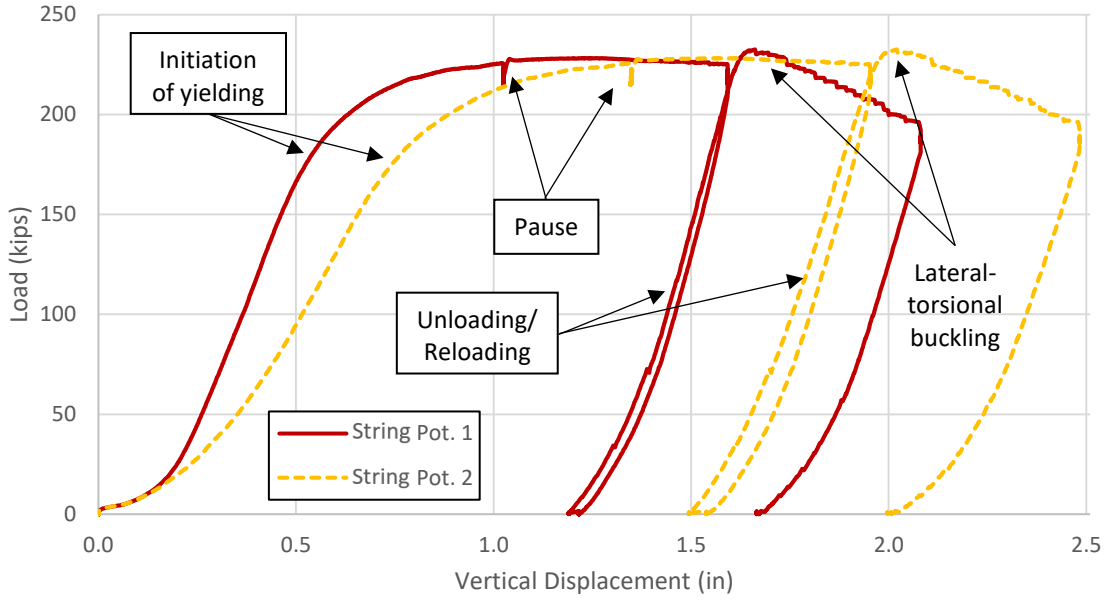


Figure 5.4.1: Test 3 load vs. vertical displacement

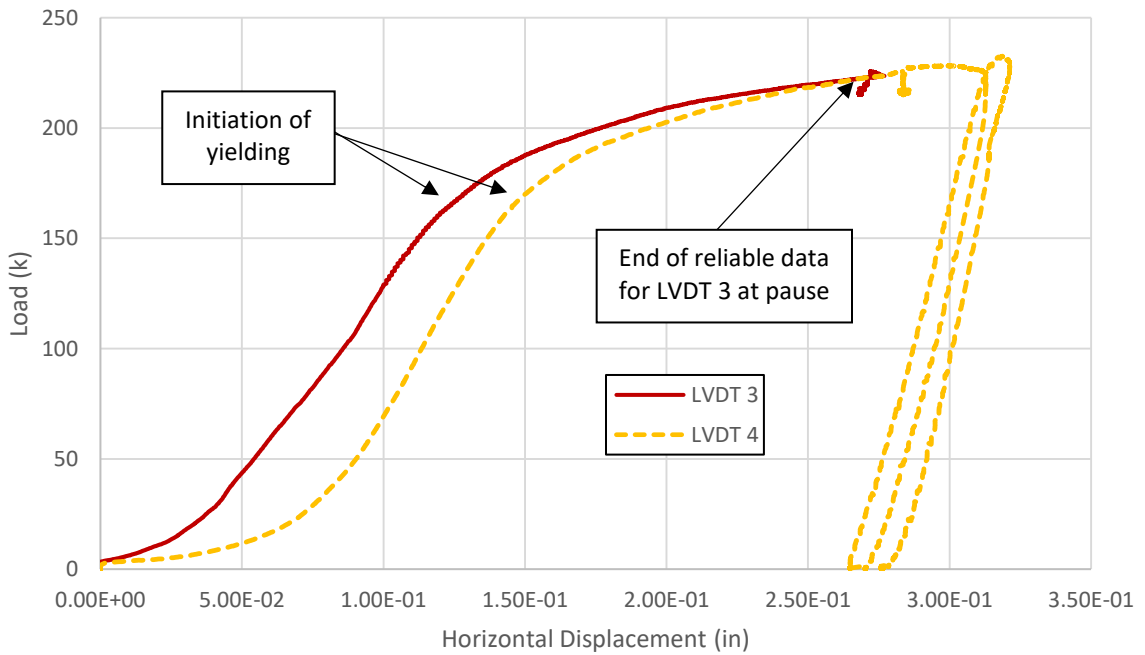


Figure 5.4.2: Test 3 load vs. horizontal LVDT displacement

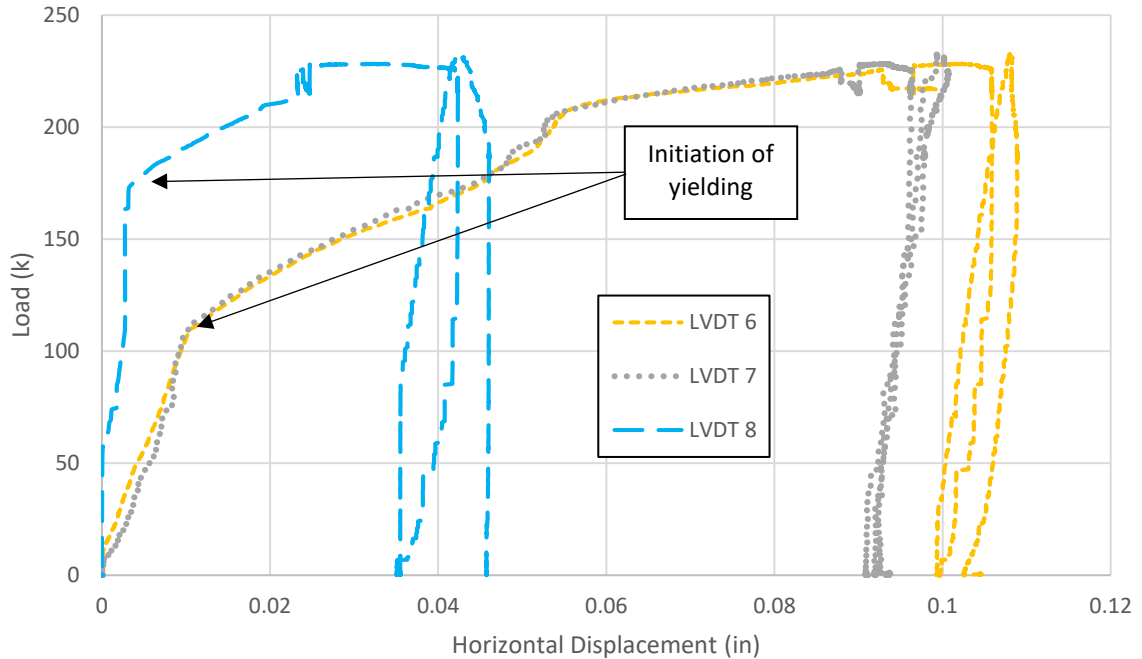


Figure 5.4.3: Test 3 load vs. angle LVDT displacement

5.4.2 Test 3 Strain Data

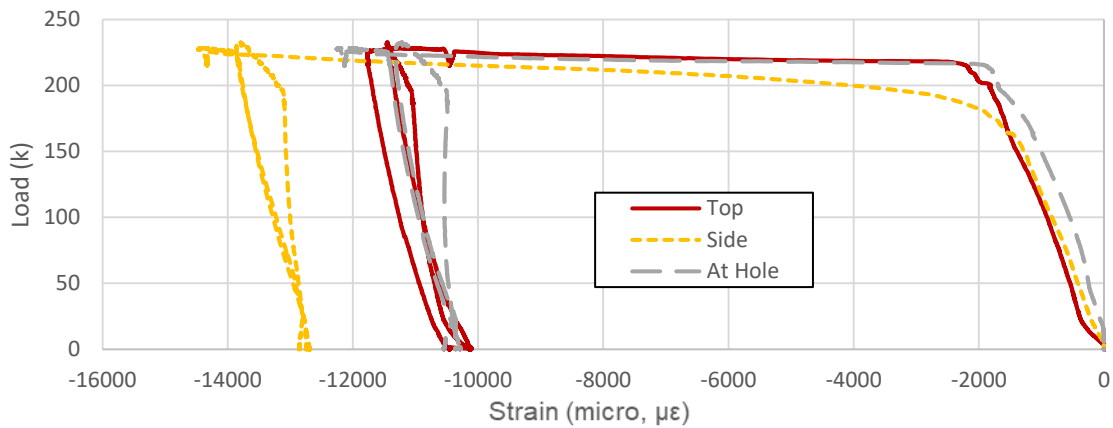
The strain gages for the beam and connection in Test 3 generated deformations that are consistent with the expected behavior, including major axis bending and shearing of the beam section, axial tension and compression of the angles, and bending and shearing of the shear plates. Strain data is presented in Figure 5.4.4 through Figure 5.4.9. Axial strain data is given for beams, angles, and one plate. One strain gage on the bottom flange of the beam section did not read data and was omitted. Strain data was recorded for one channel.

Just like Test 2, gages on the tension angles once again recorded a sudden loss in strain during the strain hardening region of the load vs. strain curves (Figure 5.4.5). The compression angles measured plasticity in each region instrumented (Figure 5.4.4).

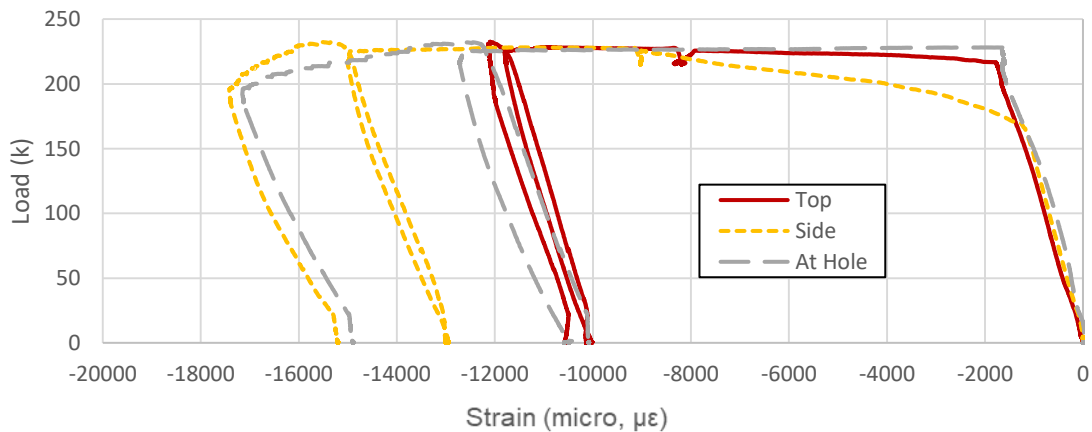
The beam data was consistent with the measurements from Test 1 and Test 2. The instruments on the bottom of the beam flange within the connection recorded

inelastic behavior only in Gage 35 and Gage 36 (Figure 5.4.7). The beam flanges once again did not record any inelastic behavior until approximately the peak load had been reached (Figure 5.4.6).

The shear plate gages recorded a distribution of strains within the linear elastic region (Figure 5.4.8). Additional comments on the distribution of strains in the shear plates are included in the discussion in Chapter 6. Relatively small strains (-0.00045 to 0.0004) existed in the top two strain gages due to permanent deformations existing in the beam section.

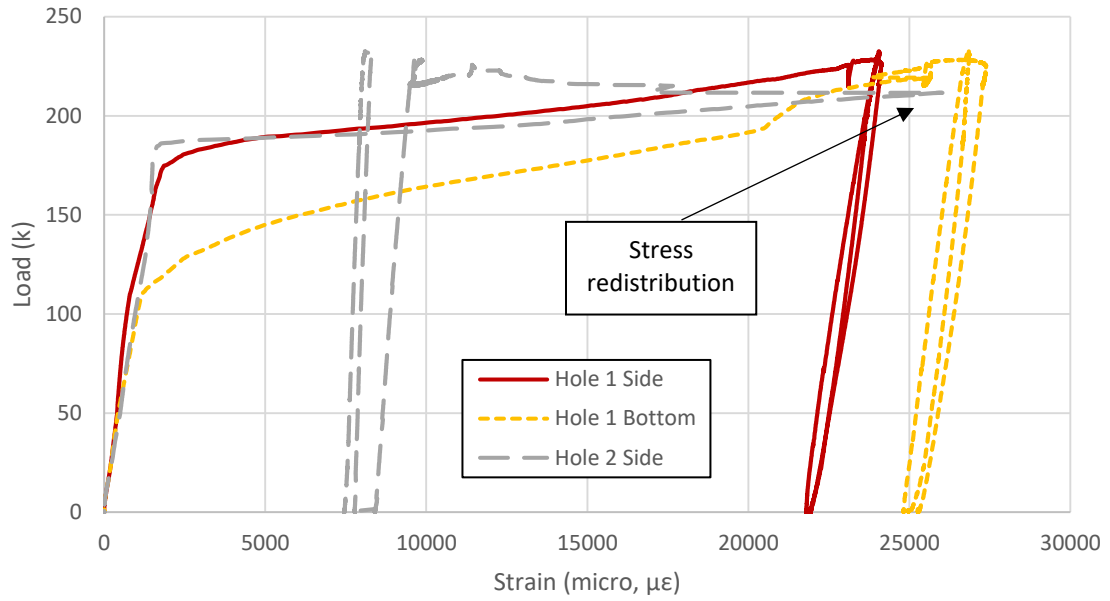


a) Angle 1

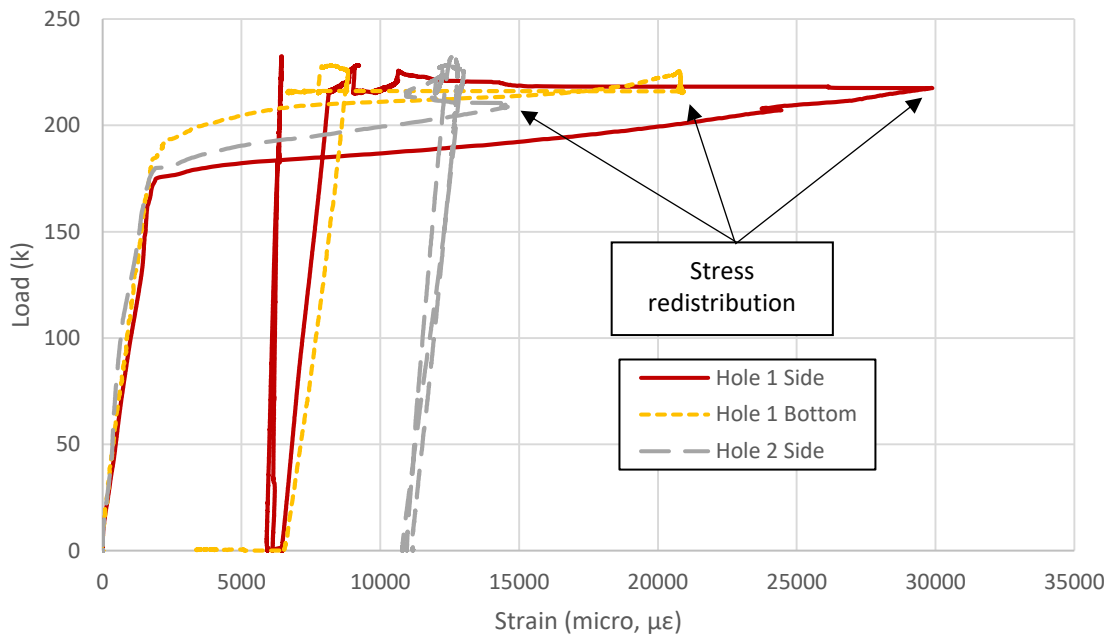


b) Angle 2

Figure 5.4.4: Test 3 load vs. compression angle axial strain

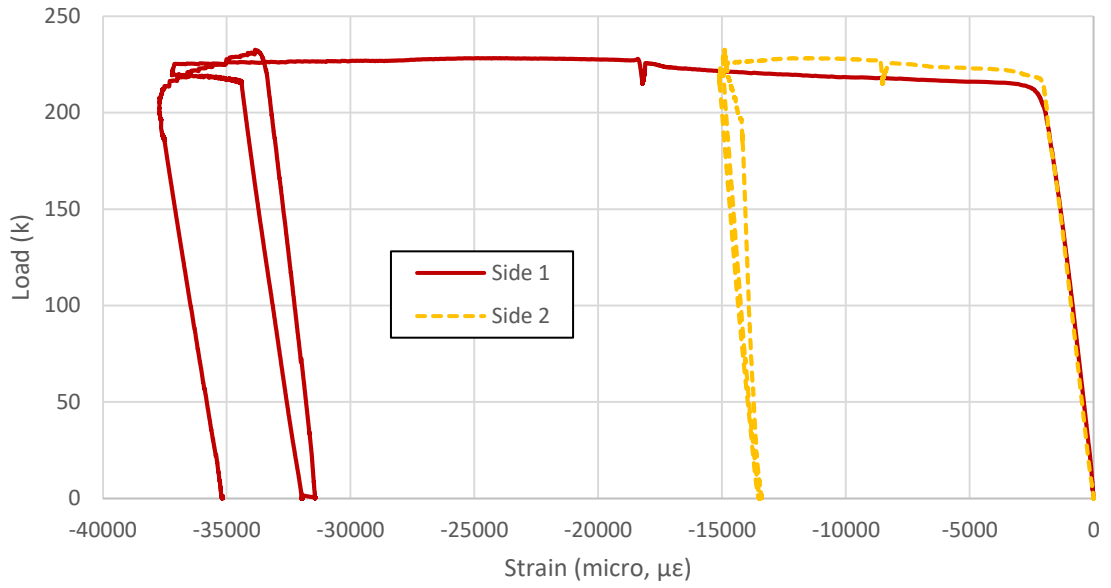


a) Angle 1

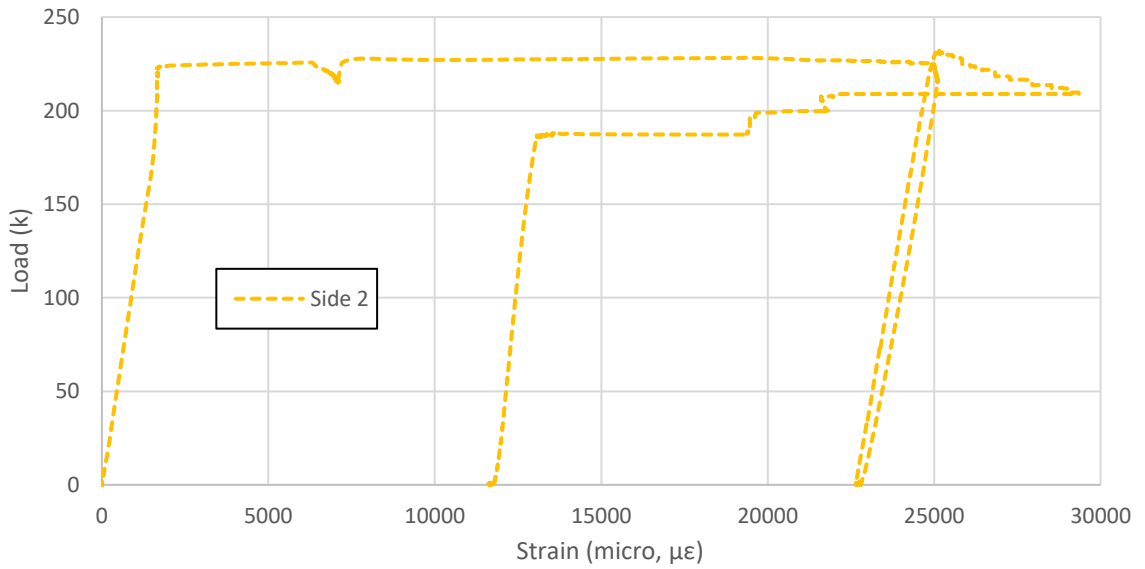


b) Angle 2

Figure 5.4.5: Test 3 load vs. tension angle axial strain



a) Top Flange



b) Bottom Flange

Figure 5.4.6: Test 3 load vs. beam flanges axial strain

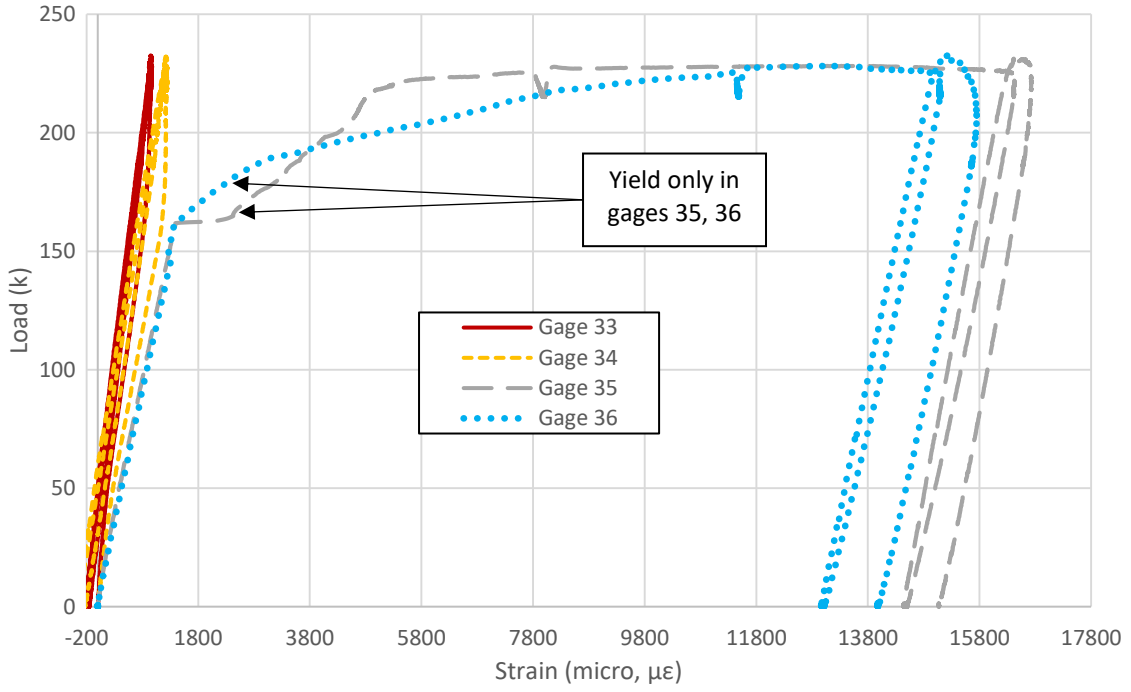


Figure 5.4.7: Test 3 load vs. beam bottom flange strain

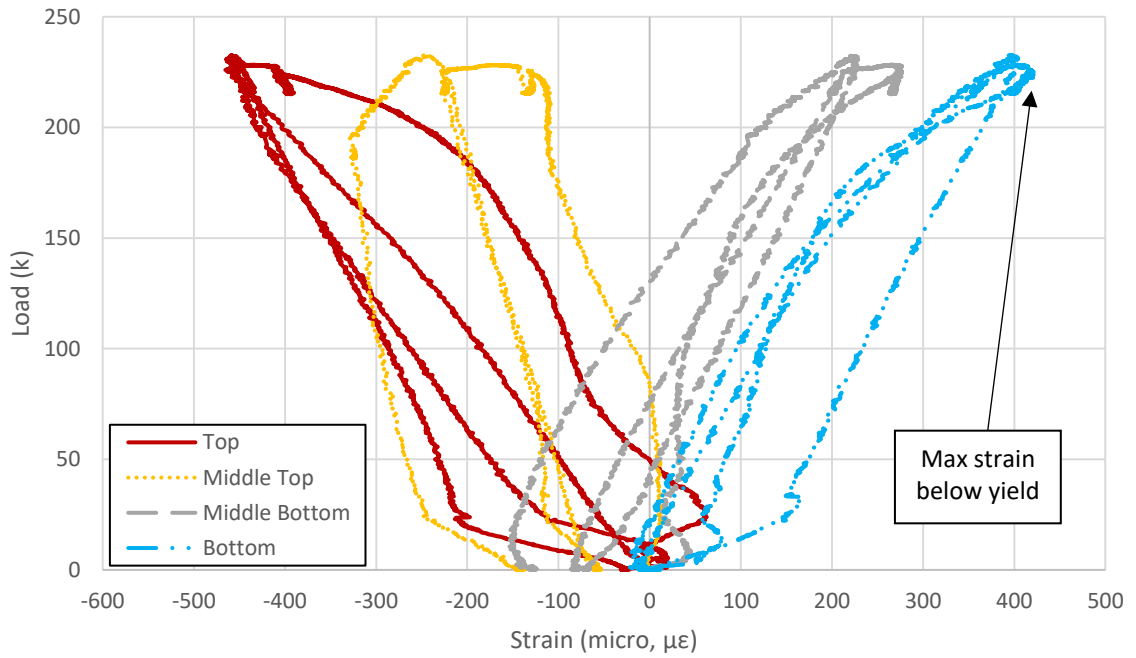


Figure 5.4.8: Test 3 load vs. shear plate axial strain

5.4.3 Test 3 Discussion

The general behavior of the connection was like that in Tests 1 and 2. Due to the presence of shear, permanent deformations of the beam flanges occurred shortly after loading began. This caused a similar deformation pattern in the angles due to vertical movement of the teeth relative to one another (Figures 5.4.11 and 5.4.14).

The lateral bracing restrained the system well until the peak load was reached and the test was paused. Since the bracing was slightly loosened for adjustment during the pause, some additional out of plane movement was allowed. This caused the top flange to deflect out-of-plane, and it loaded one of the compression angles at the peak load (Figure 5.4.12). Unfortunately, the movement allowed for the initiation of lateral buckling of the beam, even though the amount of lateral movement was small (~0.25 inches). The final deformed shape of the beam is visible in Figure 5.4.13.

In Test 3, yielding of the beam web in shear was visible in the whitewash (Figure 5.4.15). This action is assumed to be due to the formation of tension fields in the web of the beam, and it was aided by the restraint provided by the top and bottom flanges as well as the stiffeners on either side of the panels that underwent these deformations. The plastic moment of the beam section was developed, and additional comments on plastic moment are included in Chapter 6. Yield lines in the whitewash were observed on either side of the stiffener that was located under the point load.

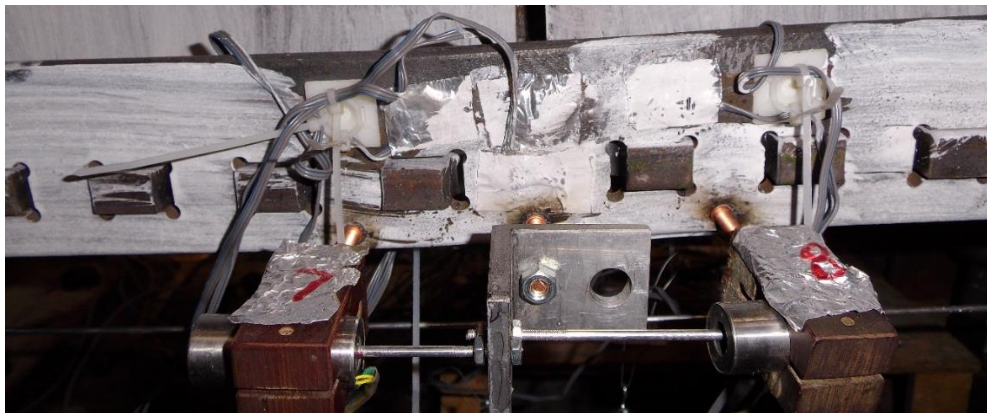


Figure 5.4.11: Test 3 movement of teeth and tension angle



Figure 5.4.12: Deformed beam flange loading the angle at peak load



Figure 5.4.13: Test 3 beam deformed shape

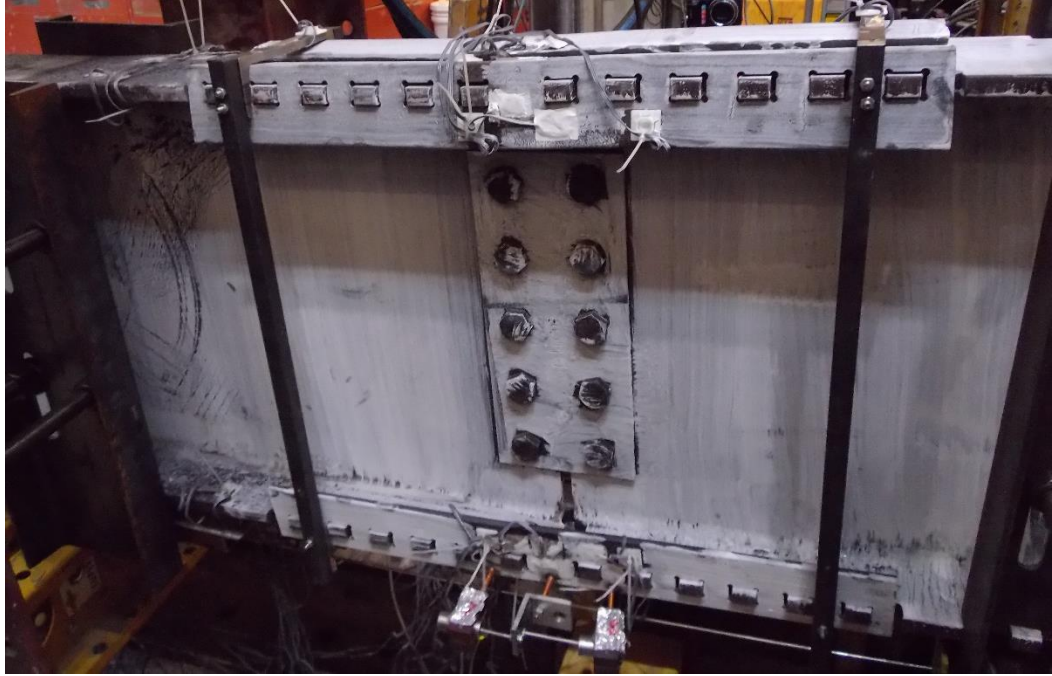


Figure 5.4.14: Test 3 connection post-test

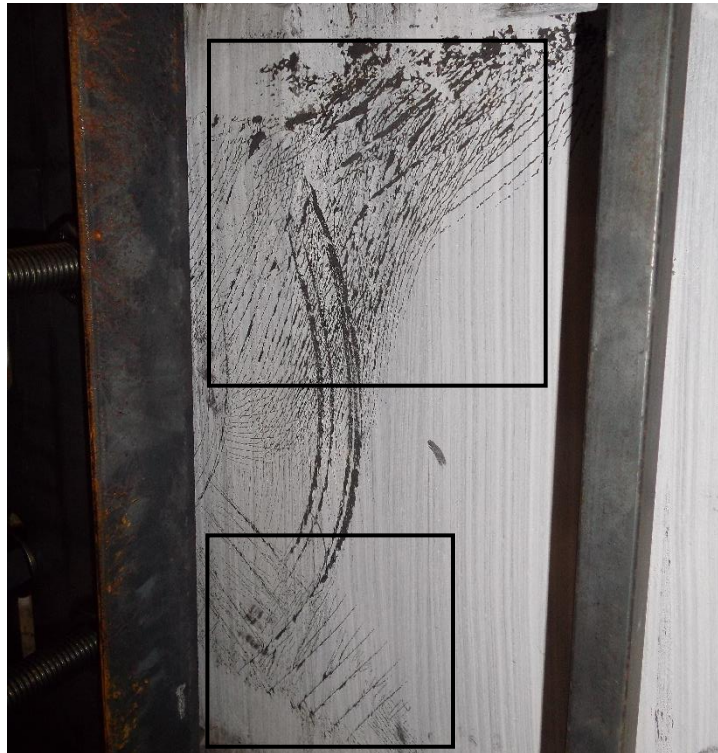


Figure 5.4.15: Test 3 beam web yielding

5.5 Test 4 Results

The fourth and final beam, another W21x57, was tested with no pauses in the loading protocol. The loading beam was elevated with steel plates to allow for up to six inches of beam vertical deflection without having to adjust the brace locations. The data gathered from Test 4 was similar to that for Test 3 since the beams were identical and loaded with the same shear span-to-depth ratio. A peak load of 287 kips was recorded, and the beam section reached peak load at its plastic moment capacity, which is demonstrated in Chapter 6.

5.5.1 Test 4 Displacement Data

The displacement data was similar to that of Test 2 and Test 3. The load vs. deflection data from string potentiometers and LVDTs is included in Figures 5.5.1 through 5.5.3. The load vs. displacement plot shown in Figure 5.5.1 indicates unequal vertical displacements due to the presence of shear, similar to Tests 2 and 3.

The horizontal LVDTs in Test 4 recorded the lowest horizontal movement of any of the four tests (Figure 5.5.2). This was due to the connection assembly and bolt hole tolerances in the shear plate. Although the connection was designed identically to the one in Test 3, it had smaller gaps from tolerances when assembled. Figure 5.5.4 is an image of the beam prior to loading, and the gap between beam webs below the shear plate is visibly larger than it is above the shear plate. Because of this serendipitous configuration, the angles started resisting load at relatively low beam deflections. In the first test, the angles did not start carrying load until the beam had deflected roughly $\frac{3}{4}$ of an inch (Figure 5.1.2), but in the fourth test they started carrying load seemingly immediately (Figure 5.5.2).

Once again, the angle LVDTs measured asymmetric behavior. LVDT 7 failed to record data and was omitted from Figure 5.5.3. A loosened restraint of the LVDT rod was likely the cause of this. LVDT 5 and 6 were located nearest the point load and both yielded at a much lower load than LVDT 8, located away from the point load. This is consistent with the plots from Test 2 and Test 3 (Figures 5.3.3 and 5.4.3).

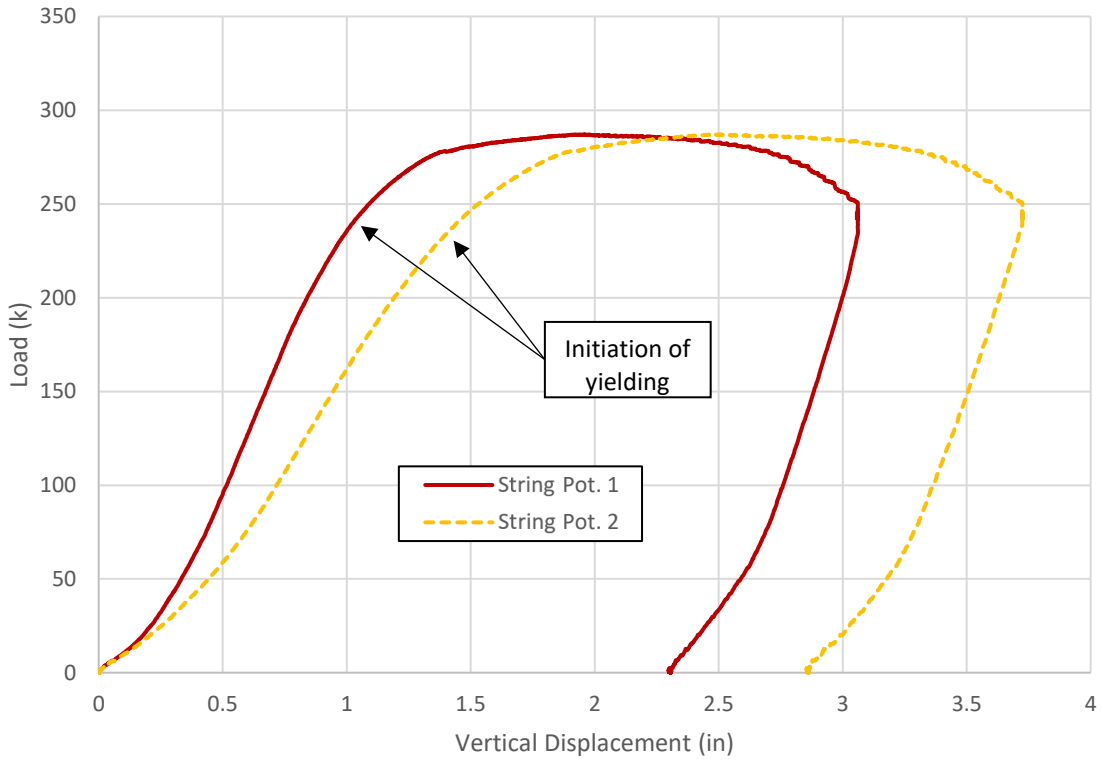


Figure 5.5.1: Test 4 load vs. vertical displacement

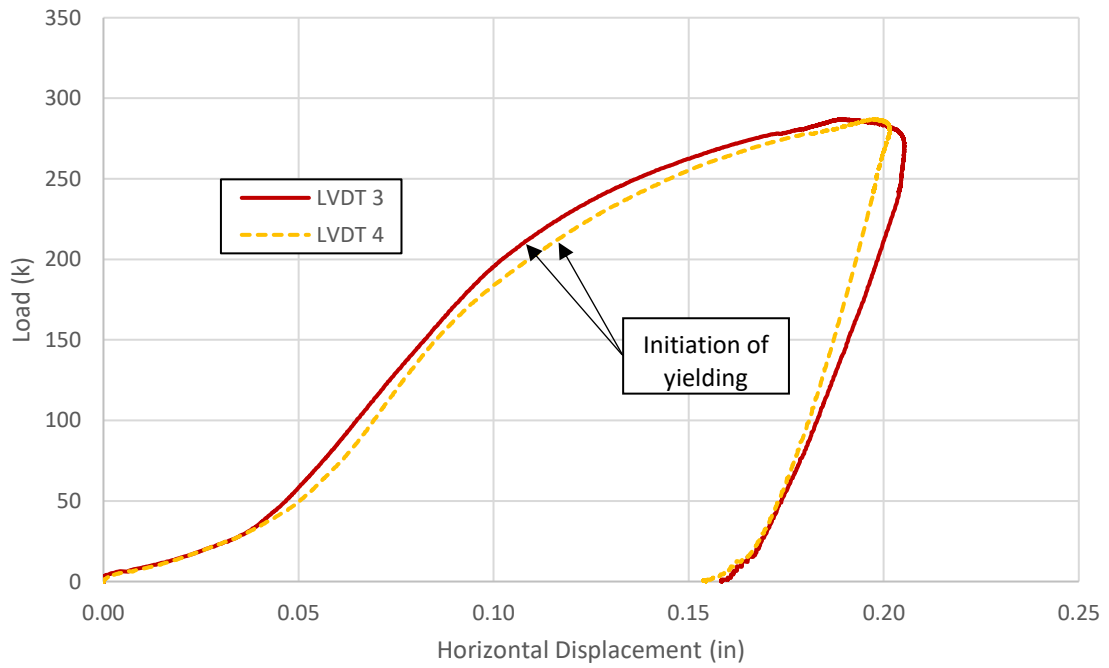


Figure 5.5.2: Test 4 load vs. horizontal LVDT displacement

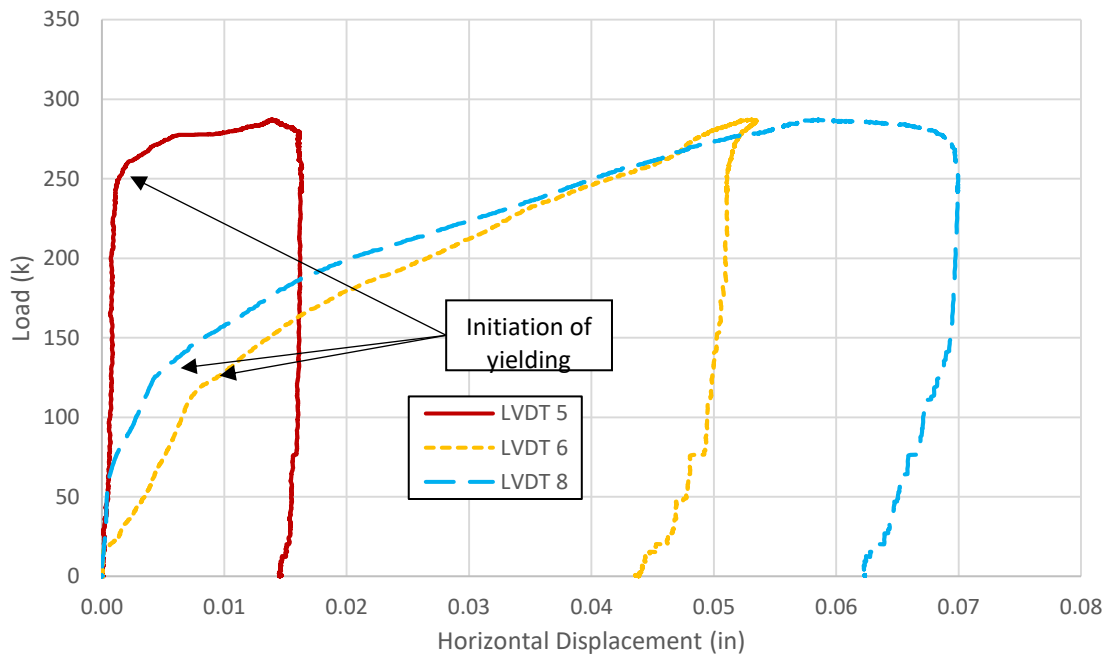


Figure 5.5.3: Test 3 load vs. angle LVDT Displacement

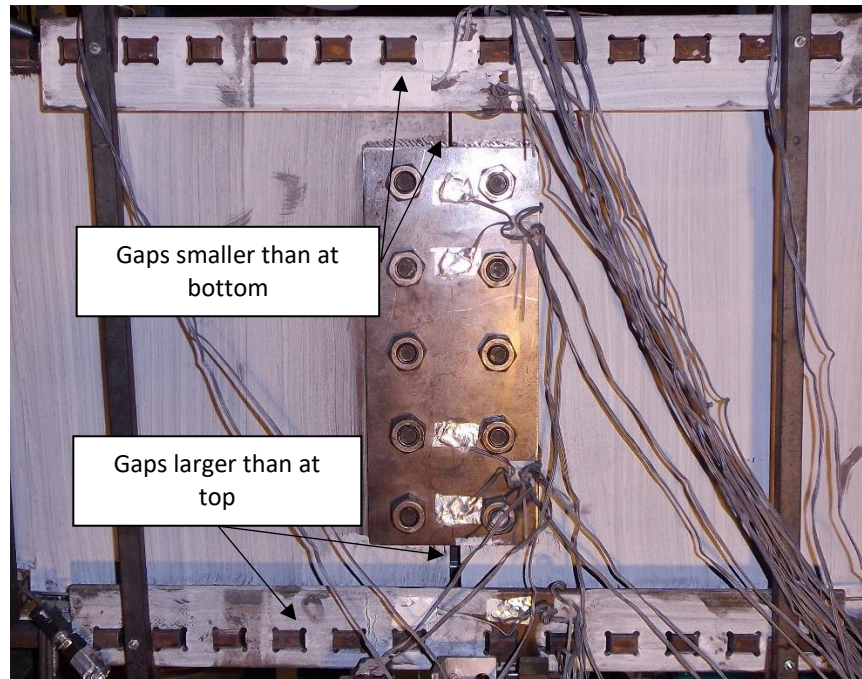


Figure 5.5.4: Test 4 connection prior to loading

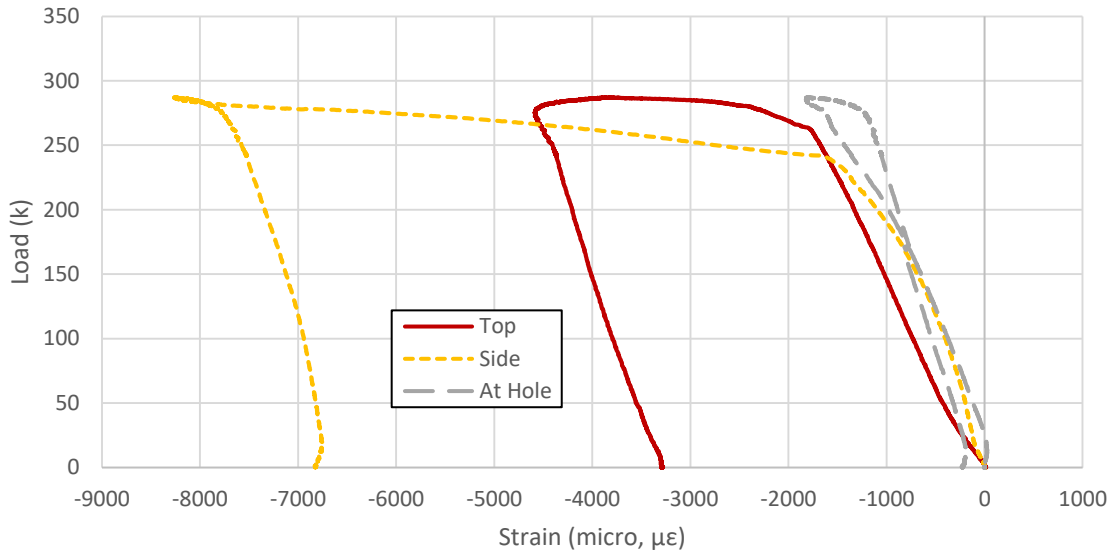
5.5.2 Test 4 Strain Data

Strain data is presented in Figure 5.5.5 through Figure 5.5.10. Axial strain data is given for beams, angles, two channels, and one plate. One strain gage on the beam flange section did not record any data and was omitted.

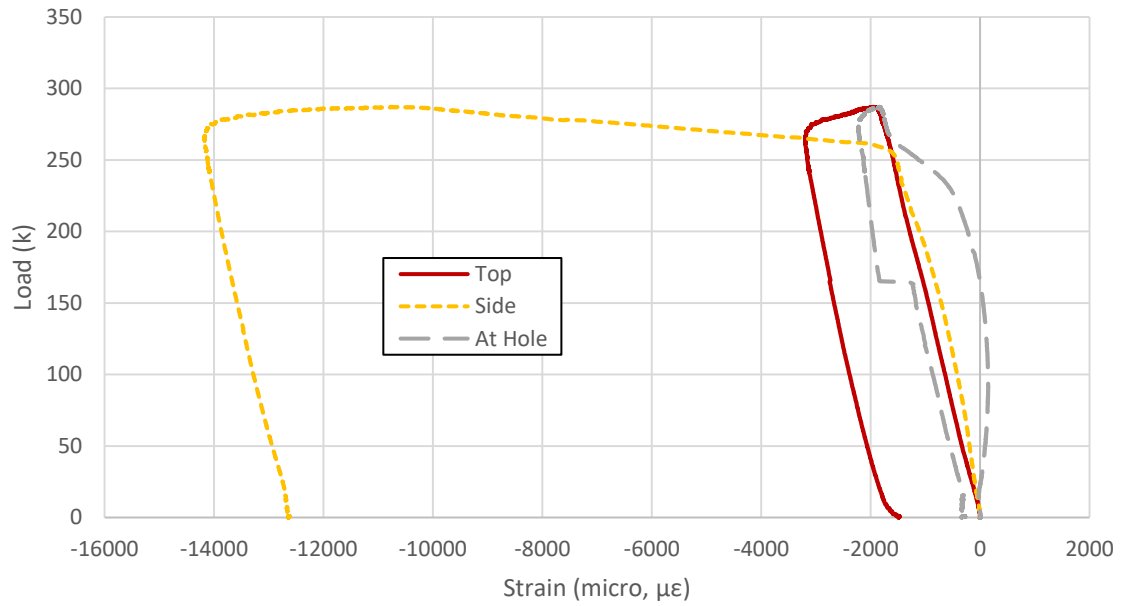
Just like Tests 2 and 3, gages on one of the tension angles recorded a sudden loss in strain during the strain hardening region of the load vs. strain curves (Figure 5.5.6). The compression angles measured plasticity in each region instrumented (Figure 5.5.5).

The beam data was consistent with the measurements from each of the other tests. The instruments on the bottom of the beam flange within the connection recorded inelastic behavior only in Gage 35 and Gage 36 (Figure 5.5.8). The beam flanges, once again, did not record any inelastic behavior until approximately the peak load had been reached (Figure 5.5.7). Most of the plasticity in the flanges of the beam sections occurred in the constant moment region of the span, which was not instrumented. It was not instrumented because the connection was not located in that region.

The shear plate gages measured strains similar to the ones measured in Test 3. Irregular strain data was measured in the “middle top” gage, and it occurred after the peak load had been reached (Figure 5.5.9). It is possible that local stress redistribution occurred within the plate to cause this. Prior to peak load, the strain distribution remained linear and elastic, and the maximum magnitude of strain recorded was approximately 0.00045.

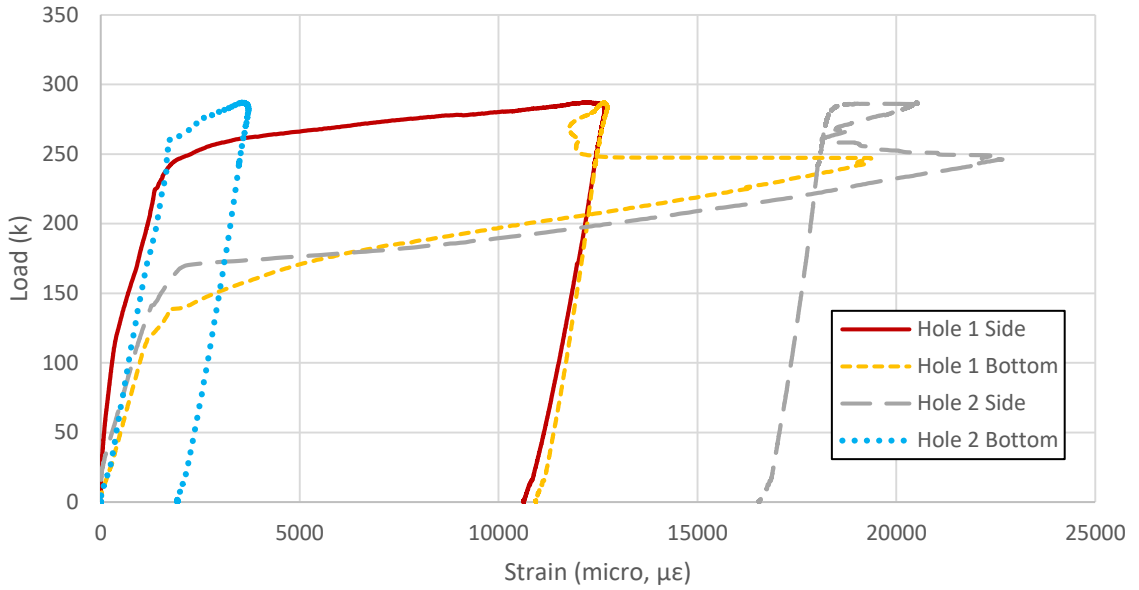


a) Angle 1

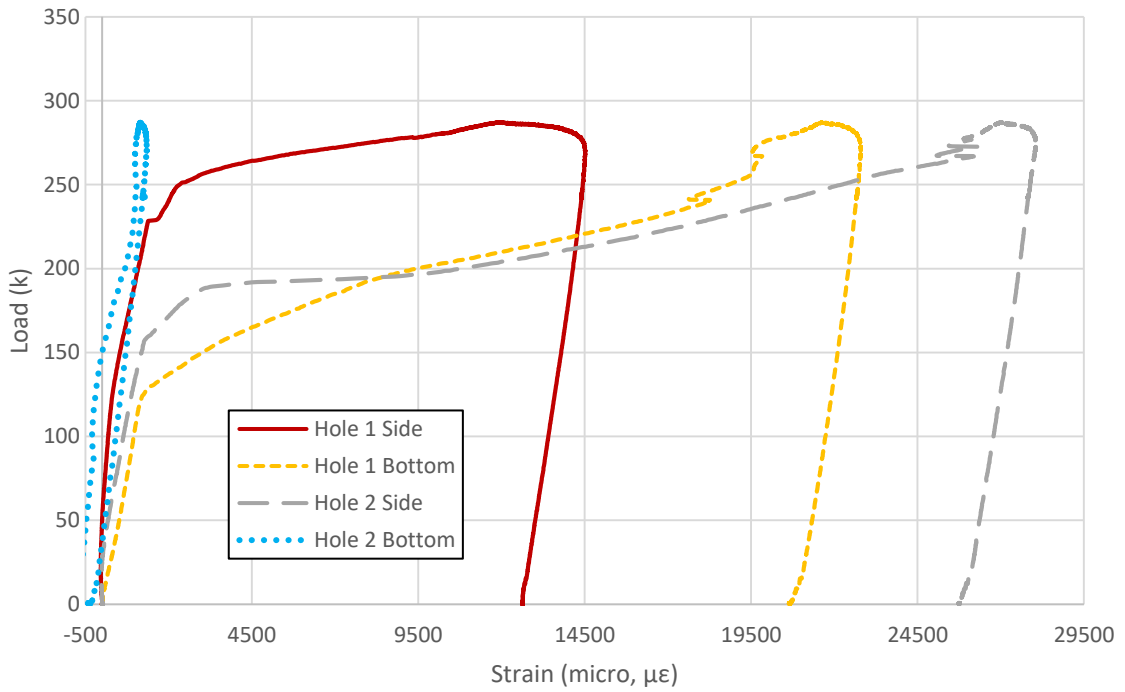


b) Angle 2

Figure 5.5.5: Test 4 load vs. compression angle axial strain

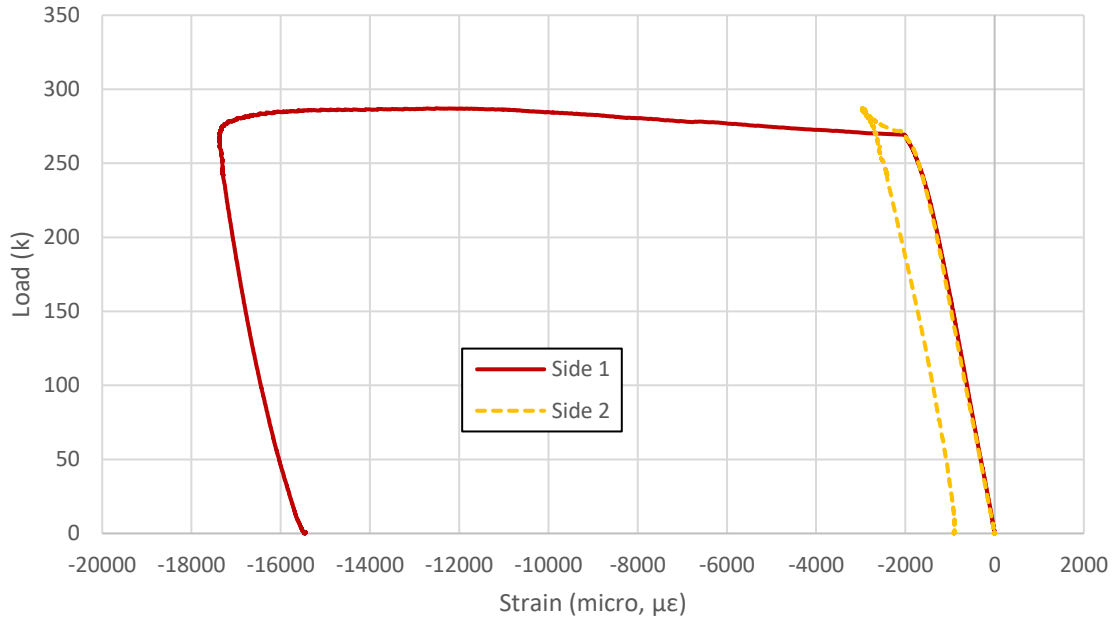


a) Angle 1

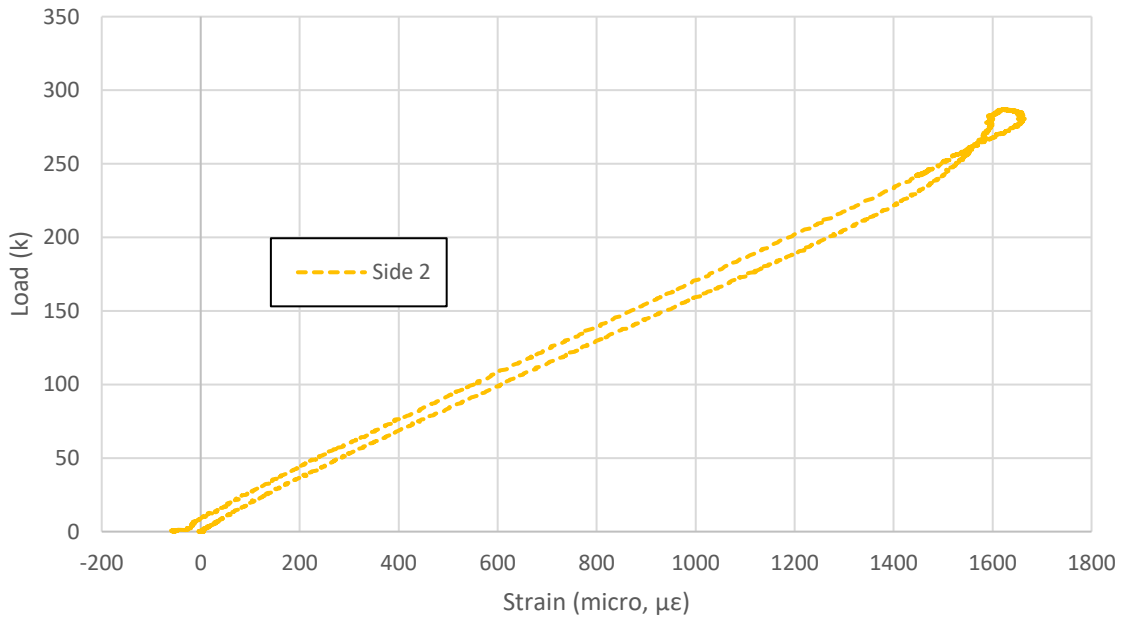


b) Angle 2

Figure 5.5.6: Test 4 load vs. tension angle axial strain



a) Top Flange



b) Bottom Flange

Figure 5.5.7: Test 4 load vs. beam flange axial strain

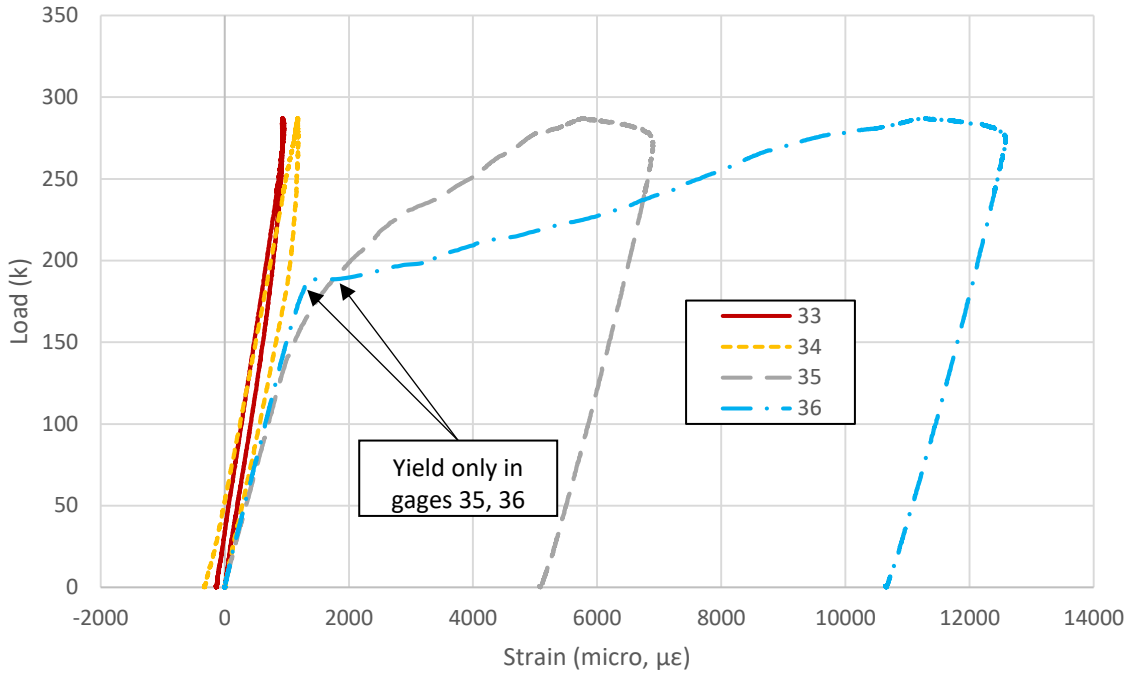


Figure 5.5.8: Test 4 load vs. beam bottom flange strain

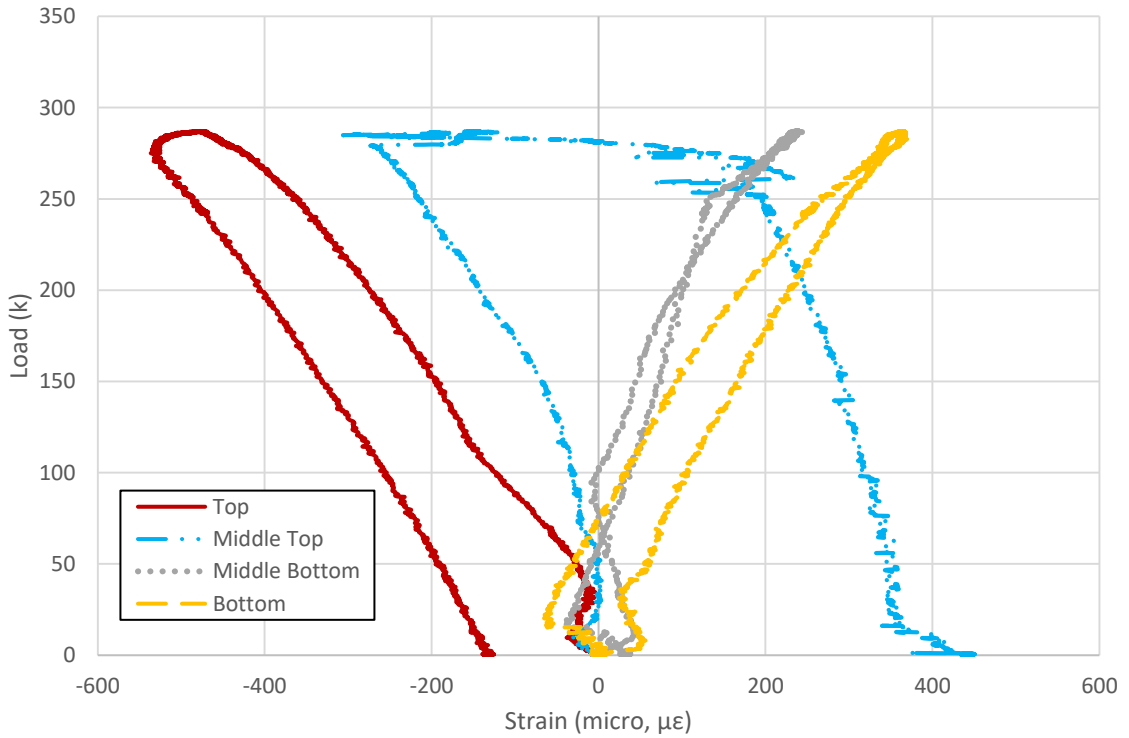


Figure 5.5.9: Test 4 load vs. shear plate axial strain

Higher flexural than axial strains were recorded in the channels, similar to the other tests. The maximum axial strain did not exceed a value of 0.0004 (Appendix D). The flexural strain data is presented in Figure 5.5.10.

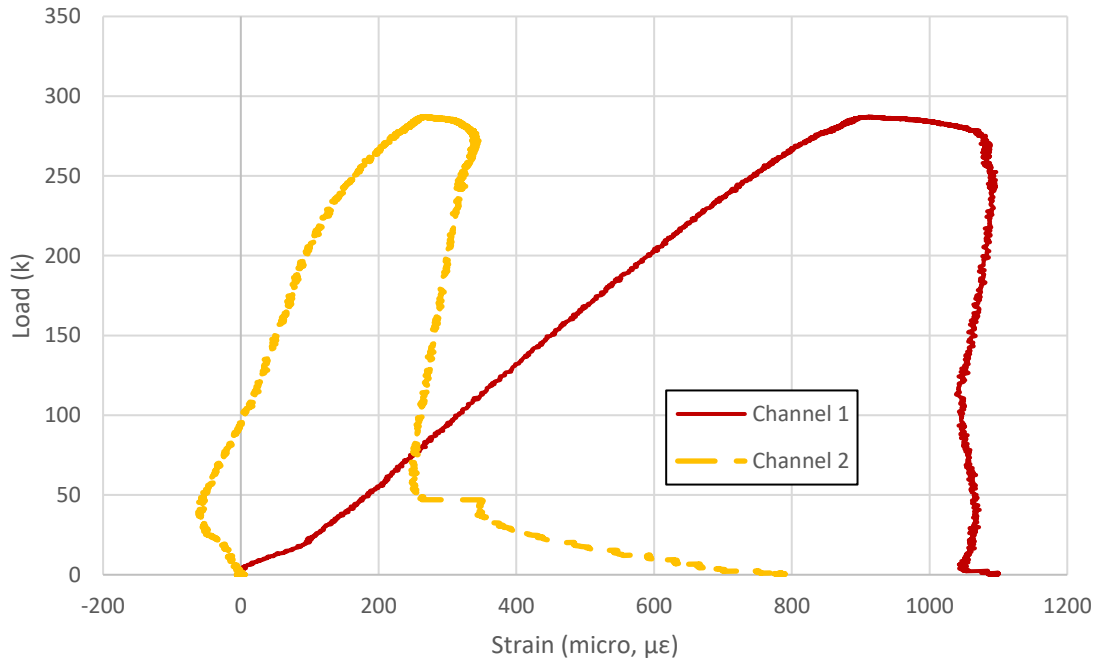


Figure 5.5.10: Test 4 load vs. channel flexural strain

5.5.3 Test 4 Discussion

Yield lines due to both moment and shear were visible in several areas along the span of the beam. The center span of the beam was in a constant moment region, and Figure 5.5.11 shows the yielding of this region after the plastic moment had been reached. Shear yielding was also visible just outside the constant moment region (5.5.13). Shear stresses were imposed on the web of the beam in the constant moment region by the flanges and welded stiffeners from the formation of tension fields. The 45-degree yield lines observed in Figure 5.5.11 are due to this stress state.

The braces restrained all visible lateral deflections until the approximate plastic moment was developed. After unloading, some lateral movement was visible in the

constant moment region (Figure 5.5.12). The lateral buckling was observed between a W12x35 brace and a weaker EFCO section brace. However, the connection region itself was not exposed to significant lateral movement (Figure 5.5.16). The connection behaved nearly identically to the connections tested in Tests 2 and 3, and images of the connection are shown in Figures 5.5.14 and 5.5.15.

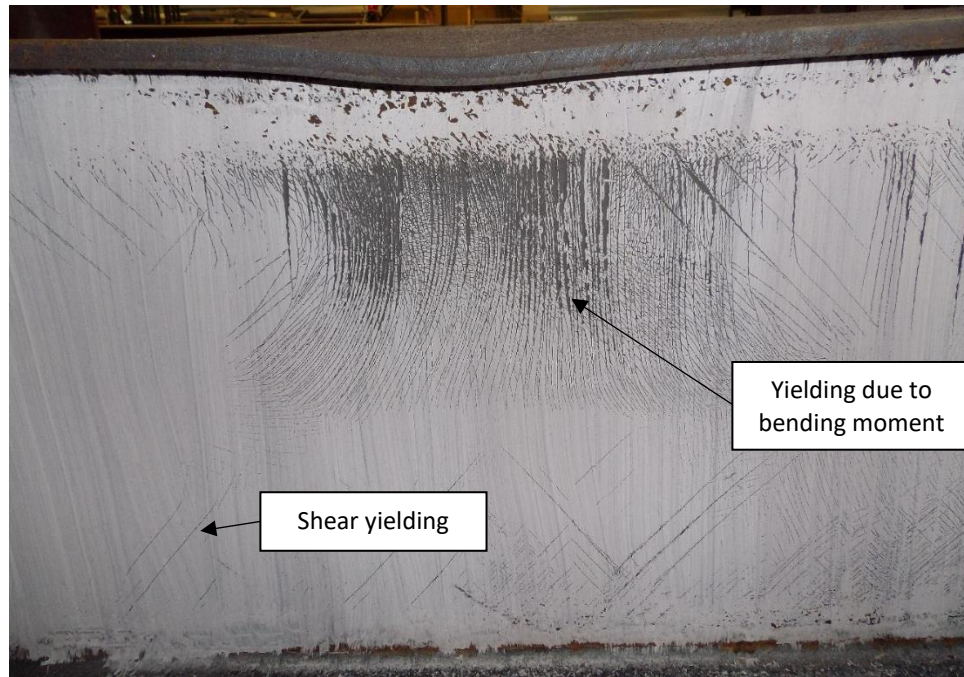


Figure 5.5.11: Test 4 yielding of the beam web at center span



Figure 5.5.12: Deformed beam shape after bracing was loosened



Figure 5.5.13: Shear yielding observed outside the constant moment region

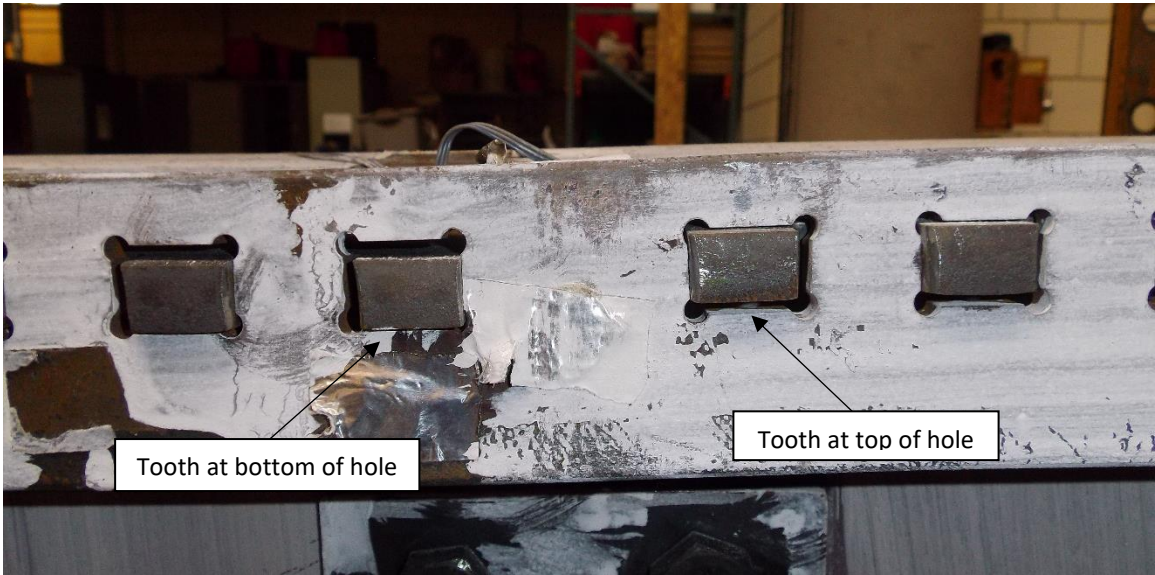


Figure 5.5.14: Test 4 top flange movement at angle centerline

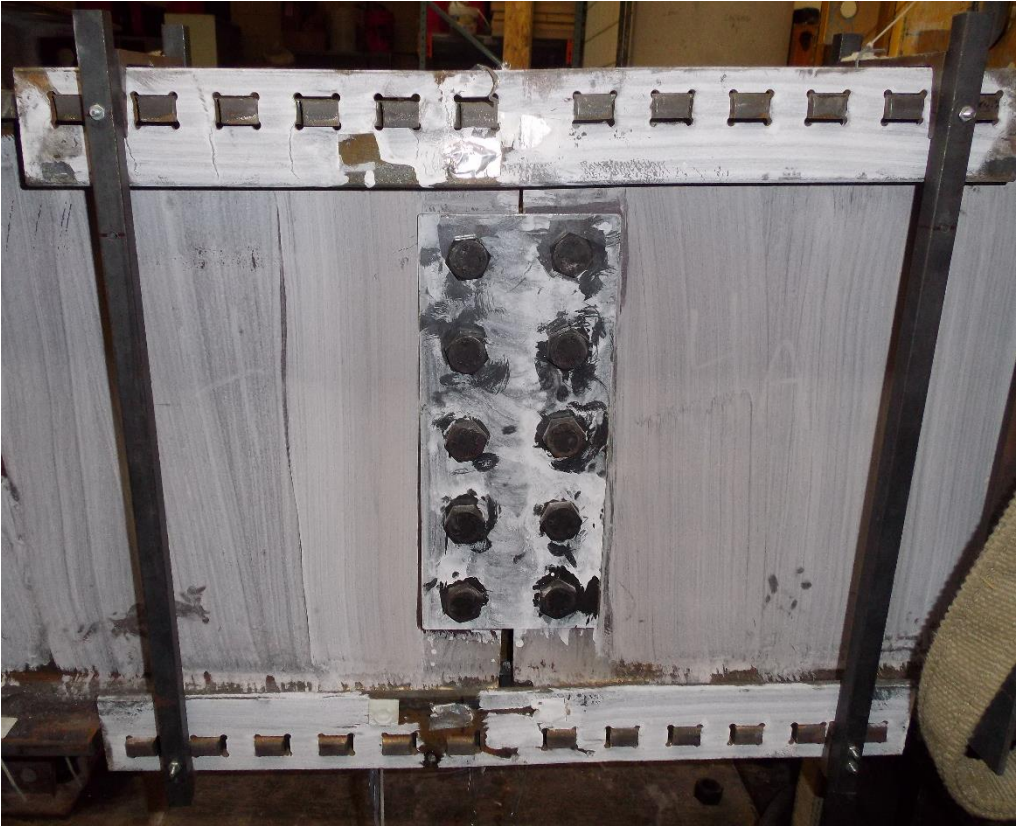


Figure 5.5.15: Test 4 connection after unloading

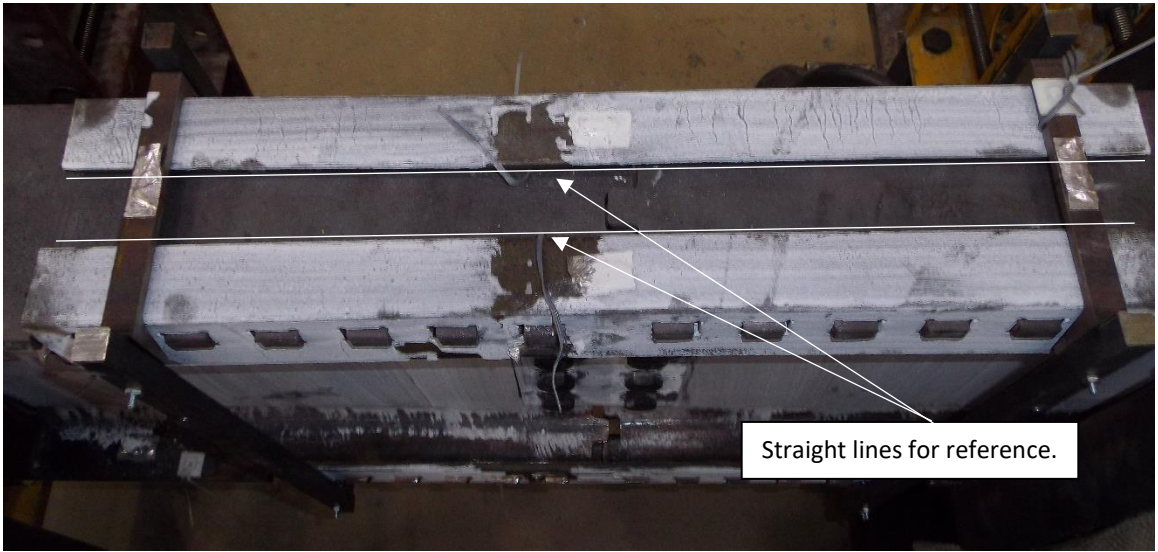


Figure 5.5.16: Test 4 top view after unloading

CHAPTER SIX

Evaluation of Experimental Observations and Measurements

6.1 Review of Test Observations

The experimental program results demonstrated globally and locally how the beam and the connection behaved at various stages of loading. In the figures presented for each test, there exists a linear elastic region, components that experienced nonlinear behavior, and a yield plateau is clearly visible. Strain hardening was also observed for some of the components following the start of yielding, and a peak load was recorded for each test. Following the peak load, the specimens lost strength and the tests were stopped. All of the beams experienced some degree of lateral-torsional buckling at peak load. However, for several of the test beams, peak loads occurred at the time that plastic moment capacity was attained.

6.2 Demands on Angles

The distribution of strains in the tension and compression angles demonstrated that the magnitude of plasticity experienced in the angles varied. Before any yielding occurred, the strain measurements recorded in tension and compression angles were roughly equal. After yielding was initiated, however, variation among strain measurements was recorded. This is demonstrated in strain distribution data from Tests 3 and 4 (Figure 6.2.1 and Figure 6.2.2). One strain measurement from each of the four angles was recorded at various instances of load, and each measurement was taken at the same location underneath a hole at the center of the angle. Test 1 and Test 2 did not have enough reliable data recorded to perform this same analysis.

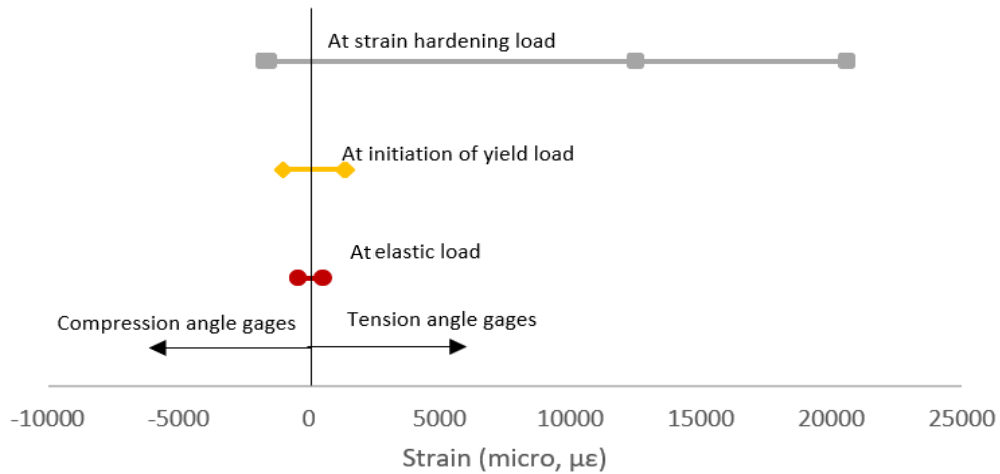


Figure 6.2.1: Test 3 distribution of strain measurements in angles

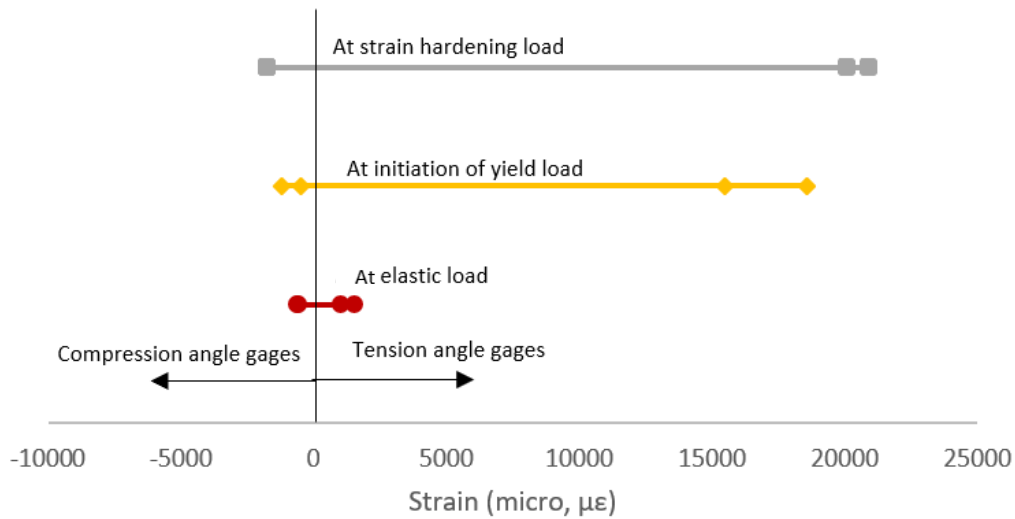


Figure 6.2.2: Test 4 distribution of strain measurements in angles

In each test, the first instruments that recorded nonlinearity were the strain gages installed on the tension angles. The strain gages on the compression angles were the next to demonstrate nonlinear behavior. In Test 1, the pure moment test, the angles were loaded symmetrically and recorded similar strains on each side of the angle. In the tests that included shear, the angles clearly began yielding on one side of the centerline before the other. Since these tests did not load the specimen with constant moment along the entire length of the connection, the moment on one end of the connection region was

higher than it was on the other. For example, in Test 3, the calculated bending moment at one end of the connection was over 300% higher than it was at the other end at peak load. Shear and moment diagrams in Figure 6.2.3 demonstrate this difference.

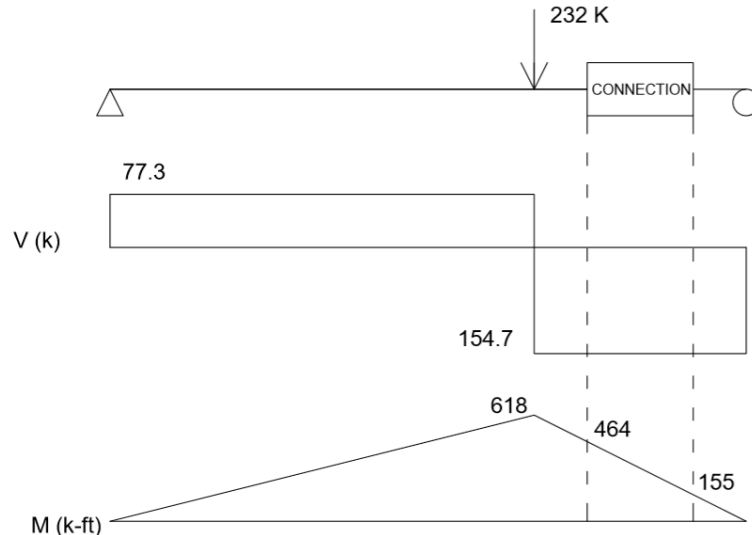


Figure 6.2.3: Shear and moment diagram for Test 3 at peak load

When the angles were designed, the entire angle was assumed to undergo the moment experienced at the centerline. Since this was not true in the angles loaded asymmetrically, some plasticity was observed in the tension angles of Tests 3 and 4 before the design loads were reached. These were the only instances of nonlinearity prior to reaching the design load that was observed in any of the four tests.

6.3 Beam Flange Development

As intended in the design procedure, the beams remained linear elastic when the angles started yielding. In each test, the first region on the beam where nonlinearity was recorded was at the centerline of the bottom flange of the beam. The highest strains on the bottom flange were recorded at the end of the connection region, and the lowest strains were recorded near the centerline of the connection. This feature is demonstrated

in Figure 6.3.1. The left side of the image is at the centerline of the connection (i.e. the end of a beam segment that is joined to another segment by means of the side intermeshed connection), and in this region accumulation of strain occurs from left to right along the flange. As the strains accumulate from left to right, the axial force on the flange increases from zero to a maximum value after the rightmost tooth. At the right side of the connection region, load transferred to the flange from all teeth was being recorded in the strain measurements. The strains measured at 90% of peak load in Test 4 are included above the image to demonstrate this. Although the teeth on the left side of the image seem to have experienced relatively low strains, these teeth were necessary to pass the tooth shear force requirement in the design procedure. All plasticity recorded on the beam bottom flanges occurred after the intended design load had been reached.

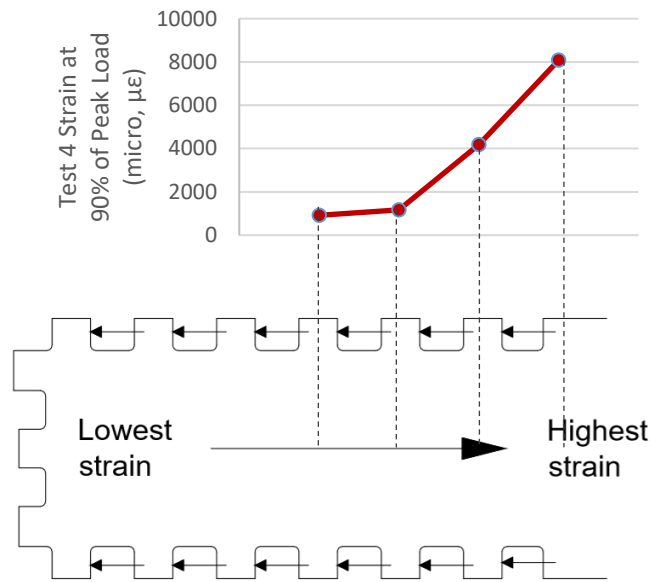


Figure 6.3.1: Test 4 beam bottom flange strain distribution

The remaining strain gages on the beam recorded flange strain measurements outside of the connection region. In each test, these instruments recorded only linear elastic behavior until the peak load was reached. This feature indicates that at the peak load the beam section itself had likely reached its capacity.

6.4 Moment Capacity of Test Beams

The plastic moment for each section was calculated using the material properties specified in the fabrication mill test certificates, and these calculations are included in Appendix C. Based upon these calculations and the yielding observed in each specimen, the plastic moment was reached in Tests 2, 3, and 4. It was not reached in Test 1 because of the early occurrence of lateral torsional buckling due to inadequate bracing. The plastic moment analysis results are tabulated in Table 7. It is also noted that in Tests 2, 3, and 4, the connections were not subject to the maximum moment due to their location along the beam.

Test	Connection Design Moment (k-ft)	Maximum Connection Moment (k-ft)	Maximum Beam Moment (k-ft)	Calculated Beam Plastic Moment (k-ft)	Moment at Connection at Mp of Beam (k-ft)	Max M in beam / Mp of beam
1	126	337	337	398	398	0.84
2	126	274	411	398	265	1.03
3	179	310	620	592	296	1.10
4	179	288	575	592	296	0.97

The first test was the only one where the connection was located in the region of maximum moment in the beam. This was also the only test where the plastic moment capacity of the beam was not developed at the peak load. In each of the other tests, the maximum moment occurred away from the connection and caused a failure in the beam section, a beam section that did not contain the side-intermeshed connection. It is possible that the connection could have resisted additional load in Tests 2,3, and 4, but the beam section reached its peak load and controlled the failure of the specimen. Conversely, it is possible that the beam in Test 1 could have resisted more load if the bracing system had prevented lateral-torsional buckling as early as it occurred.

6.5 Sources of Moment Overstrength

The peak moment that was reached in Test 1 indicated that the connection possessed more capacity than initially calculated. The sources that contributed to this overstrength are listed and discussed in this section.

6.5.1 Moment Contribution of the Shear Plates

Although the connection was designed assuming only the angles resist bending moment forces, moment was resisted by the shear plates as well. The data recorded in the shear plates can be used to estimate how much moment capacity they contributed. In the shear plates, only linear elastic behavior was recorded. Figures 6.5.1 and 6.5.2 show the distribution of strain measurements at 90% of peak load for the shear plates instrumented in Test 3 and Test 4. The four data points represent the strain gages located from the top to the bottom of the plate. The coefficient of determination of the trendline, R^2 , is approximately 1.00 in each plot, and it indicates that the linear trendline matches the data points very closely.

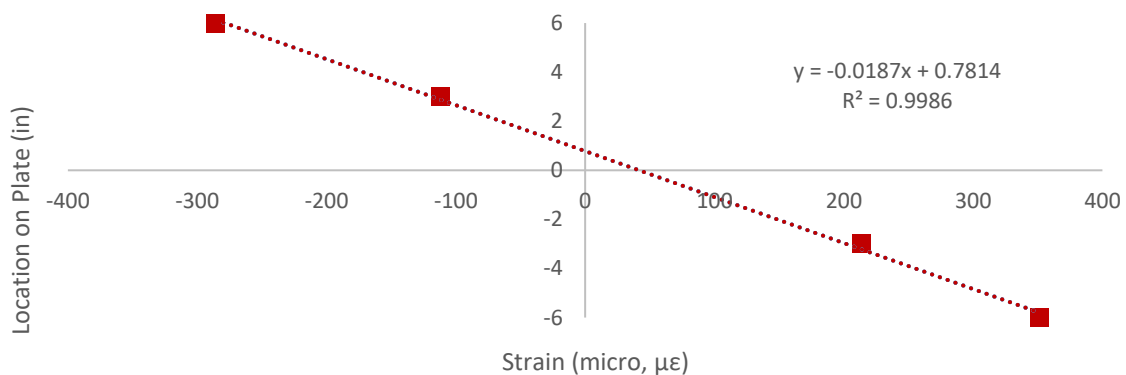


Figure 6.5.1: Test 3 shear plate strain distribution at 90% of peak load

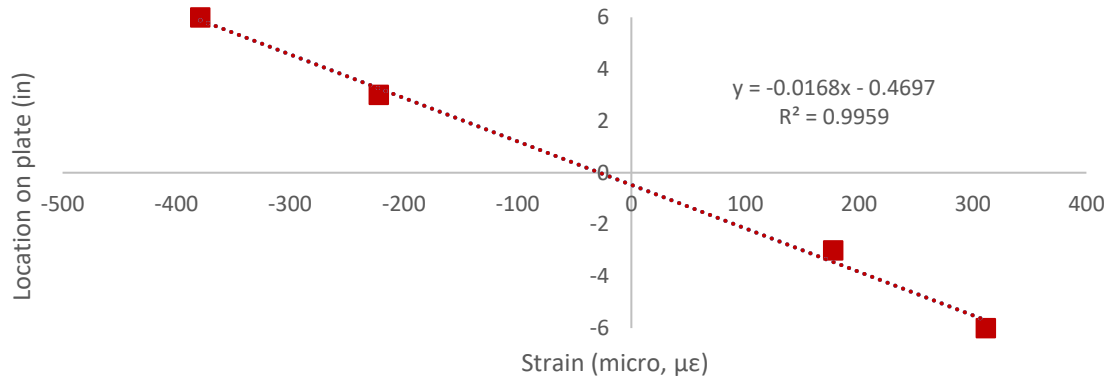


Figure 6.5.2: Test 4 shear plate strain distribution at 90% of peak load

Because of the linear elastic behavior recorded in the plate, the distribution of strains could be used to estimate curvature, k , in the shear plate. Curvature is equal to the inverse of the slope of the linear regression line. Curvature can then be used to solve for the moment in a single shear plate using equation 6.1.

$$M = EIk \quad [6.1]$$

Although the side intermeshed connection was designed assuming that the angles were the only element resisting bending moment forces, the plate moment due to curvature proved that plates did resist some moment. The moments resisted by shear plates at various stages of loading were calculated using the strain gage data, and the results are tabulated in Table 8 for Test 3 and Table 9 for Test 4. The data in the tables indicates very high correlation between strain and location along height of the plates, as well as moments in the shear plates as large as 7.6% of the connection moment.

Table 8: Test 3 Shear Plate Moments						
Load (k)	Moment (k-ft)	% of Peak Load	R²	Curvature (1x10⁻⁵)	Moment in Plates (k-ft)	% of Total Moment Resisted by Plates
139	186	60	1.00	2.49	7.6	4.1
186	247	80	1.00	3.86	11.9	4.8
209	278	90	1.00	5.35	16.4	5.9
220	294	95	0.99	6.49	19.9	6.8
229	305	100	0.99	7.14	21.9	7.2

Table 9: Test 4 Shear Plate Moments						
Load (k)	Moment (k-ft)	% of Peak Load	R²	Curvature (1x10⁻⁵)	Moment in Plates (k-ft)	% of Total Moment Resisted by Plates
172	172	60	0.99	3.38	10.4	6.0
229	229	80	1.00	5.0	15.3	6.7
257	257	90	1.00	5.95	18.3	7.1
272	272	95	0.99	6.58	20.2	7.4
286	286	100	0.98	7.04	21.6	7.6

6.5.2 Moment Contribution from Bearing of Beam Webs

Moment forces at the connection were also resisted by bearing contact between the two beams. As load increased, the top flanges of the two beams moved closer together until contact was established. Additional resistance at the top flange would have theoretically elevated the neutral axis of the connection region.

The couple comprising the compression from bearing in the top flange and added tension in the shear plates can be defined using the strain data in the shear plates. That is, the shear plates are subjected to combined flexure and axial tension, in addition to vertical shear. The added tension stress can be computed from the strains measured in the shear plates because they remain linear elastic. The strains in the shear plates are obtained from the superposition of axial tension and bending. Thus, the tensile strain is obtained as follows.

$$e_{sp,a} = \frac{1}{2}(e_t - e_s) \quad [6.2]$$

e_t = the larger (tensile) strain in the bottom fiber (face) of the shear plates
 e_s = the smaller (compressive) strain in the top fiber (face) of the shear plates
Tension is assumed to be positive and compression negative

The net tensile force in the bearing plates is obtained as follows.

$$T_{bg} = 2A_{sp} E_s e_{sp,a} \quad [6.3]$$

A_{sp} = the area of one shear plate

The moment from the bearing-plate tension mechanism is obtained as follows.

$$M_{bg,2} = T_{bg} d_{sp,f} \quad [6.4]$$

$d_{sp,f}$ = the distance from the shear plate center to beam compression flange centroid

These calculations could be performed using the strain data from Test 3 and Test 4. For each test, the moment from the bearing-plate tension mechanism was calculated to be nearly 30 kip-ft, which represented approximately 11% of the total moment at the connection.

6.5.3 Decomposition of Moment Overstrength

Analysis was performed to decompose the moment overstrength of the connection in Test 1. Test 1 was selected since the angles experienced the highest stresses in this test. To perform the analysis, the stress in the angle was assumed to be the yield stress from mill test certificates (Table 2). The moment from bearing-plate tension action was also

assumed to remain consistent between each test. This produced a value of 30 kip-ft of moment, as calculated in Section 6.5.2.

$$\frac{\text{Connection } M_{max}}{\text{Target } M_{max}} = \frac{0.84}{\frac{1}{3}} = 2.52 \quad [6.5]$$

So, the connection experienced 2.52 times the moment that it was designed to resist. The following calculations explain why this overstrength existed.

$$\frac{\text{Actual } F_y}{\text{Specified } F_y} = \frac{58.6}{36} = 1.63 \quad [6.6]$$

$$\text{Additional overstrength} = \frac{2.52}{1.63} = 1.55 \quad [6.7]$$

The shear plates were calculated to have contributed to nearly 8% of the bending moment capacity. The overstrength can then be reduced by this amount.

$$\frac{1.55}{1.08} = 1.44 \quad [6.8]$$

Since the flexural contribution from the flange bearing and shear plate axial tension is assumed to remain at 30 kip-ft, this also reduces the overstrength.

$$\text{Flange bearing moment contribution} = \frac{30 \text{ k-ft}}{398 \text{ k-ft}} \times 100\% = 8\% \quad [6.9]$$

$$\frac{1.44}{1.08} = 1.33 \quad [6.10]$$

Additional contribution from flange bearing and post-yield straining of the tension angles could also be calculated from the following equation.

$$\Delta f_{y,actual} = f_{u,actual} - f_{y,actual} = 75.3 - 58.6 = 16.7 \text{ ksi} \quad [6.11]$$

$$\begin{aligned} \Delta M &= 2A_{angle}\Delta f_{y,actual}d_c = 2(1.55)(16.7)(18 - 0.605) \quad [6.12] \\ &= 75 \text{ k} - ft \end{aligned}$$

$$\frac{75 \text{ k} - ft}{398 \text{ k} - ft} \times 100\% = 19\% \quad [6.13]$$

$$\frac{1.33}{1.19} = 1.12 \quad [6.14]$$

Since the design procedure included a factor of 1.1 when calculating the failure load of the angles, the remaining overstrength factor may be divided by 1.1.

$$\frac{1.12}{1.1} = 1.02 \quad [6.15]$$

Since a final value of 1.02 was calculated, it may be concluded that moment overstrength was likely due to the mechanisms outlined in the calculations performed in this section.

6.6 Side Angle Contributions to Shear Resistance

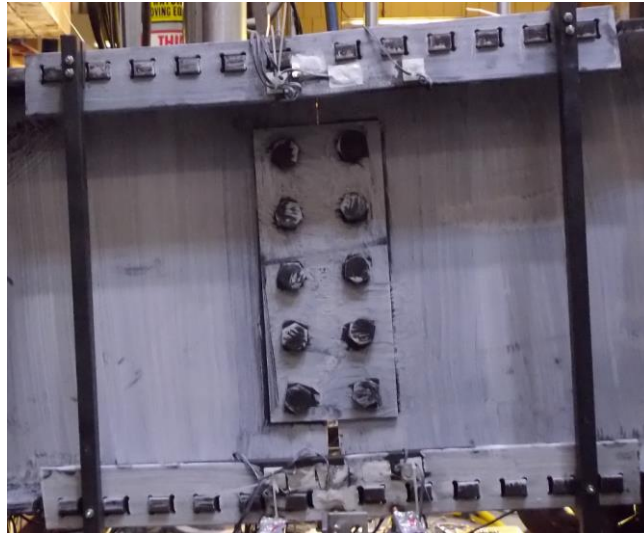
The side angles contributed to the resistance of shear forces. Roughly 150 kips of shear force was resisted at the connection in Tests 3 and 4, and although this was well within the loads that the plates were designed to resist, it was evident that the side angles contributed to shear resistance also. The deformed shape of the angles from Tests 2, 3, and 4 demonstrated the presence of shear forces in the angles. Had no shear force

been resisted, the angles would have deformed due to bending only and looked like the angles from Test 1. A comparison of angles from Test 1 and Test 3 is pictured in Figure 6.6.1.

Although the magnitude of the shear force that was resisted by the angles was unknown, it can still be inferred that the shear plates carried most of the shear load. The angles had little stiffness and shear resistance, and even if they hadn't contributed any shear capacity at all, the plates still would have been sufficient.



a) Test 1 angle deformation with no shear



b) Test 3 angle deformation with shear

Figure 6.6.1: Angle deformation with and without shear

6.7 Channel Restraint Forces

The channels used to restrain the angles proved the importance of a lateral restraint device on the angles. The channels restraining the angles in compression experienced the highest strains, and the flexural strains were higher than the axial strains. This was because the loads applied on the channels were eccentric and created bending in the web of the channel, as shown in Figure 6.7.1. The maximum axial strain that was measured was approximately 0.0004 in Test 1 (Figure 5.1.8). This strain corresponds to a stress of 11.6 ksi and a lateral force of approximately 1.8 kips.

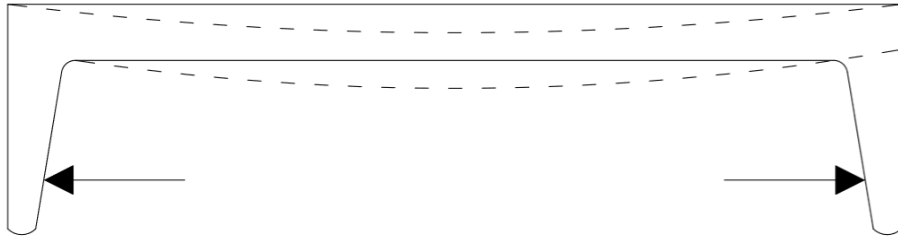


Figure 6.7.1: Channel loading

Since an axial force was measured in the channel restraints, it can be concluded that frictional resistance alone was not enough to prevent the angles from sliding off the teeth. Table 10 summarizes the channel axial forces from each of the four tests. The ratio of maximum compression angle axial strain to maximum channel axial strain is included in this table.

Table 10: Load in Channel Restraints				
Test	Max Axial Strain (micro)	Max Axial Stress (ksi)	Max Axial Force (k)	Max Angle Axial Strain/ Max Channel Axial Strain
1	400	11.6	1.8	37
2	190	5.5	0.9	210
3	395	11.5	1.8	44
4	340	9.9	1.6	41

6.8 Local Nonlinearity

Plasticity may have also occurred in various components of the specimens due to local yielding. For example, in Test 3 the top flange buckled to where it came into contact and started loading the end of one of the angles. This resulted in local plasticity at the end of the angle, and it is pictured in Figure 6.8.1.



Figure 6.8.1: Local plasticity in Test 3

Another location where local plasticity likely occurred was at the bolts in the shear plate. Finite element modelling was conducted in conjunction with the experimental testing, and the model showed plastic behavior of the bolts and in the plates directly around the bolt holes. It was not possible to measure these deformations with strain gages, and it was also not visible without disassembling the connection. The resistance to removal by the bolts in the shear plates indicated that plastic deformation of the bolts did occur.

Restraint in the removal of the angles after the tests indicates that the permanent deformations in these angles kept them locked in place on the beam flange teeth.

6.9 Potential Design Procedure Modifications

The experimental testing program proved that the intermeshed connection can successfully resist gravity loads. The connection possessed the required strength for design loads, and it showed ductility at extreme loads. Although the results from this experimental program were largely positive, modifications to the design procedure could lead to more optimal results. The potential design procedure modifications are included in Table 11.

Table 11: Potential Design Procedure Modifications	
Modification	Description
Asymmetrical connections	Uniform load was not always applied along the length of the connection. Asymmetrical connections could be designed in these cases.
Include shear plate moment resistance	The shear plates were proven to resist some of the bending moment forces. These could be included in a future design to create a less conservative connection.
Elimination of 1.1 factor in peak angle load calculations	This factor contributed to the moment overstrength.

6.9.1 Asymmetrical Connections

As discussed in section 5.6, Tests 3 and 4 each had locations on the tensile angles that yielded before the design load was reached. This happened because the connection was designed to resist loads at its centerline, but higher loads existed at one end of the connection region. In future designs, the connection could be designed for the load experienced at the connection centerline initially. Then, once the length of this initial connection is known, the maximum forces within the connection region could be identified. If these forces are larger than what the initial design from analysis at the centerline can withstand, another design iteration may be performed. However, this approach could lead to an overdesigned angle if load greatly varies over the length of the connection region as it did in tests three and four. Because of this, perhaps the connection could be longer on one side of the centerline than on the other.

6.9.2 Moment Overstrength

The connection resisted design loads well, but it generally resisted higher loads than it was expected to at peak load. The design procedure intended for the angles to be the only component of the specimens that yielded. Although the angles were the first component to yield, the beam sections experienced yielding prior to the ultimate load. Part of this occurred because maximum moment was away from the connection in Tests 2, 3, and 4. Also, since the shear plate moment contribution was neglected during the design procedure, the angles were not required to resist as much moment as was calculated.

To better estimate loads in the angles, perhaps moment contribution from the shear plate could be estimated and included in the design procedure. Stress distributions in wide flange beams create the highest tensile and compressive forces in flanges rather than the web, and this is largely due to the high width of the flange relative to the width of the web. From the strains measured in the testing program, the shear plates were estimated to carry up to almost 8% of the moment. In both W18x46 and W21x57 beams, the web thickness is approximately 6% of the beam flange width. Perhaps the ratio of web thickness to beam flange width could be used in future designs to estimate how much moment is resisted by the shear plates.

The factor of 1.1 used to calculate peak angle load could also be eliminated in future designs. This factor contributed to the moment overstrength that was observed in the testing program. Additional moment overstrength did occur due to bearing of the flanges and webs of the beams, however, this moment contribution was only able to be calculated after the test. A rational way to estimate this moment contribution in the design phase would need to be developed to include this in the design procedure.

CHAPTER SEVEN

Summary, Observations, Conclusions and Recommendations

7.1 Summary

This new type of intermeshed steel connection was designed to connect steel beams. The connections included four steel angles that were intermeshed onto rectangular teeth cut into the sides of the top and bottom flanges of wide flange steel sections. A pair of bolted, rectangular plates was used to connect the beam webs. The angles were intended to develop the axial forces in the beam flanges, and the plates the shear forces in the webs. Simply supported beams featuring these connections were fabricated using high-definition plasma cutting for the rectangular teeth in the flanges and water jet cutting for the holes in the angles. Two variations of the side intermeshed connections were tested for a total of four simply supported beam tests. Forces, strains and displacements were measured in each test, and data analysis was performed to verify the procedure that was developed to design the connection. The results from this experimental study expanded the knowledge base concerning intermeshed steel connections and how they may be implemented in the design and construction of steel frame buildings in the future.

7.2 Observations

The intermeshed steel connection was proven to be a robust and ductile connection that could transfer bending moment and shear forces. The connections were able to resist the imposed forces from the simulated gravity loading, develop ample plasticity in the intended components (the angles), undergo some unintended cycles of repeated loading, and ultimately enable the beam to develop bending moments that approached, matched, or exceeded the calculated plastic moment capacity of the beam section. The angles were designed solely to resist axial forces to generate the moment resistance of the connection, but it was evident that they also experienced shear at high loads. The shear plates located at the web were designed to resist only shear, but these elements resisted some bending

moment as well. Linear elastic behavior was recorded at the design level loads the connections were designed to resist, and nonlinearity was observed at loads approaching and exceeding the strength limits of the beams. Nonlinear behavior started in the angles, and as the peak load was approached, nonlinear behavior was observed in the beam sections as well.

It is concluded that the angles served to transfer loads across the joint between beam sections, and eventually became the sacrificial component of the connection once the beam capacity was reached. The geometry of the teeth in the beam flanges and the rectangular holes in the angles, supplemented with the stress-reducing radii at the corners, performed as intended. The angles developed plastic strains exceeding 20% without any evidence of fracture or ductile tearing in any of the tests.

Most observations from the testing were consistent with the predictions made prior to the experimental program. Stress distributions created the highest local demands at the center of the side angles, and the highest local demands in the beams existed at the ends of the connections. Local failures in the angles, namely fracture and ductile tearing, were avoided with the inclusion of radii at the hole corners, and some local failures in beams were avoided with stiffeners and lateral bracing. In all four tests, there was some degree of lateral or lateral-torsional buckling, even though the measured moment in the last three tests matched or exceeded the plastic moment capacity calculated using the actual yield stress of the beam steel as reported in the mill certification documents. The bracing system that was used did not provide sufficient stiffness to avoid the lateral and lateral-torsional modes, even though it was modified throughout the testing program to enhance its stiffness. Channel restraints were necessary to keep the side angles in place during loading, but the axial force demands on the channels were relatively low, that is, under 2 kips, which represents less than 1% of the axial force in the compression angles. Higher initial seating and lateral loads than originally anticipated were observed, but otherwise testing assumptions projected the outcomes of the experimental program well.

In three of the four tests, the plastic moment of the beam section was developed. The connection remained intact and maintained its ability to carry load in each of these

cases, but it was not located at the maximum moment region. The only test that failed to develop the plastic moment of the beam was the only one with the connection located in the maximum constant moment region. This specimen failed due to lateral torsional buckling of the beam, and this outcome is partly the result of an inadequate bracing system. However, the design target for the moment capacity of the connection was much lower than the plastic moment capacity. The connection was designed to develop one-third of the moment capacity of the beam section calculated using the minimum specified yield stress for the beam steel. By virtue of a larger actual yield stress, as well as strain hardening, and a conservative design procedure, which is patterned after the capacity approach for seismic design, the connection developed a moment capacity equal to 84% of the plastic moment capacity (calculated using the actual yield stress).

7.3 Conclusions

The experimental program confirmed that intermeshed steel connections can resist gravity loads experienced in typical moment frames. The connections may be designed to remain linear elastic under the expected service loads. If an overloading event were to occur, the angles would be the first element to experience inelastic behavior. The tests also showed ample capacity to resist cases of large amounts of overloading.

Intermeshed steel connections are ideally placed near inflection points for gravity loading for beams in moment frames, thus moment demands are relatively low. Such an approach will reduce the length of the connection and number of cuts required during fabrication. This may allow for connections to be designed with a shorter length and fewer teeth than what was tested in this study.

The side intermeshed connection is a complex system that relies on the interaction of many different elements. The connection was designed to avoid stress concentrations and local plasticity when these elements interact. Side angles resist most, but not all, of the bending moment force, and they are also subject to some shear forces. Shear plates resist most, but not all, of the shear force in the connection, and they contribute to some bending moment resistance, thus increasing the total bending moment capacity of the

connection. Initial seating was observed in test data, and visual observations indicated that beam deflection occurs before the elements of the connection (i.e. teeth, angles, bolts and plates) become engaged and resist load.

Plasma cutting and water jet cutting were found to be successful procedures for creating the precise geometry of the intermeshed steel connection. Moreover, this capability was found at steel fabrication shops near the University of Minnesota, and the fabricators were able to meet the needs of the projects without significant changes to their fabrication procedures. The connection was quickly and easily assembled for each test and required no skilled or time-consuming labor. Disassembly of the connection after testing was difficult due to the plasticity experienced in the angles and shear plate bolts. The use of a torch or pry bar may aid with disassembly.

7.4 Recommendations

Optimization of intermeshed steel connection geometry may also be investigated in future research. Finite element analysis can be used to investigate in more detail the performance of these connections. For example, the shear forces and bending moments at the base of the teeth would be difficult to obtain experimentally, and the distribution of these forces along the connection would help in efforts to improve the efficiency of the connection. Additionally, the contributions of the angles to shear strength, and of the shear plates to bending moment strength, could be investigated in greater detail. The influence of the magnitude and distribution of the gaps from tolerances to the various bearing surfaces could also be evaluated, as well as their influence on connection performance under vertical loads. Finally, laboratory testing could explore alternatives to the geometry used in this study.

Different loading scenarios could be used for additional laboratory tests. Every test conducted in this study was a simply supported beam test, but the connection was conceptualized for use in moment frames, in which large negative moments would be present at the supports. Connection performance under these conditions is of interest. Additionally, while the intermeshed connection was not developed for lateral load

resisting elements, it would be part of a building that undergoes drift when subjected to lateral loads. The ability of the gravity frames which feature these connections under such conditions is essential because vertical load capacity would have to be ensured for expected levels of drift. Thus, a cruciform assembly with beams attached to either side of a column could simulate a moment frame and test the intermeshed connection under lateral drift with reversals in the load direction. Lastly, testing of a full-scale moment frame that features intermeshed connections could be used to investigate the performance of an entire system, including any interactions between the connections and the other frame components. Successes in future research could lead to code acceptance and commercialization of intermeshed steel connections for steel frame buildings.

Future work should investigate construction methods that make the intermeshed steel connection marketable and practical in real building construction. For example, the lateral restraint system using channels was important and could be easily instrumented for testing. However, it would not be as practical in construction. A pneumatic steel strapping tool could be used to lock steel restraint straps around the connection instead, or a simple restraint that utilizes threads and bolts could be attached to the connection. The advantage of these devices is that they could be installed minimizing flexural stresses in the restraint device, thus the only force demand would be from axial stress. Vertical deflections, such as those observed during initial seating, would also be impractical in a building, and perhaps some camber could be introduced to eliminate deflections from floor deck weight. Alternatives such as these must be studied in more detail.

REFERENCES

- Al Sabah, S.A., Laefer, D.F., GB Patent Application No 1718746.9, 2017.
- Al Sabah, S.A., Laefer, D.F., GB Patent Application No 1718744.4, 2017.
- American Institute of Steel Construction (2010), *Seismic Provisions for Structural Steel Buildings*, ANSI/AISC 341-10, American Institute of Steel Construction, Chicago, IL.
- American Institute of Steel Construction (2016). *Prequalified Connections for Special and Intermediate Steel Moment Frames for Seismic Applications*, ANSI/AISC 358-16, American Institute of Steel Construction, Chicago, IL.
- American Institute of Steel Construction (2017). *Steel Construction Manual*, 15th Ed., American Institute of Steel Construction Inc, Chicago, IL.
- American Institute of Steel Construction (2019). "Construction Costs." *American Institute of Steel Construction (AISC)*, <https://www.aisc.org/why-steel/resources/construction-costs/>.
- "ConX Systems." *ConXTech Inc.*, <http://www.conxtech.com/conx-systems/>.
- Cordova, P. P., Hamburger, R. O. (2011). "Steel Connections: Proprietary or Public Domain?" *Modern Steel Construction* (Oct 2011), 24-31.
- Dahil, L., Dahil, I., Karabulut, A. (2014). "Comparison of Advanced Cutting Techniques on Hardox 500 Steel Material and the Effect of Structural Properties of the Material." *Metalurgia 53* (2014), 3, 291-294.
- Eurocode3. (1992). ENV-1993-1-1, *Design of Steel Structures*, Commission of the European Communities, European Prenorm, Brussels, Belgium.
- "Facts About Plasma Technology and Plasma Cutting." *BOC*, www.boc-gas.co.nz/en/legacy/attachment?files=tcm:y435-68107,tcm:435-68107,tcm:35-68107.
- Garlock, R. B. (1993). "ATLSS Connections With Moment Capacity." *Theses and Dissertations*. Paper 200.
- Gerfen, K. (2009). "Pin-Furse Joint". *The Journal of the American Institute of Architects*. Retrieved from www.architectmagazine.com
- Krajcarz, D. (2014). "Comparison Metal Water Jet Cutting with Laser and Plasma Cutting." *Procedia Engineering* (Dec 2014). 10.1016/j.proeng.2014.03.061

Matis, P., Martin, T., McGetrick, P.J., Schultz, A., Le, J.-L., Shemshadian, M.E., Labbane, R., Laefer, D., Al-Sabah, S., Truong-Hong, L., Huynh, M.P., "Numerical modelling of the axial load behaviour of flange plate geometries for a novel intermeshed steel connection", *Journal of Constructional Steel Research*, in review.

Perreira, N. D., Fleischman, R. B., Viscomi, B. V., Lu, Le-Wu (1993). Automated Construction and ATLSS Connections; Development, Analysis, Experimentation, and Implementation of ATLSS Connections for Automated Construction. *ATLSS Reports*. ATLSS report number 93-02. <http://preserve.lehigh.edu/engr-civil-environmental-atlss-reports/183>

Schultz, A., Le, J.-L., Shemshadian, M.E., Labbane, R., Laefer, D., Al-Sabah, S., Truong-Hong, L., Huynh, M.P., McGetrick, P., Martin, T., Matis, P., AMASS: Advanced Manufacturing for the Assembly of Structural Steel, in: *Tenth Int. Struct. Eng. Constr. Conf.*, Chicago, May 20-25, 2019.

Shan, Y., Kim, J. Y., Goodrum, P. M., Caldas, C. H., Haas, C. (2014). "Impact of Steel Quick Connection System on Steel Erection Labor Productivity: Case Studies and Simulation Based Analyses." *Canadian Journal of Civil Engineering*, Vol. 41, 1036-1045.

Shemshadian, M. E., Le, J. L., Schultz, A. E., McGetrick, P., Al-Sabah, S., Laefer, D. F., Martin, A., Hong, L. T., Huynh, M. P. Numerical study of the behavior of intermeshed steel connections under mixed-mode loading. *Journal of Constructional Steel Research*. 2019 Sep 1;160:89-100.

Sikora, J. A Summary of Stress Concentrations in the Vicinity of Openings in Ship Structures. Naval Ship Research and Development Center, Report 3889, 1973.

"Tech Tips." *SidePlate Systems*, <https://www.sideplate.com/media/1404/20170930-tech-tips.pdf>.

Tsavdaridis K.D. (2014). "Strengthening Techniques: Code-Deficient Steel Buildings." *Encyclopedia of Earthquake Engineering*. Springer, Berlin, Heidelberg

Viana, D. D., Tommelein, I. D., Formoso, C. T. (2017). "Using Modularity to Reduce Complexity of Industrialized Building Systems for Mass Customization." *Energies*, 10. 10.3390/en10101622.

Winter, G. (1960). "Lateral Bracing of Columns and Beams." *ASCE Transactions*, Vol. 125, pp. 809-825.

APPENDIX A

Connection Design

This section contains details of the dimensions used to manufacture the side intermeshed connection specimens that were tested. The dimensions were selected by using a spreadsheet that followed the design procedure presented in Chapter 3. The spreadsheet data for the angles and beam teeth is presented in section A.1. The drawings presented in A.2 are the same drawings that were used by Grunau Metals and Am-Tec Designs for fabrication. Connections for two W18x46 beams and two W21x57 beams were detailed. The connection design for each beam size is different, but the details for the angles are identical for both W18x46 beams and for both W21x57 beams. Tables that include dimensions from the actual specimen after delivery are also included. Lastly, Section A.4 includes the mill certificates for the steel components used for the beam specimens.

A.1 Design Spreadsheets

Section Properties	
Section Name	W18X46
Section Depth, d	18.1 in
Section Width, w	6.06 in
Flange Thickness, tf	0.605 in
Web Thickness, tw	0.36 in
Zp	90.7 in ³

Angle Properties	
Section Name	L2-1/2X2X3/8
Side Plate Width (Vertical)	2.5 in
Side Plate Width (Horiz)	2 in
Angle Thickness	0.375 in
Clearance (Angle to Flange)	0.3125 in
Angle Area	1.55 in ²

Material Properties	
Fy Section	50 ksi
Fy Side Plate	36 ksi
Fu Side Plate	58 ksi

Design Effects	
Design Moment, Md	126 k-ft

Connection Properties	
# of teeth-one flange side	6
Tooth width, b	0.9
Tolerance, g0	1/16
Tolerance, g1	1/16
Tolerance, g2	1/16

Assumptions	
LRFD ϕ (bending, shear)	0.9
LRFD ϕ (rupture)	0.75
U	0.8
Ry Gr 36	1.5
Ry Gr 50	1.1

Angle	
Yielding	
Flange Force	79.14 k
Flange Force per Side	39.57 k
Side Angle capacity	50.22 k
Side Plate Utilization	79 %
Rupture	
Side Plate Force	39.57 k
Ae (effective area)	1.02 in ²
Side Plate Rupture Strength	44.41 k
Side Plate Utilization	89 %
Yield before rupture?	NO
Teeth Properties	
tooth area, Atooth	0.5445 in ²
tooth plastic section mod, Mptooth	0.1225125 in ³

Max force from an angle	92.1 k
Tooth Force, Ved	15.3 k
Tooth Resistance, VRd	15.6 k
Shear Utilization Ratio	99 %

Bending Stress Reduction Factor	1.000
Tooth Moment, Med	3.8 k-ft
Tooth Moment Resistance, MRd	6.1 k-ft
Moment Utilization	63 %

Figure A1: W18x46 Design Spreadsheet

Section Properties	
Section Name	W21X57
Section Depth, d	21.1 in
Section Width, w	6.56 in
Flange Thickness, tf	0.65 in
Web Thickness, tw	0.405 in
Zp	129 in ³

Angle Properties	
Section Name	L3X2X3/8
Side Plate Width (Vertical)	3 in
Side Plate Width (Horiz)	2 in
Angle Thickness	0.375 in
Clearance (Angle to Flange)	0.375 in
Angle Area	1.75 in ²

Material Properties	
Fy Section	50 ksi
Fy Side Plate	36 ksi
Fu Side Plate	58 ksi

Design Effects	
Design Moment, Md	179.17 k-ft

Connection Properties	
# of teeth-one flange side	6
Tooth width, b	1
Tolerance, g0	1/16
Tolerance, g1	1/16
Tolerance, g2	1/16

Assumptions	
LRFD ϕ (bending, shear)	0.9
LRFD ϕ (rupture)	0.75
U	0.8
Ry Gr 36	1.5
Ry Gr 50	1.1

Angle	
Yielding	
Flange Force	96.74 k
Flange Force per Side	48.37 k
Side Plate capacity	56.70 k
Side Plate Utilization	85 %
Rupture	
Side Plate Force	48.37 k
Ae (effective area)	1.17 in ²
Side Plate Rupture Strength	50.79 k
Side Plate Utilization	95 %
Yield before rupture?	NO

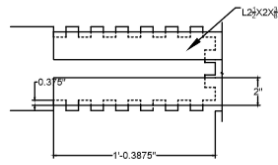
Teeth Properties	
tooth area, Atooth	0.65 in ²
tooth plastic section mod, Mptooth	0.1625 in ³

Max force from an angle	104.0 k
Tooth Force, Ved	17.3 k
Tooth Resistance, VRd	18.6 k
Shear Utilization Ratio	93 %

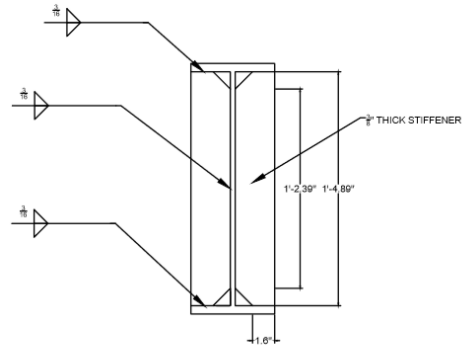
Bending Stress Reduction Factor	1.000
Tooth Moment, Med	4.3 k-ft
Tooth Moment Resistance, MRd	8.0 k-ft
Moment Utilization	54 %

Figure A.2: W21x57 Design Spreadsheet

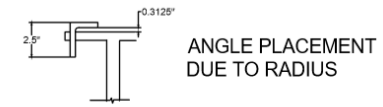
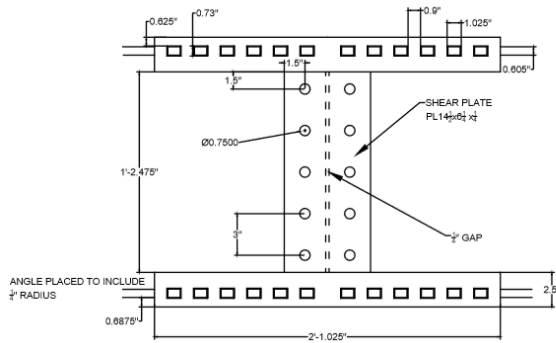
W18 TOP VIEW - WITH ANGLES



STIFFENER



W18 SIDE VIEW



ANGLE TOLERANCE DIMENSIONS

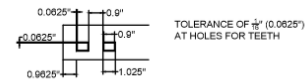


Figure A.5: Test 1 and 2 Connection Details

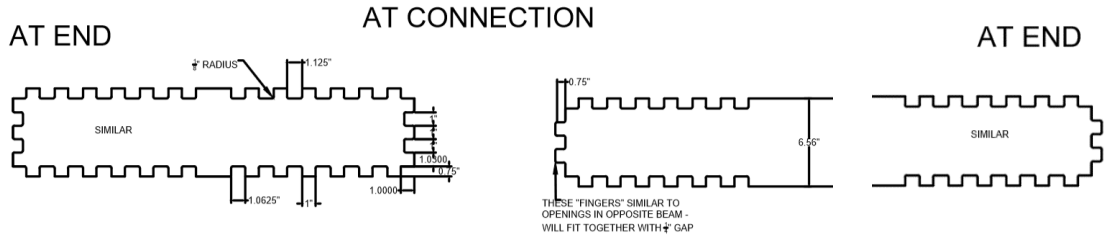
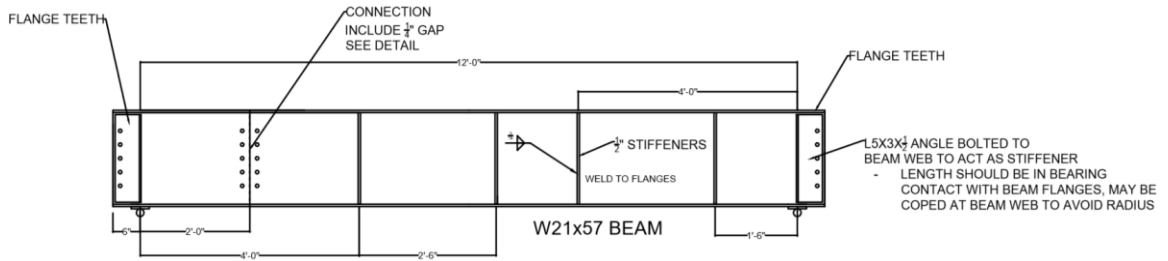


Figure A.6: Test 3 Beam Dimensions

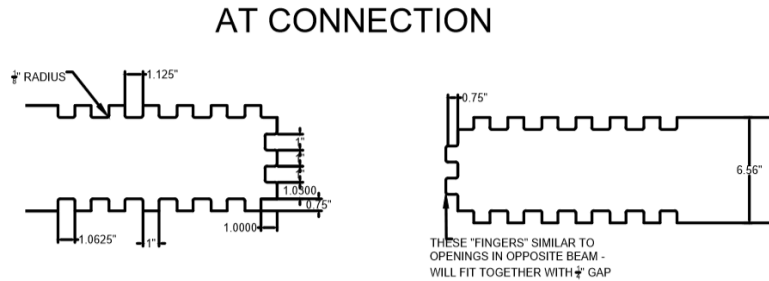
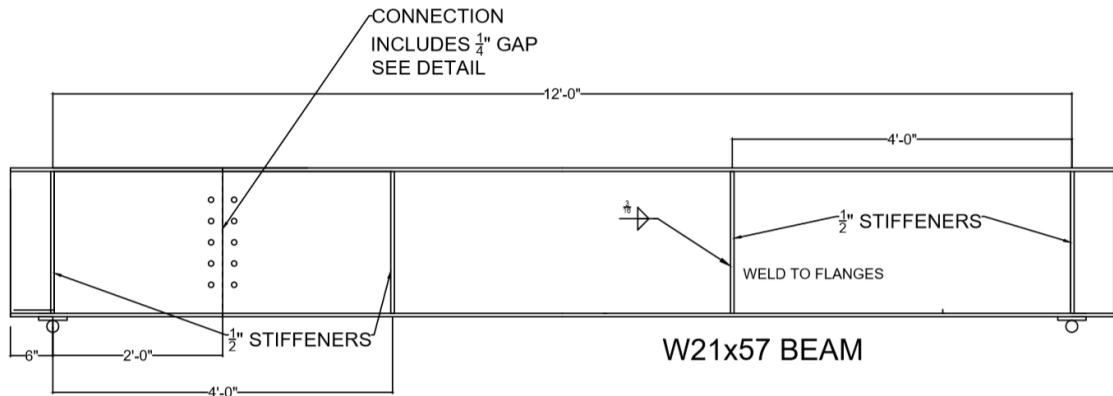


Figure A.7: Test 4 Beam Dimensions

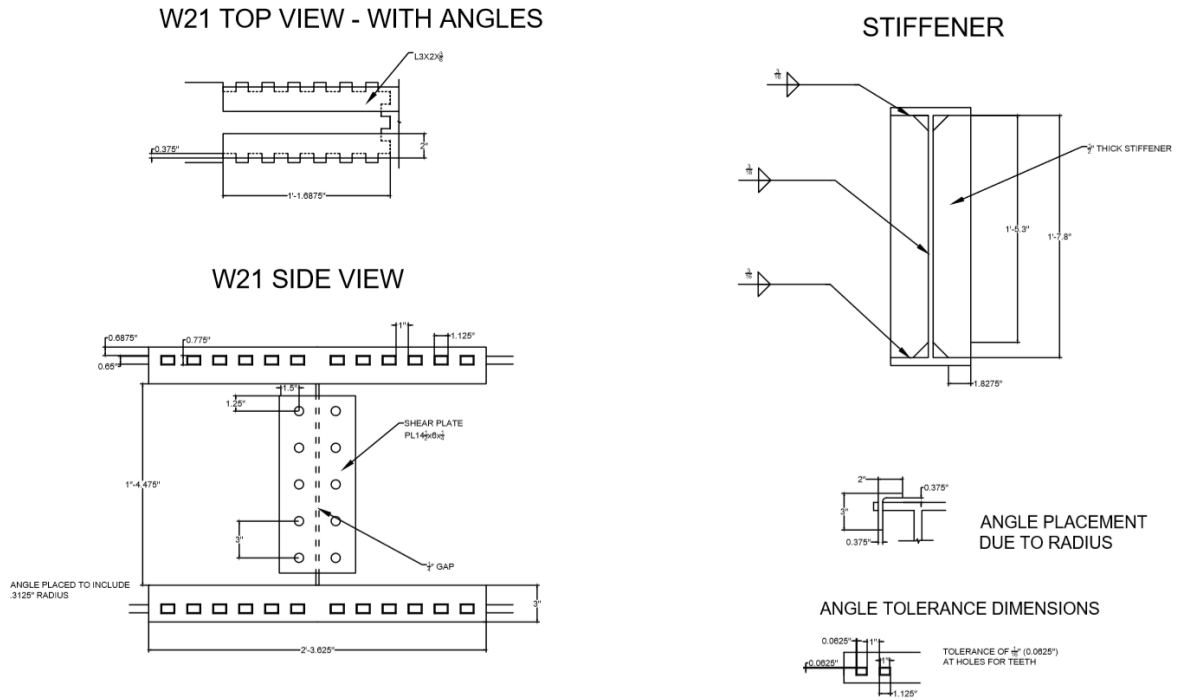


Figure A.8: Test 3 and 4 Connection Details

A.3 Specimen Measurements

After the specimens were received, the critical components on them were measured to check the precision of the fabrication. The critical components measured on the beams included the teeth dimensions on both flanges, and on the angles they were the hole width and height dimensions. It was assumed that the members prior to cutting were selected by the fabricators to meet AISC criteria for imperfections and tolerances, and that the cutting processes would not alter member dimensions. Tables are included for every beam and angle tested. All measurements taken were well within the acceptable range of measurements.

Table A1: Beam 1 Specimen Measurements

TOP FLANGE							
Tooth #	Measurement (in)	Design (in)	Diff (in)	Gap #	Measurement (in)	Design (in)	Diff (in)
1	0.882	0.9	-0.018	1	1.058	0.9625	0.0955
2	0.8695	0.9	-0.0305	2	1.056	1.025	0.031
3	0.8615	0.9	-0.0385	3	1.072	1.025	0.047
4	0.8615	0.9	-0.0385	4	1.07	1.025	0.045
5	0.8665	0.9	-0.0335	5	1.069	1.025	0.044
6	0.8735	0.9	-0.0265	6	1.077	1.025	0.052
7	0.866	0.9	-0.034	7	1.063	0.9625	0.1005
8	0.867	0.9	-0.033	8	1.059	1.025	0.034
9	0.8615	0.9	-0.0385	9	1.063	1.025	0.038
10	0.8625	0.9	-0.0375	10	1.061	1.025	0.036
11	0.855	0.9	-0.045	11	1.06	1.025	0.035
12	0.854	0.9	-0.046	12	1.059	1.025	0.034
13	0.865	0.9	-0.035	13	1.074	1.025	0.049
14	0.855	0.9	-0.045	14	1.082	1.025	0.057
15	0.868	0.9	-0.032	15	1.077	1.025	0.052
16	0.855	0.9	-0.045	16	1.077	1.025	0.052
17	0.859	0.9	-0.041	17	1.076	1.025	0.051
18	0.853	0.9	-0.047	18	1.015	0.9625	0.0525
19	0.869	0.9	-0.031	19	1.067	1.025	0.042
20	0.865	0.9	-0.035	20	1.061	1.025	0.036
21	0.867	0.9	-0.033	21	1.062	1.025	0.037
22	0.859	0.9	-0.041	22	1.06	1.025	0.035
23	0.867	0.9	-0.033	23	1.059	1.025	0.034
24	0.861	0.9	-0.039	24	1	0.9625	0.0375
AVG:			-0.037	AVG:			0.047
BOTTOM FLANGE							
Tooth #	Measurement (in)	Design (in)	Diff (in)	Gap #	Measurement (in)	Design (in)	Diff (in)
1	0.903	0.9	0.003	1	1.071	0.9625	0.1085
2	0.887	0.9	-0.013	2	1.049	1.025	0.024
3	0.881	0.9	-0.019	3	1.065	1.025	0.04
4	0.865	0.9	-0.035	4	1.06	1.025	0.035
5	0.883	0.9	-0.017	5	1.065	1.025	0.04
6	0.878	0.9	-0.022	6	1.06	1.025	0.035
7	0.858	0.9	-0.042	7	1.06	0.9625	0.0975
8	0.879	0.9	-0.021	8	1.066	1.025	0.041
9	0.869	0.9	-0.031	9	1.069	1.025	0.044
10	0.858	0.9	-0.042	10	1.069	1.025	0.044
11	0.863	0.9	-0.037	11	1.068	1.025	0.043
12	0.867	0.9	-0.033	12	1.079	1.025	0.054
13	0.863	0.9	-0.037	13	1.061	1.025	0.036
14	0.865	0.9	-0.035	14	1.073	1.025	0.048
15	0.866	0.9	-0.034	15	1.064	1.025	0.039
16	0.873	0.9	-0.027	16	1.058	1.025	0.033
17	0.859	0.9	-0.041	17	1.064	1.025	0.039
18	0.863	0.9	-0.037	18	1.012	0.9625	0.0495
19	0.869	0.9	-0.031	19	1.065	1.025	0.04
20	0.866	0.9	-0.034	20	1.071	1.025	0.046
21	0.865	0.9	-0.035	21	1.07	1.025	0.045
22	0.865	0.9	-0.035	22	1.066	1.025	0.041
23	0.869	0.9	-0.031	23	1.067	1.025	0.042
24	0.866	0.9	-0.034	24	1.004	0.9625	0.0415
AVG:			-0.030	AVG:			0.046

Table A2: Beam 2 Specimen Measurements

TOP FLANGE							
Tooth #	Measurement (in)	Design (in)	Diff (in)	Gap #	Measurement (in)	Design (in)	Diff (in)
1	0.861	0.9	-0.039	1	1.048	0.9625	0.0855
2	0.867	0.9	-0.033	2	1.055	1.025	0.03
3	0.869	0.9	-0.031	3	1.059	1.025	0.034
4	0.867	0.9	-0.033	4	1.061	1.025	0.036
5	0.865	0.9	-0.035	5	1.065	1.025	0.04
6	0.88	0.9	-0.02	6	1.056	1.025	0.031
7	0.846	0.9	-0.054	7	1.071	0.9625	0.1085
8	0.871	0.9	-0.029	8	1.069	1.025	0.044
9	0.852	0.9	-0.048	9	1.072	1.025	0.047
10	0.858	0.9	-0.042	10	1.069	1.025	0.044
11	0.863	0.9	-0.037	11	1.074	1.025	0.049
12	0.865	0.9	-0.035	12	1.071	1.025	0.046
13	0.857	0.9	-0.043	13	1.078	1.025	0.053
14	0.856	0.9	-0.044	14	1.058	1.025	0.033
15	0.846	0.9	-0.054	15	1.065	1.025	0.04
16	0.855	0.9	-0.045	16	1.079	1.025	0.054
17	0.854	0.9	-0.046	17	1.063	1.025	0.038
18	0.848	0.9	-0.052	18	0.992	0.9625	0.0295
19	0.863	0.9	-0.037	19	1.064	1.025	0.039
20	0.863	0.9	-0.037	20	1.07	1.025	0.045
21	0.86	0.9	-0.04	21	1.057	1.025	0.032
22	0.866	0.9	-0.034	22	1.066	1.025	0.041
23	0.861	0.9	-0.039	23	1.056	1.025	0.031
24	0.862	0.9	-0.038	24	0.997	0.9625	0.0345
AVG:			-0.039	AVG:			#REF!
BOTTOM FLANGE							
Tooth #	Measurement (in)	Design (in)	Diff (in)	Gap #	Measurement (in)	Design (in)	Diff (in)
1	0.873	0.9	-0.027	1	1.1052	0.9625	0.1427
2	0.872	0.9	-0.028	2	1.06	1.025	0.035
3	0.873	0.9	-0.027	3	1.066	1.025	0.041
4	0.865	0.9	-0.035	4	1.061	1.025	0.036
5	0.858	0.9	-0.042	5	1.068	1.025	0.043
6	0.863	0.9	-0.037	6	1.068	1.025	0.043
7	0.868	0.9	-0.032	7	1.061	0.9625	0.0985
8	0.871	0.9	-0.029	8	1.063	1.025	0.038
9	0.865	0.9	-0.035	9	1.06	1.025	0.035
10	0.858	0.9	-0.042	10	1.064	1.025	0.039
11	0.882	0.9	-0.018	11	1.067	1.025	0.042
12	0.88	0.9	-0.02	12	1.053	1.025	0.028
13	0.882	0.9	-0.018	13	1.063	1.025	0.038
14	0.897	0.9	-0.003	14	1.062	1.025	0.037
15	0.86	0.9	-0.04	15	1.051	1.025	0.026
16	0.873	0.9	-0.027	16	1.06	1.025	0.035
17	0.855	0.9	-0.045	17	1.065	1.025	0.04
18	0.868	0.9	-0.032	18	1.008	0.9625	0.0455
19	0.866	0.9	-0.034	19	1.047	1.025	0.022
20	0.891	0.9	-0.009	20	1.067	1.025	0.042
21	0.873	0.9	-0.027	21	1.069	1.025	0.044
22	0.872	0.9	-0.028	22	1.07	1.025	0.045
23	0.866	0.9	-0.034	23	1.065	1.025	0.04
24	0.87	0.9	-0.03	24	1.006	0.9625	0.0435
AVG			-0.029	AVG:			0.045

Table A3: Beam 3 Specimen Measurements


TOP FLANGE							
Tooth #	Measurement (in)	Design (in)	Diff (in)	Gap #	Measurement (in)	Design (in)	Diff (in)
1	0.982	1	-0.018	1	1.097	1.0625	0.0345
2	0.98	1	-0.02	2	1.153	1.125	0.028
3	0.995	1	-0.005	3	1.159	1.125	0.034
4	0.998	1	-0.002	4	1.141	1.125	0.016
5	0.986	1	-0.014	5	1.15	1.125	0.025
6	0.982	1	-0.018	6	1.16	1.125	0.035
7	0.966	1	-0.034	7	1.084	1.0625	0.0215
8	0.968	1	-0.032	8	1.138	1.125	0.013
9	0.981	1	-0.019	9	1.132	1.125	0.007
10	0.996	1	-0.004	10	1.128	1.125	0.003
11	0.969	1	-0.031	11	1.138	1.125	0.013
12	0.958	1	-0.042	12	1.145	1.125	0.02
13	0.969	1	-0.031	13	1.143	1.125	0.018
14	0.982	1	-0.018	14	1.156	1.125	0.031
15	0.974	1	-0.026	15	1.141	1.125	0.016
16	0.969	1	-0.031	16	1.153	1.125	0.028
17	0.978	1	-0.022	17	1.161	1.125	0.036
18	0.977	1	-0.023	18	1.097	1.0625	0.0345
19	0.978	1	-0.022	19	1.126	1.125	0.001
20	0.99	1	-0.01	20	1.144	1.125	0.019
21	0.972	1	-0.028	21	1.127	1.125	0.002
22	1.002	1	0.002	22	1.128	1.125	0.003
23	0.975	1	-0.025	23	1.146	1.125	0.021
24	0.968	1	-0.032	24	1.069	1.0625	0.0065
AVG			-0.02092	AVG			0.01941667
BOTTOM FLANGE							
Tooth #	Measurement (in)	Design (in)	Diff (in)	Gap #	Measurement (in)	Design (in)	Diff (in)
1	0.98	1	-0.02	1	1.099	1.0625	0.0365
2	0.983	1	-0.017	2	1.164	1.125	0.039
3	0.972	1	-0.028	3	1.159	1.125	0.034
4	0.968	1	-0.032	4	1.159	1.125	0.034
5	0.978	1	-0.022	5	1.162	1.125	0.037
6	0.982	1	-0.018	6	1.156	1.125	0.031
7	0.961	1	-0.039	7	1.102	1.0625	0.0395
8	0.983	1	-0.017	8	1.175	1.125	0.05
9	0.974	1	-0.026	9	1.171	1.125	0.046
10	0.965	1	-0.035	10	1.167	1.125	0.042
11	0.978	1	-0.022	11	1.163	1.125	0.038
12	0.985	1	-0.015	12	1.151	1.125	0.026
13	0.974	1	-0.026	13	1.171	1.125	0.046
14	0.981	1	-0.019	14	1.165	1.125	0.04
15	0.969	1	-0.031	15	1.164	1.125	0.039
16	0.959	1	-0.041	16	1.156	1.125	0.031
17	0.986	1	-0.014	17	1.16	1.125	0.035
18	0.965	1	-0.035	18	1.106	1.0625	0.0435
19	0.96	1	-0.04	19	1.176	1.125	0.051
20	0.974	1	-0.026	20	1.167	1.125	0.042
21	0.956	1	-0.044	21	1.153	1.125	0.028
22	0.966	1	-0.034	22	1.165	1.125	0.04
23	0.961	1	-0.039	23	1.161	1.125	0.036
24	0.984	1	-0.016	24	1.098	1.0625	0.0355
AVG			-0.027333333	AVG			0.03833333

Table A4: Beam 4 Specimen Measurements


TOP FLANGE							
Tooth #	Measurement (in)	Design (in)	Diff (in)	Gap #	Measurement (in)	Design (in)	Diff (in)
1	0.977	1	-0.023	1	1.0875	1.0625	0.025
2	0.981	1	-0.019	2	1.159	1.125	0.034
3	0.993	1	-0.007	3	1.167	1.125	0.042
4	0.982	1	-0.018	4	1.15	1.125	0.025
5	0.975	1	-0.025	5	1.159	1.125	0.034
6	0.977	1	-0.023	6	1.156	1.125	0.031
7	0.975	1	-0.025	7	1.096	1.0625	0.0335
8	0.962	1	-0.038	8	1.163	1.125	0.038
9	0.976	1	-0.024	9	1.163	1.125	0.038
10	0.969	1	-0.031	10	1.162	1.125	0.037
11	0.977	1	-0.023	11	1.166	1.125	0.041
12	0.958	1	-0.042	12	1.159	1.125	0.034
13	0.972	1	-0.028	13	1.161	1.125	0.036
14	0.982	1	-0.018	14	1.162	1.125	0.037
15	0.997	1	-0.003	15	1.145	1.125	0.02
16	0.985	1	-0.015	16	1.156	1.125	0.031
17	0.975	1	-0.025	17	1.152	1.125	0.027
18	0.988	1	-0.012	18	1.073	1.0625	0.0105
19	0.955	1	-0.045	19	1.17	1.125	0.045
20	0.962	1	-0.038	20	1.159	1.125	0.034
21	0.971	1	-0.029	21	1.157	1.125	0.032
22	0.972	1	-0.028	22	1.16	1.125	0.035
23	0.975	1	-0.025	23	1.155	1.125	0.03
24	0.995	1	-0.005	24	1.1	1.0625	0.0375
AVG:			-0.023708333	AVG:			0.0328125
BOTTOM FLANGE							
Tooth #	Measurement (in)	Design (in)	Diff (in)	Gap #	Measurement (in)	Design (in)	Diff (in)
1	0.966	1	-0.034	1	1.108	1.0625	0.0455
2	0.964	1	-0.036	2	1.166	1.125	0.041
3	0.965	1	-0.035	3	1.165	1.125	0.04
4	0.965	1	-0.035	4	1.164	1.125	0.039
5	0.968	1	-0.032	5	1.165	1.125	0.04
6	0.958	1	-0.042	6	1.17	1.125	0.045
7	0.96	1	-0.04	7	1.108	1.0625	0.0455
8	0.961	1	-0.039	8	1.172	1.125	0.047
9	0.965	1	-0.035	9	1.158	1.125	0.033
10	0.981	1	-0.019	10	1.166	1.125	0.041
11	0.984	1	-0.016	11	1.164	1.125	0.039
12	0.971	1	-0.029	12	1.162	1.125	0.037
13	0.977	1	-0.023	13	1.157	1.125	0.032
14	0.964	1	-0.036	14	1.16	1.125	0.035
15	0.964	1	-0.036	15	1.164	1.125	0.039
16	0.965	1	-0.035	16	1.167	1.125	0.042
17	0.985	1	-0.015	17	1.169	1.125	0.044
18	0.959	1	-0.041	18	1.109	1.0625	0.0465
19	0.966	1	-0.034	19	1.157	1.125	0.032
20	0.971	1	-0.029	20	1.16	1.125	0.035
21	0.967	1	-0.033	21	1.164	1.125	0.039
22	0.967	1	-0.033	22	1.167	1.125	0.042
23	0.984	1	-0.016	23	1.169	1.125	0.044
24	0.961	1	-0.039	24	1.103	1.0625	0.0405
AVG			-0.03175	AVG			0.040166667

Table A5: Angle Specimen Measurements											
L 2.5 X 2 X 3/8											
Hole	Width (in)	Height (in)	Hole	Width (in)	Height (in)	Hole	Width (in)	Height (in)	Hole	Width (in)	Height (in)
Angle 1			Angle 2			Angle 3			Angle 4		
1	1.018	0.724	1	1.019	0.724	1	1.019	0.731	1	1.02	0.727
2	1.0205	0.726	2	1.021	0.725	2	1.019	0.738	2	1.02	0.736
3	1.021	0.73	3	1.018	0.723	3	1.02	0.736	3	1.02	0.732
4	1.021	0.734	4	1.018	0.728	4	1.02	0.739	4	1.018	0.734
5	1.022	0.724	5	1.017	0.726	5	1.017	0.735	5	1.018	0.735
6	1.02	0.732	6	1.021	0.731	6	1.019	0.736	6	1.02	0.73
7	1.018	0.736	7	1.019	0.725	7	1.016	0.738	7	1.017	0.733
8	1.02	0.732	8	1.018	0.736	8	1.018	0.738	8	1.017	0.734
9	1.019	0.734	9	1.018	0.728	9	1.013	0.742	9	1.019	0.732
10	1.021	0.729	10	1.019	0.726	10	1.018	0.731	10	1.021	0.739
11	1.019	0.73	11	1.019	0.732	11	1.016	0.733	11	1.018	0.734
12	1.018	0.735	12	1.02	0.733	12	1.018	0.731	12	1.02	0.729
AVG	1.020	0.731		1.019	0.728		1.018	0.736		1.019	0.733
Angle 5			Angle 6			Angle 7			Angle 8		
1	1.022	0.734	1	1.019	0.726	1	1.017	0.734	1	1.025	0.733
2	1.02	0.737	2	1.02	0.727	2	1.017	0.739	2	1.022	0.73
3	1.021	0.727	3	1.018	0.728	3	1.015	0.728	3	1.021	0.737
4	1.018	0.734	4	1.019	0.734	4	1.015	0.731	4	1.02	0.726
5	1.017	0.734	5	1.022	0.735	5	1.019	0.732	5	1.02	0.732
6	1.021	0.736	6	1.02	0.729	6	1.013	0.729	6	1.02	0.726
7	1.019	0.738	7	1.018	0.734	7	1.014	0.728	7	1.017	0.729
8	1.019	0.732	8	1.02	0.729	8	1.016	0.728	8	1.018	0.732
9	1.019	0.733	9	1.02	0.731	9	1.015	0.737	9	1.02	0.731
10	1.02	0.735	10	1.019	0.736	10	1.016	0.732	10	1.018	0.726
11	1.017	0.734	11	1.018	0.732	11	1.017	0.73	11	1.018	0.734
12	1.018	0.733	12	1.016	0.734	12	1.016	0.728	12	1.016	0.735
AVG	1.019	0.734		1.019	0.731		1.016	0.731		1.020	0.731
L 3 X 2.5 X 3/8											
Angle 1			Angle 2			Angle 3			Angle 4		
1	1.115	0.778	1	1.116	0.773	1	1.117	0.776	1	1.119	0.779
2	1.117	0.777	2	1.114	0.772	2	1.118	0.777	2	1.117	0.773
3	1.115	0.785	3	1.118	0.775	3	1.115	0.777	3	1.117	0.775
4	1.117	0.776	4	1.116	0.777	4	1.116	0.776	4	1.116	0.775
5	1.118	0.774	5	1.116	0.776	5	1.118	0.775	5	1.116	0.775
6	1.113	0.78	6	1.114	0.778	6	1.116	0.774	6	1.116	0.774
7	1.118	0.777	7	1.115	0.775	7	1.113	0.776	7	1.113	0.777
8	1.118	0.786	8	1.116	0.774	8	1.113	0.774	8	1.111	0.776
9	1.118	0.774	9	1.116	0.775	9	1.117	0.778	9	1.113	0.775
10	1.116	0.778	10	1.116	0.778	10	1.117	0.772	10	1.116	0.778
11	1.117	0.775	11	1.119	0.779	11	1.116	0.775	11	1.115	0.777
12	1.114	0.777	12	1.114	0.776	12	1.117	0.775	12	1.114	0.773
AVG	1.116	0.778		1.116	0.776		1.116	0.775		1.115	0.776
Angle 5			Angle 6			Angle 7			Angle 8		
1	1.116	0.775	1	1.117	0.77	1	1.121	0.781	1	1.125	0.776
2	1.115	0.775	2	1.12	0.773	2	1.123	0.778	2	1.126	0.774
3	1.115	0.773	3	1.117	0.778	3	1.126	0.781	3	1.126	0.778
4	1.117	0.773	4	1.124	0.775	4	1.124	0.778	4	1.124	0.775
5	1.118	0.776	5	1.123	0.771	5	1.126	0.773	5	1.125	0.773
6	1.115	0.777	6	1.122	0.777	6	1.122	0.776	6	1.124	
7	1.113	0.776	7	1.112	0.778	7	1.123	0.774	7	1.126	0.776
8	1.113	0.777	8	1.12	0.774	8	1.125	0.771	8	1.125	0.774
9	1.117	0.775	9	1.122	0.774	9	1.123	0.776	9	1.124	0.776
10	1.118	0.775	10	1.121	0.776	10	1.124	0.773	10	1.123	0.774
11	1.116	0.777	11	1.123	0.776	11	1.125	0.773	11	1.123	0.773
12	1.116	0.778	12	1.125	0.775	12	1.125	0.773	12	1.126	0.775
AVG	1.116	0.776		1.121	0.775		1.124	0.776		1.125	0.775

A.4 Mill Test Certificates

CERTIFIED MATERIAL TEST REPORT														Page 1/1																									
 US-ML-MIDLOTHIAN 300 WARD ROAD MIDLOTHIAN, TX 76065 USA		CUSTOMER SHIP TO KLOECKNER METALS US 14806 W RIDGE LN DUBUQUE, IA 52003-8465 USA				CUSTOMER BILL TO KLOECKNER METALS CORPORATION 500 COLONIAL CENTER PKWY ROSWELL, GA 30076-8853 USA				GRADE A992/A572-50		SHAPE / SIZE Wide Flange Beam / 21 X 57# / 530 X 85		DOCUMENT ID: 000000000																									
		SALES ORDER 6337062000220		CUSTOMER MATERIAL N° B2157W401400		LENGTH 4000"		PCS 0	WEIGHT 6,840 LB		HEAT / BATCH 59080425/04																												
CUSTOMER PURCHASE ORDER NUMBER 7259657				BILL OF LADING 1327-0000292145				DATE 08/21/2018				SPECIFICATION / DATE of REVISION ASTM A6-17 ASTM A709-17 ASTM A992-11 (2015), A572-15 CSA G40.21-13 345WM																											
CHEMICAL COMPOSITION <table border="1"> <tr> <th>C %</th> <th>Mn %</th> <th>P %</th> <th>S %</th> <th>Si %</th> <th>Cu %</th> <th>Ni %</th> <th>Cr %</th> <th>Mo %</th> <th>Sn %</th> <th>V %</th> <th>Nb %</th> <th>Al %</th> </tr> <tr> <td>0.08</td> <td>0.87</td> <td>0.016</td> <td>0.043</td> <td>0.22</td> <td>0.30</td> <td>0.11</td> <td>0.18</td> <td>0.023</td> <td>0.005</td> <td>0.002</td> <td>0.017</td> <td>0.003</td> </tr> </table>														C %	Mn %	P %	S %	Si %	Cu %	Ni %	Cr %	Mo %	Sn %	V %	Nb %	Al %	0.08	0.87	0.016	0.043	0.22	0.30	0.11	0.18	0.023	0.005	0.002	0.017	0.003
C %	Mn %	P %	S %	Si %	Cu %	Ni %	Cr %	Mo %	Sn %	V %	Nb %	Al %																											
0.08	0.87	0.016	0.043	0.22	0.30	0.11	0.18	0.023	0.005	0.002	0.017	0.003																											
CHEMICAL COMPOSITION CEq _{A6} % 0.30																																							
MECHANICAL PROPERTIES <table border="1"> <tr> <th>YS 0.2% PSI</th> <th>UTS PSI</th> <th>YS MPa</th> <th>UTS MPa</th> <th>Y/T_{ratio} %</th> <th>G/L Inch</th> </tr> <tr> <td>54314</td> <td>71652</td> <td>374</td> <td>494</td> <td>0.760</td> <td>8.000</td> </tr> <tr> <td>55689</td> <td>72605</td> <td>384</td> <td>501</td> <td>0.770</td> <td>8.000</td> </tr> </table>														YS 0.2% PSI	UTS PSI	YS MPa	UTS MPa	Y/T _{ratio} %	G/L Inch	54314	71652	374	494	0.760	8.000	55689	72605	384	501	0.770	8.000								
YS 0.2% PSI	UTS PSI	YS MPa	UTS MPa	Y/T _{ratio} %	G/L Inch																																		
54314	71652	374	494	0.760	8.000																																		
55689	72605	384	501	0.770	8.000																																		
MECHANICAL PROPERTIES <table border="1"> <tr> <th>G/L mm</th> <th>Elong. %</th> </tr> <tr> <td>200.0</td> <td>25.10</td> </tr> <tr> <td>200.0</td> <td>25.70</td> </tr> </table>														G/L mm	Elong. %	200.0	25.10	200.0	25.70																				
G/L mm	Elong. %																																						
200.0	25.10																																						
200.0	25.70																																						

a) W21x57

CERTIFIED MATERIAL TEST REPORT														Page 1/1																									
 US-ML-PETERSBURG 25801 HOFHEIMER WAY PETERSBURG, VA 23803-8905 USA		CUSTOMER SHIP TO KLOECKNER METALS US 14806 W RIDGE LN DUBUQUE, IA 52003-8465 USA				CUSTOMER BILL TO KLOECKNER METALS CORPORATION 500 COLONIAL CENTER PKWY ROSWELL, GA 30076-8853 USA				GRADE A992/A572-50		SHAPE / SIZE Wide Flange Beam / 18 X 46# / 460 X 68		DOCUMENT ID: 000000000																									
		SALES ORDER 6866070000240		CUSTOMER MATERIAL N° B1846W601400		LENGTH 6000"		PCS 0	WEIGHT 13,800 LB		HEAT / BATCH 60125827/08																												
CUSTOMER PURCHASE ORDER NUMBER 7305528				BILL OF LADING 1330-0000108541				DATE 09/14/2018				SPECIFICATION / DATE of REVISION ASTM A6-17 ASTM A709-17 ASTM A992-11 (2015), A572-15 CSA G40.21-13 345WM																											
CHEMICAL COMPOSITION <table border="1"> <tr> <th>C %</th> <th>Mn %</th> <th>P %</th> <th>S %</th> <th>Si %</th> <th>Cu %</th> <th>Ni %</th> <th>Cr %</th> <th>Mo %</th> <th>Sn %</th> <th>V %</th> <th>Nb %</th> <th>Al %</th> </tr> <tr> <td>0.08</td> <td>0.96</td> <td>0.010</td> <td>0.037</td> <td>0.19</td> <td>0.28</td> <td>0.13</td> <td>0.11</td> <td>0.030</td> <td>0.009</td> <td>0.001</td> <td>0.015</td> <td>0.003</td> </tr> </table>														C %	Mn %	P %	S %	Si %	Cu %	Ni %	Cr %	Mo %	Sn %	V %	Nb %	Al %	0.08	0.96	0.010	0.037	0.19	0.28	0.13	0.11	0.030	0.009	0.001	0.015	0.003
C %	Mn %	P %	S %	Si %	Cu %	Ni %	Cr %	Mo %	Sn %	V %	Nb %	Al %																											
0.08	0.96	0.010	0.037	0.19	0.28	0.13	0.11	0.030	0.009	0.001	0.015	0.003																											
CHEMICAL COMPOSITION CEq _{A6} % 0.30																																							
MECHANICAL PROPERTIES <table border="1"> <tr> <th>YS 0.2% PSI</th> <th>UTS PSI</th> <th>YS MPa</th> <th>UTS MPa</th> <th>Y/T_{ratio} %</th> <th>G/L Inch</th> </tr> <tr> <td>52200</td> <td>68500</td> <td>360</td> <td>472</td> <td>0.760</td> <td>8.000</td> </tr> <tr> <td>53200</td> <td>68700</td> <td>367</td> <td>474</td> <td>0.770</td> <td>8.000</td> </tr> </table>														YS 0.2% PSI	UTS PSI	YS MPa	UTS MPa	Y/T _{ratio} %	G/L Inch	52200	68500	360	472	0.760	8.000	53200	68700	367	474	0.770	8.000								
YS 0.2% PSI	UTS PSI	YS MPa	UTS MPa	Y/T _{ratio} %	G/L Inch																																		
52200	68500	360	472	0.760	8.000																																		
53200	68700	367	474	0.770	8.000																																		
MECHANICAL PROPERTIES <table border="1"> <tr> <th>G/L mm</th> <th>Elong. %</th> </tr> <tr> <td>200.0</td> <td>28.30</td> </tr> <tr> <td>200.0</td> <td>27.40</td> </tr> </table>														G/L mm	Elong. %	200.0	28.30	200.0	27.40																				
G/L mm	Elong. %																																						
200.0	28.30																																						
200.0	27.40																																						
COMMENTS / NOTES 																																							

b) W18x46

Figure A.9: Grunau Metals mill test certificates for beams

Customer PO	1053_385	Sales Order #	10013650 - 4.1
Product Group	Hot Roll - Merchant Bar Quality	Product #	3006985
Grade	Nucor Multigrade	Lot #	10089294822
Size	3" x 2" x 0.375"	Heat #	100892948
BOL #	BOL-175259	Load #	80334
Description	Hot Roll - Merchant Bar Quality Unequal Angle 3" x 2" x 3/8" Nucor Multigrade 20' 0" [240"] 2001-6000 lbs	Customer Part #	1A318020
Production Date	07/15/2018	Qty Shipped LBS	4957
Product Country Of Origin	United States	Qty Shipped EA	42
Original Item Description	Hot Roll - Merchant Bar Quality Unequal Angle 3" x 2" x 3/8" Nucor Multigrade 20' 0" [240"]	Original Item Number	1023429

I hereby certify that the material described herein has been manufactured in accordance with the specifications and standards listed above and that it satisfies those requirements.

Melt Country of Origin : United States

Melting Date: 07/12/2018

C (%)	Mn (%)	P (%)	S (%)	Si (%)	Ni (%)	Cr (%)	Mo (%)	Cu (%)	Ti (%)	V (%)	Nb (%)
0.16	0.71	0.019	0.027	0.19	0.09	0.16	0.03	0.25	0.000	0.014	0.003
Sn (%)											
0.010											

ASTM A529 S78.2 CE (%) : 0.37

ASTM A992 5.4 CE (%) : 0.34

Other Test Results

Yield (PSI) : 52500

Yield (PSI) : 51400


Tensile (PSI) : 72600

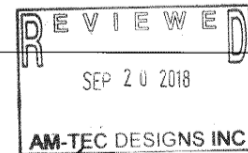
Tensile (PSI) : 72700

Elongation in 8" (%) : 27.0

Elongation in 8" (%) : 28.0

a) 3 x 2 x 3/8

 <p>US-ML-WILTON 1500-2500 WEST 3RD STREET WILTON, IA 52778 USA</p>	CERTIFIED MATERIAL TEST REPORT				Page 1/1																																																		
	CUSTOMER SHIP TO		CUSTOMER BILL TO		GRADE	SHAPE / SIZE	DOCUMENT ID:																																																
	WEST CENTRAL STEEL INC 105 19TH ST NW WILLMAR, MN 56201-2426 USA		WEST CENTRAL STEEL INC WILLMAR, MN 56201-1178 USA		GGMULTI	Angle / 2 1/2X2X3/8	0000000000																																																
	SALES ORDER 6464520/000010		CUSTOMER MATERIAL N°		LENGTH	WEIGHT	HEAT / BATCH																																																
CUSTOMER PURCHASE ORDER NUMBER 131780		BILL OF LADING 1334-0000048606		DATE 05/15/2018		20'00" 4,876 LB 6405913602																																																	
<table border="1"> <tr> <td colspan="7">CHEMICAL COMPOSITION</td> </tr> <tr> <td>C %</td> <td>Mn %</td> <td>P %</td> <td>S %</td> <td>Si %</td> <td>Cr %</td> <td>Ni %</td> </tr> <tr> <td>0.14</td> <td>0.61</td> <td>0.015</td> <td>0.046</td> <td>0.20</td> <td>0.26</td> <td>0.15</td> </tr> <tr> <td colspan="7">MECHANICAL PROPERTIES</td> </tr> <tr> <td>Elong %</td> <td>G/L Inch</td> <td>UTS PSI</td> <td>UTS MPa</td> <td>YS PSI</td> <td>YS MPa</td> <td></td> </tr> <tr> <td>26.30</td> <td>8.000</td> <td>75300</td> <td>519</td> <td>59000</td> <td>407</td> <td></td> </tr> <tr> <td>25.00</td> <td>8.000</td> <td>75300</td> <td>519</td> <td>58200</td> <td>401</td> <td></td> </tr> </table>							CHEMICAL COMPOSITION							C %	Mn %	P %	S %	Si %	Cr %	Ni %	0.14	0.61	0.015	0.046	0.20	0.26	0.15	MECHANICAL PROPERTIES							Elong %	G/L Inch	UTS PSI	UTS MPa	YS PSI	YS MPa		26.30	8.000	75300	519	59000	407		25.00	8.000	75300	519	58200	401	
CHEMICAL COMPOSITION																																																							
C %	Mn %	P %	S %	Si %	Cr %	Ni %																																																	
0.14	0.61	0.015	0.046	0.20	0.26	0.15																																																	
MECHANICAL PROPERTIES																																																							
Elong %	G/L Inch	UTS PSI	UTS MPa	YS PSI	YS MPa																																																		
26.30	8.000	75300	519	59000	407																																																		
25.00	8.000	75300	519	58200	401																																																		
<table border="1"> <tr> <td colspan="7">GEOMETRIC CHARACTERISTICS</td> </tr> <tr> <td colspan="7">R.R</td> </tr> <tr> <td colspan="7">19.75</td> </tr> </table>							GEOMETRIC CHARACTERISTICS							R.R							19.75																																		
GEOMETRIC CHARACTERISTICS																																																							
R.R																																																							
19.75																																																							
<p>COMMENTS / NOTES</p> <p>This grade meets the requirements for the following grades: ASTM Grades: A36; A529-50; A572-50; A709-36; A709-50 CSA Grades: 44W; 50W AASHTO Grades: M270-36; M270-50 ASME Grades: SA36</p>																																																							



b) 2 1/2 x 2 x 3/8

Figure A.10: Am-Tec Designs angle mill test certificates

CERTIFICATE OF TEST FOR COIL 5215046 HEAT# NLK1763313						
SOLD TO:		CUSTOMER PO: 303061-2		ORDER: 3044694		ITEM: 41208169
SHIP TO:		RESULTS FOR COIL: 5215046		EDGE: MILL		INDUSTRY SPEC: CONV TO ASTM A38
		PRODUCT TYPE: HR		FINISH: BLACK		CUSTOMER SPEC: NA
		PRODUCT CATEGORY: CONV TO A38		HARDNESS: NA		CUSTOMER PART #: 14
		ORDERED GRADE: 1012		HARDNESS RANGE: NA		CERT #: 14
		ORDERED GAUGE: 0.2400 MM		YIELD: 36000		CUSTOMER NOTE:
		GAGE TOL: +0.015/-0.000		TENSILE: 5800/80000		
		ORDERED WIDTH: 48.0000 MM		ELONGATION: 22%		
		WIDTH TOL: +1.1250/0.0000		BEND:		
JOB #	COIL #	SIZE	WGT	YIELD	TENSILE	ELONGATION
3044694-01	5215043	0.2400 x 48.0000	46050	51,900	73,500	31.0
HEAT# NLK1763313 (Country of Origin: RUSSIA) C: .20 - MN: .75 - P: .017 - S: .008 - SE: .02 - AL: .047 - CU: .04 - NI: .02 - CR: .03 - MO: * - SN: * - TI: .001 - V: .001 - NB: .003 - N: .003 - B: .0002 - CA: * - CE: * - ZR: * - AS: * - SB: *						
JOB #	COIL #	SIZE	WGT	YIELD	TENSILE	ELONGATION
3044694-01	5215046	0.2400 x 48.0000	46810	54,500	75,900	24.0
HEAT# NLK1763313 (Country of Origin: RUSSIA) C: .20 - MN: .75 - P: .017 - S: .008 - SE: .02 - AL: .047 - CU: .04 - NI: .02 - CR: .03 - MO: * - SN: * - TI: .001 - V: .001 - NB: .003 - N: .003 - B: .0002 - CA: * - CE: * - ZR: * - AS: * - SB: *						

9040860

Figure A.11: Shear plate mill test certificate

APPENDIX B

Test Design Calculations

Several calculations were necessary to properly design the testing setup. This section contains information regarding the design of stiffeners and bracing that prevent local failures. Checks were also performed on the surfaces where flange teeth bear on the angle holes. Local bearing forces were examined, and they were used to study the potential for slip-out of the angles.

B.1 Stiffener Design

Stiffeners were located at point loads and reactions to help prevent local buckling. The equations presented in this section were used to size the stiffeners.

$$I_{st} \geq bt_w^3j \quad [B1]$$

I_{st} = Stiffener moment of inertia

b = beam flange width

t_w = web thickness

j = assumed as 0.5

For the W18x46 beam, $I_{st} \geq (6.05)(0.36)^3(0.5) = 0.14 \text{ in}^4$. For the 3/8" stiffener, $I_{st} = \frac{1}{12}(0.375)(2.5)^3 = 0.49 \text{ in}^4$. The stiffener capacity, P , is given by the equation below.

$$P = A_{pb}F_{yst} \quad [B2]$$

P = Stiffener plate capacity

A_{pb} = Area of plate bearing

F_{yst} = Stiffener yield strength, 36 ksi

Each stiffener used on the W18x46 beam has a capacity, P , of at least 46.9 kips from $P = (2.5)(0.375)(50) = 46.9$. Since there were stiffeners on each side of the web, at each load point there was additional capacity of at least 93.8 kips at stiffener locations for the W18x46 beam.

Similarly, for the W21x57 beam, $I_{st} \geq (6.56)(0.405)^3(0.5) = 0.218 \text{ in}^4$. A ½” stiffener was selected, and $I_{st} = \frac{1}{12}(0.5)(2.5)^3 = 0.65 \text{ in}^4$. The plate capacity was calculated to be 62.5 kips using equation B2, and the total additional capacity from stiffeners under point loads was 125 kips.

Finally, both stiffeners were checked to meet the steel construction manual’s width-to-thickness ratio requirements for tension field action given by equation B3.

$$\left(\frac{b}{t}\right)_{st} \leq 0.56 \sqrt{E/F_{yst}} \quad [\text{B3}]$$

For both plates, $\left(\frac{b}{t}\right)_{st} \leq 0.56\sqrt{29000/36} = 15.9$. The W18x46 beam stiffeners had a width-to-thickness ratio of about 6.7, and the W21x57 beam stiffeners had one of about 5.

B.2 Original Bracing Design

The lateral force requirement for the bracing system was estimated using the two-percent rule (Winter 1960), which states that bracing must resist 2% of the compressive force in the member it braces. The maximum design moment in the beam was about 180 kip-ft, but the maximum moment a W21x57 beam can be expected to withstand is 490 kip-ft. As an upper bound estimate, this moment was divided into couple forces, and the distance between the forces was taken as the distance between the centroids of the top and bottom flanges. Example calculations using the W21x57 beam are provided below, and steel angles were deemed appropriate to resist the resulting lateral force of 5.5 kips.

$$M = \text{Force} \times \text{Distance}$$

$$\text{Force} = \frac{(480)(12)}{21} = 274 \text{ kips}$$

$$(0.02)(274) = 5.5 \text{ kips}$$

B.3 Revised Bracing Design

The lateral restraint provided by the angles was deemed insufficient after running two tests. Neither the angles nor the EFCO supporting them were stiff enough to resist the loads. The two-percent rule seemed to have underestimated the lateral forces applied to the bracing. As a result, the two percent value was replaced with ten percent, and this produced a demand of nearly 30 kips.

The EFCO was replaced with W12x35 beams, and the angles were replaced with C8x11.5 channels. The beams were bolted to the support below with four 7/8" A490 bolts. The channels, wide flange beams, and bolts each had their capacities checked against the demand. The loading for the system is shown in Figure B1.

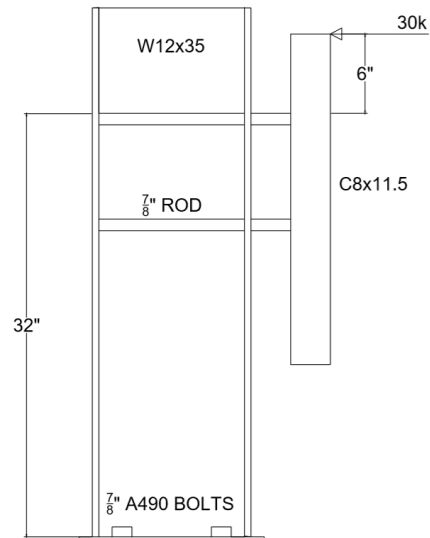


Figure B1: Loading on Revised Bracing

The bending moment in the channel was calculated by assuming the channel was a 6” long cantilever with a 30 kip point load on the end. This loading created 15 kip-ft of bending moment, and the capacity of a C8x11.5 is around 26 kip-ft. The W12x35 was also treated as a cantilever with a 30 kip point load and a 32” span. This created a bending moment of 80 kip-ft, and the capacity of a W12x35 is around 192 kip-ft. The beam’s maximum deflection was then checked using equation B4. The maximum lateral deflection was estimated to be only 0.04 inches, and up to one eighth of an inch of deflection was considered acceptable.

$$\Delta = \frac{PL^3}{3EI} \quad [B4]$$

$$\Delta = \frac{(30)(32)^3}{3(29000)(285)} = 0.04 \text{ in}$$

Finally, the bolt capacity was checked. Only two of the bolts were assumed to resist tensile forces. The tensile force was estimated by using the maximum moment in the W12x35, 80 kip-ft, and separating it into couple forces acting on the beam’s two flanges. This resulted in a tensile force of approximately 40 kips per bolt, and each bolt can carry a tensile force of 51.0 kips.

B.4 Local Bearing at Angle Holes

Since the teeth apply load to the angles on a relatively small surface, local bearing forces were checked. The teeth had a higher yield stress than the angles do, therefore only the angles needed to be checked. The bearing capacity was estimated by referencing section J3-6c in the steel construction manual (AISC 2017). This is the bearing strength for a connection with long slotted holes, which is what the side intermeshed connection most closely resembles. An R_t value was also included. The equation, B5, is provided below.

$$\phi R_n = \phi 2.0 d t F_u R_t \quad [B5]$$

R_n = bearing capacity

d = depth of surface

t = thickness of surface

R_t = factor from seismic design provisions

The design force from a single tooth in the W18x46 was 15.3 kips, and in the W21x57 it was 17.3 kips. The bearing capacity of the angles for each specimen is calculated below. The capacity of each angle exceeded the demand.

$$\phi R_{n(18x46)} = (0.75)(2)(0.451)(0.375)(58)(1.1) = 16.3 \text{ kips} > 15.3 \text{ kips}$$

$$\phi R_{n(21x57)} = (0.75)(2)(0.496)(0.375)(58)(1.1) = 17.8 \text{ kips} > 17.3 \text{ kips}$$

B.5 Potential for Slippage of Angle

The friction forces at the surfaces where the teeth and angles meet help to keep the angles in place once they are loaded. Calculations were performed to see if the friction force would be high enough to keep the angles in place without any sort of external restraint. The angles could potentially move whenever they reach their buckling load. The buckling load is the same as the angle capacity that was used in the connection design procedure. The two percent rule may be used to estimate the amount of friction force required to restrain the angles. For example, the capacity of one of the 3x2.5x3/8 angles is 56.7 kips. Two percent of this value is 1.13 kips. Therefore, the friction force provided between a single tooth and the angle must be at least 1.13 kips to avoid an external restraint system.

The bearing force on a single tooth must be calculated. Since there are six teeth on each side of one flange, the angle capacity may be divided by six for a single tooth. This force may then be multiplied by the coefficient of friction between the surfaces. The coefficient of friction was estimated as 0.15. This was a conservative lower bound estimate that would more closely represent a lubricated surface. The friction force calculated was 1.4 kips, so no external restraint system was deemed necessary. However, the channel restraints were provided for safety purposes and to measure lateral forces with strain gages. The calculations performed in this section are provided below.

$$\text{Restraint required for } 3 \times 2 \frac{1}{2} \times \frac{3}{8} = 56.7(0.02) = 1.13 \text{ kips}$$

$$\text{Bearing Force} = \frac{56.7}{6 \text{ teeth}} = 9.45 \text{ kips per tooth}$$

$$\text{Friction force} = F * \mu = (9.45)(0.15) = 1.4 \text{ kips}$$

$$1.4 \text{ kips} > 1.13 \text{ kips}$$

APPENDIX C

Testing Prediction Calculations

C.1 Expected Failure Load for Connection

The moment at which the connection failed was estimated for each beam prior to testing. Since angle rupture controlled the design, the expected failure load of the connection is when the angle ruptures. The R_t factor was again included in these calculations. The equations used to estimate moment and the connection when it fails are provided below.

$$F = F_u A_e R_t \quad [C1]$$

F_u = specified rupture stress

A_e = effective area of the angle

R_t = factor from seismic design provisions, 1.2

$$F_{tot} = 2F \quad [C2]$$

F_{tot} = Total force both tension angles can resist together

$$M = F_{tot} d_r \quad [C3]$$

d_r = distance between the centroids of the top and bottom angle legs parallel to the ground

Once the maximum moment was estimated, the corresponding point loads in Table 3 were obtained using static equilibrium and the geometry from Figure 4.7. C.1.1 and C.1.2 show the maximum moment calculations performed for each beam size.

C.1.1 W18x46 Maximum Moment Calculation

$$F = (58)(1.02)(1.2) = 71 \text{ kips}$$

$$F_{tot} = 2(71) = 142 \text{ kips}$$

$$M = (142)(18.1 + 2(0.3125) + 0.375) = 226 \text{ kip} - \text{ft}$$

C.1.2 W21x57 Maximum Moment Calculation

$$F = (58)(1.17)(1.2) = 81.4 \text{ kips}$$

$$F_{tot} = 2(81.4) = 162.9 \text{ kips}$$

$$M = (162.9)(21.1 + 2(0.3125) + 0.375) = 300 \text{ kip} - \text{ft}$$

C.2 Deflection Estimation

The maximum deflection was estimated using the maximum point loads expected into the beam deflection equations or the various beam configurations in the test program. The equations for simply supported beams with one and two point loads were used.

Deflections during the tests exceeded these calculations because the beams were loaded to forces exceeding the maximum expected values.

Additional deflection was predicted since the beams may slip due to the tolerances at the angle holes. Since there is a vertical tolerance at angle holes of 1/16" both above and below a single tooth, a total of 1/8" of additional deflection may occur due to vertical tolerances. An additional inch of deflection was then added to this total to account for plasticity and vertical deflection due to horizontal movement. As an example, the deflection calculations for the first beam test are given in C.2.1.

$$\Delta = \frac{Pab(a+2b)\sqrt{3a(a+2b)}}{27EI} \quad [C4]$$

$$\Delta = \frac{Pa}{24EI}(3l^2 - 4a^2) \quad [C5]$$

C.2.1 Deflection Calculations

a) Beam test 1

$$\Delta = \frac{(75.3)(3)(12)}{(24)(29000)(712)}(3(12 \times 12)^2 - 4(3 \times 12)^2) = 0.31''$$

$$0.31 + 0.125 + 1.0 = 1.44''$$

b) Beam test 2

$$\begin{aligned} \Delta &= \frac{(150.7)(3 \times 12)(9 \times 12)(3 \times 12 + 2(9 \times 12))\sqrt{3(3 \times 12)(3 \times 12 + 2(9 \times 12))}}{(27)(29000)(712)(12 \times 12)} \\ &= 0.30'' \end{aligned}$$

$$0.30 + 0.125 + 1.0 = 1.43''$$

c) Beam test 3

$$\Delta = \frac{(225)(4 \times 12)(8 \times 12)(4 \times 12 + 2(8 \times 12))\sqrt{3(4 \times 12)(4 \times 12 + 2(8 \times 12))}}{(27)(29000)(1170)(12 \times 12)} = 0.35$$

$$0.35 + 0.125 + 1.0 = 1.48''$$

d) Beam test 4

$$\Delta = \frac{(150)(4)(12)}{(24)(29000)(1170)} (3(12 \times 12)^2 - 4(4 \times 12)^2) = 0.47''$$

$$0.47 + 0.125 + 1.0 = 1.59''$$

C.3 Plastic Moment Calculations

$$M_p = \sigma_y Z_p$$

W18x46:

$$M_p = \frac{(52.7)(90.7)}{12} = 398.3 \text{ k-ft}$$

W21x57:

$$M_p = \frac{(55.02)(129)}{12} = 591.5 \text{ k-ft}$$

APPENDIX D

Additional Data

D.1 Strain Calculations

Most strain gages were placed in groups of two so that strain data could be separated into axial and flexural components, as demonstrated in Figure D1. The calculations used for each component of strain are given in equations D1 and D2. Compressive strain was negative, and tensile strain was positive.

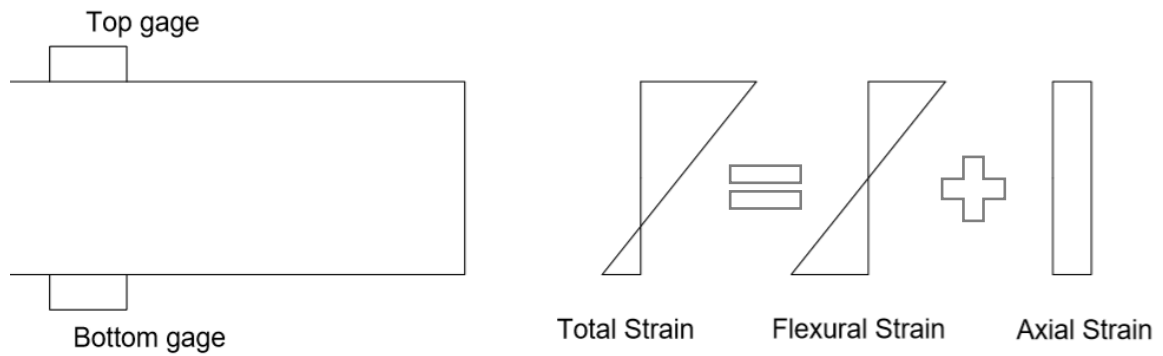


Figure D1: Strain components

$$\epsilon_{axial} = \frac{1}{2}(\epsilon_{top} + \epsilon_{bottom}) \quad [D1]$$

$$\epsilon_{flexure} = \frac{1}{2}(\epsilon_{top} - \epsilon_{bottom}) \quad [D2]$$

D.2 Test 1 Supplementary Figures

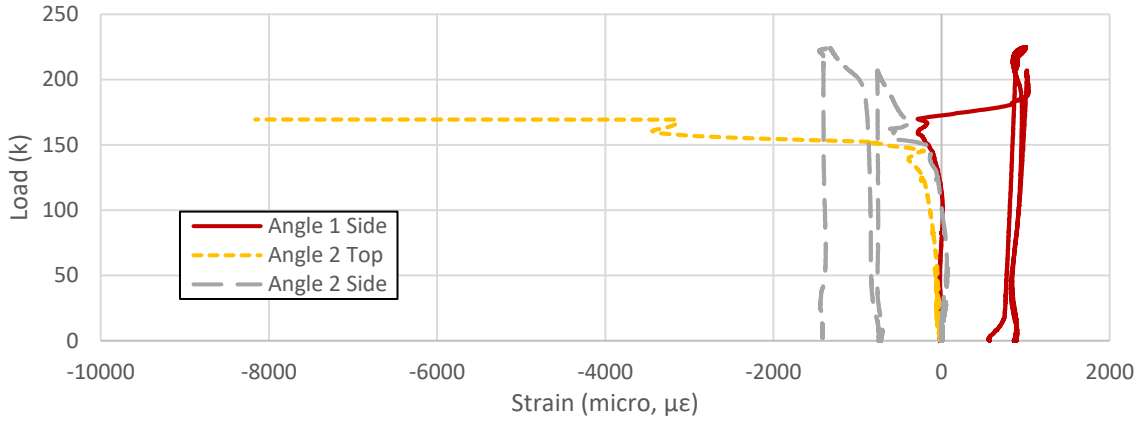


Figure D2: Test 1 compression angle load vs. flexural strain

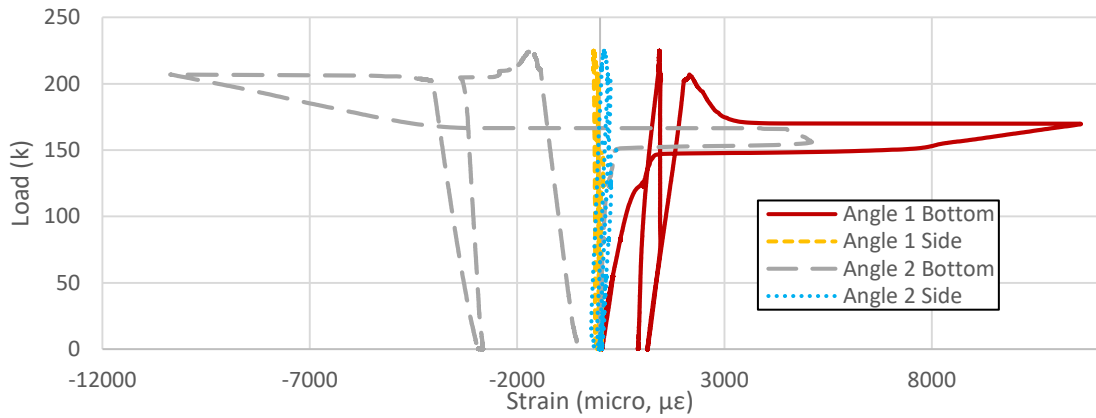


Figure D3: Test 1 tension angle load vs. flexural strain

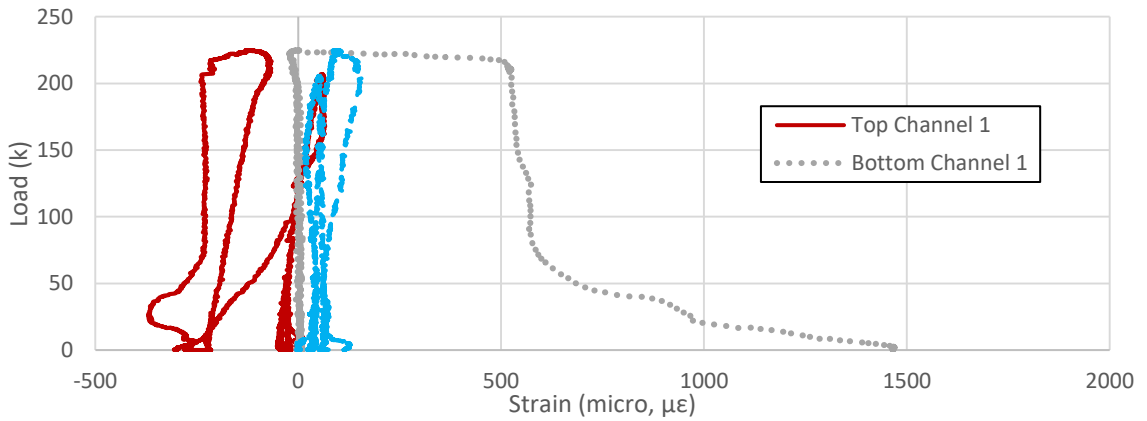


Figure D4: Test 1 channel load vs. flexural strain

D.3 Test 2 Supplementary Figures

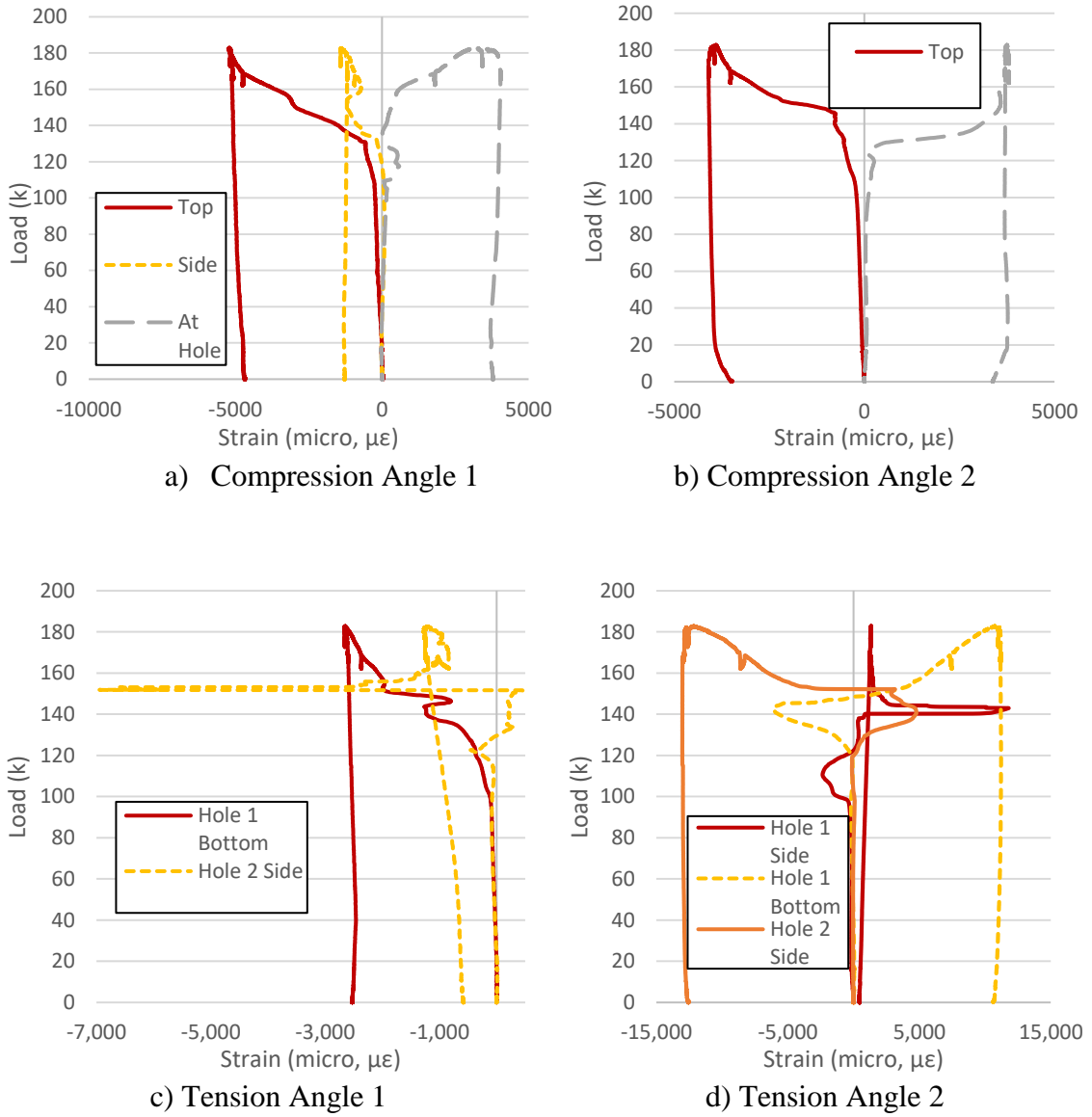


Figure D5: Test 2 angle load vs. flexural strain

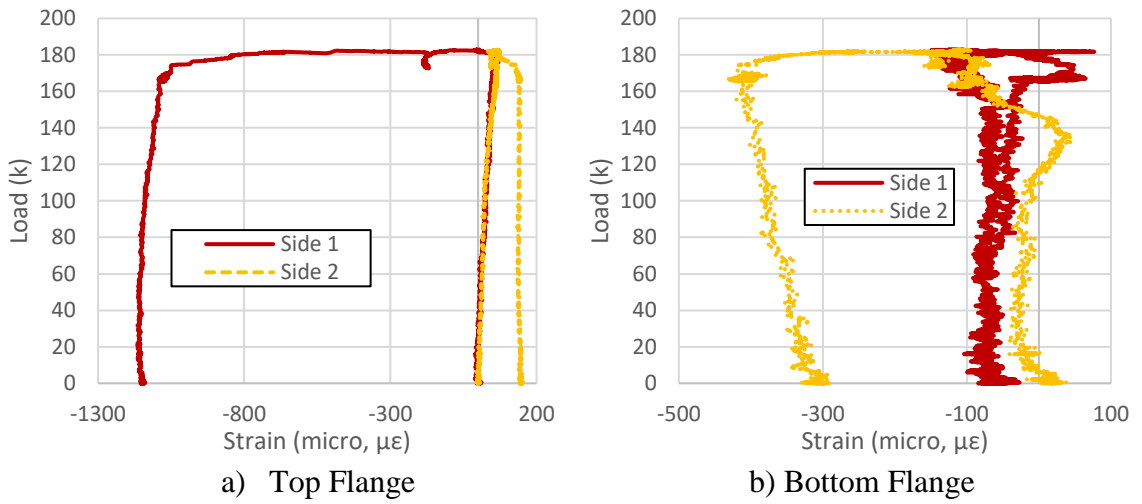


Figure D6: Test 2 beam flange load vs. flexural strain

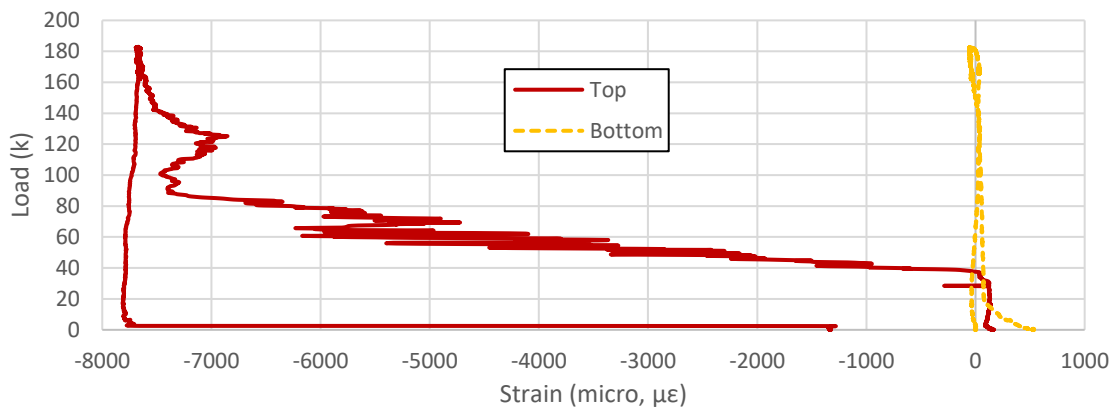


Figure D7: Test 2 shear plate load vs. flexural strain

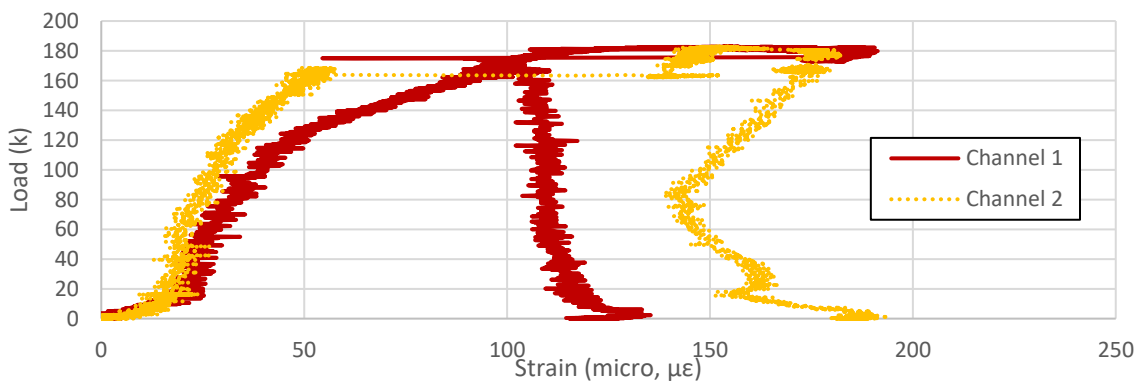


Figure D8: Test 2 compression region channel load vs. axial strain

D.4 Test 3 Supplementary Figures

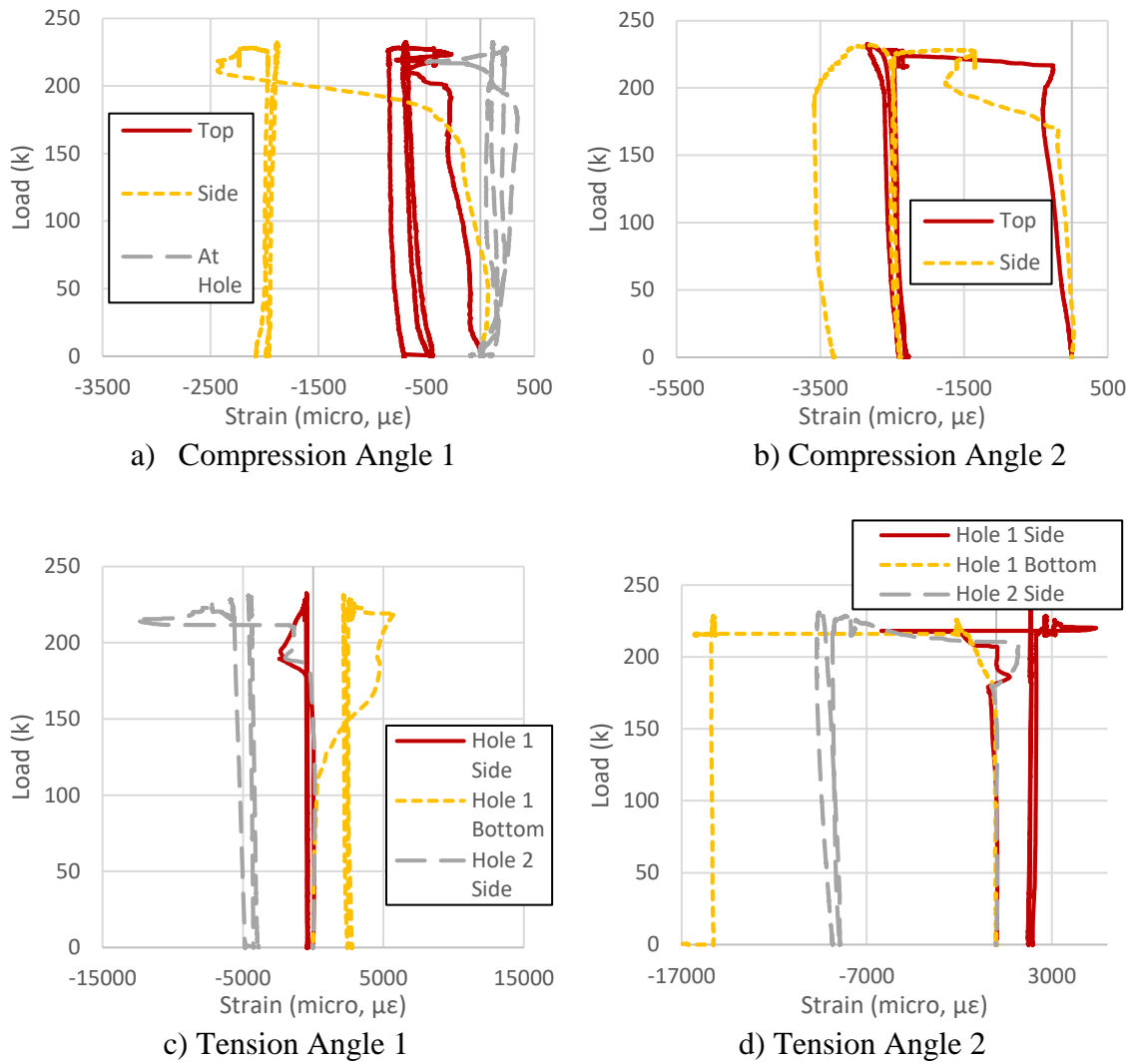


Figure D9: Test 3 angle load vs. flexural strain

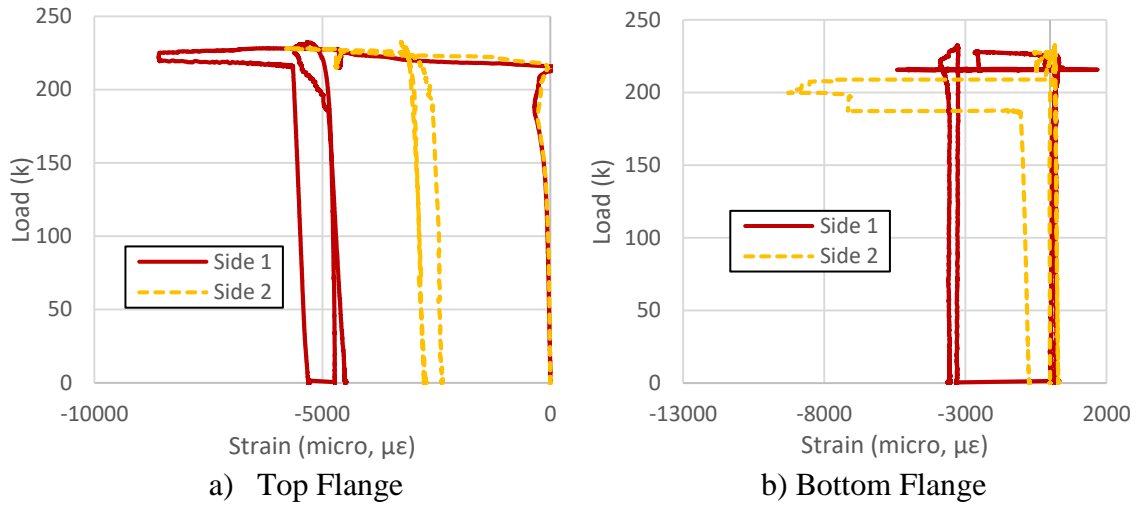


Figure D10: Test 3 beam flange load vs. flexural strain

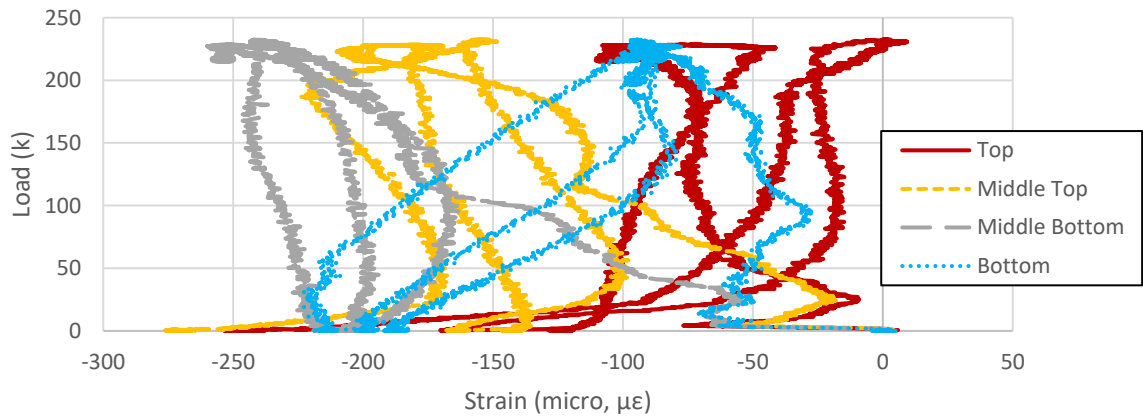


Figure D11: Test 3 shear plate load vs. flexural strain

D.5 Test 4 Supplementary Figures

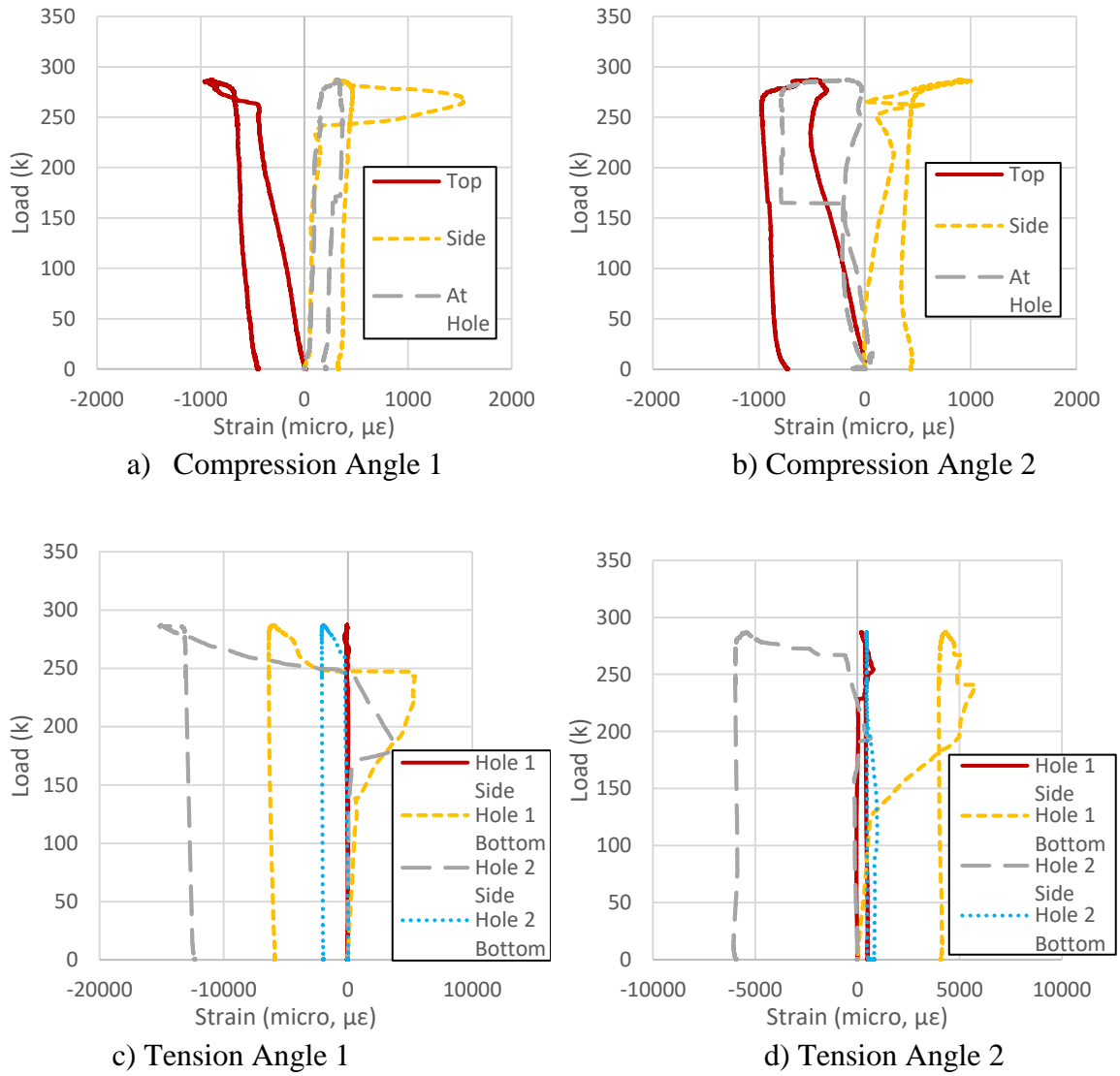


Figure D13: Test 4 angle load vs. flexural strain

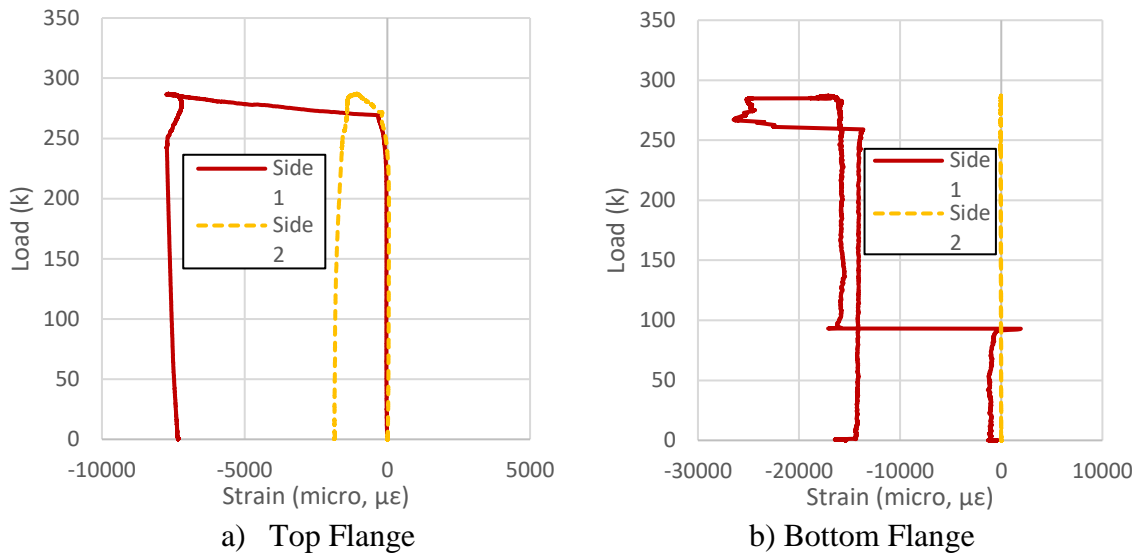


Figure D14: Test 4 beam flange load vs. flexural strain

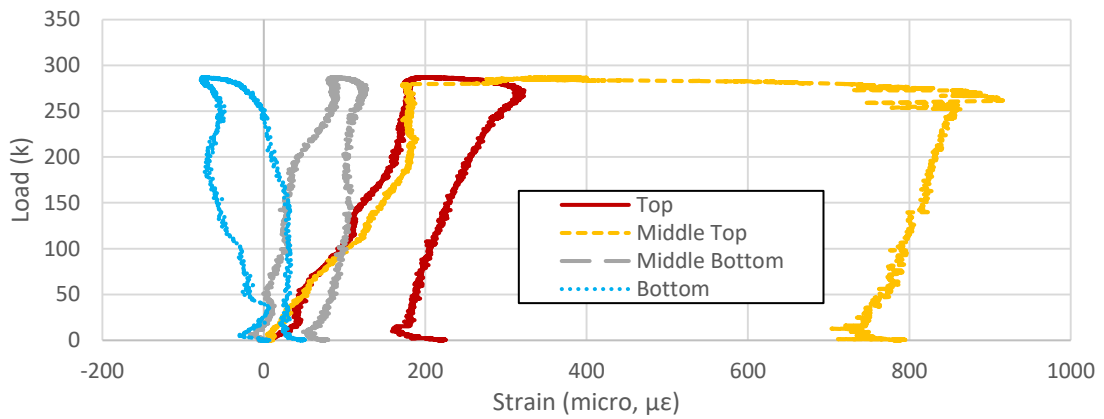


Figure D15: Test 4 shear plate load vs. flexural strain

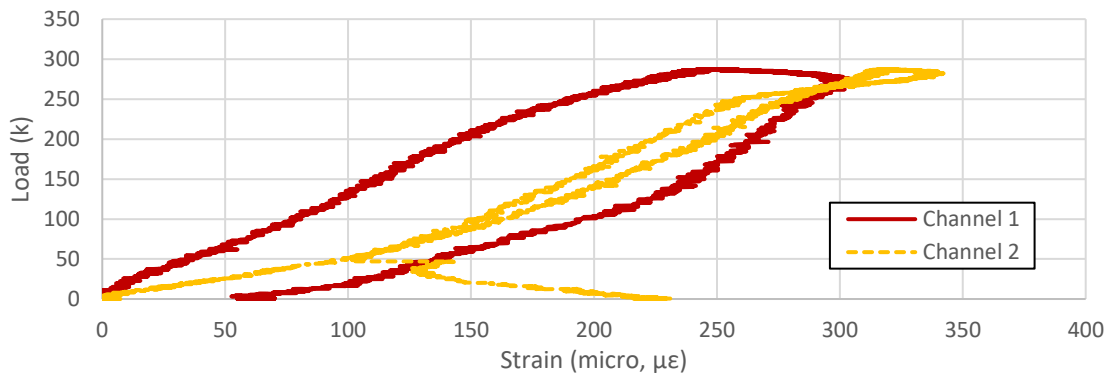


Figure D16: Test 4 compression region channel load vs. axial strain